OPTICAL PROPERTIES OF METAL/DIELECTRIC COMPOSITES WITH PASSIVE AND ACTIVE HOST MATRICES

By

Sisay Shewamare

SUBMITTED AS A
REQUIREMENT FOR THE DEGREE OF
DOCTOR OF PHILOSOPHY
AT
ADDIS ABABA UNIVERSITY
ADDIS ABABA
JUNE 2013

ADDIS ABABA UNIVERSITY
DEPARTMENT OF
PHYSICS

The undersigned hereby certify that they have read and recommend to the School of Graduate Studies for acceptance a thesis entitled "**OPTICAL PROPERTIES OF METAL/DIELECTRIC COMPOSITES WITH PASSIVE AND ACTIVE HOST MATRICES**" by **Sisay Shewamare** as a requirement for the degree of **Doctor of Philosophy**.

Dated: June 2013

External Examiner: _____
Prof. Viktor Reshetnyak

Research Supervisor: _____
Prof. Vadim Mal'nev

Internal examiner: _____
Dr. Mulugeta Bekele

_____

ADDIS ABABA UNIVERSITY

Date: **June 2013**

Author: **Sisay Shewamare**

Title: **OPTICAL PROPERTIES OF METAL/DIELECTRIC COMPOSITES WITH PASSIVE AND ACTIVE HOST MATRICES**

Department: **Physics**

Degree: **Ph.D.** Convocation: Year: **2013**

Permission is herewith granted to Addis Ababa University to circulate and to have copied for non-commercial purposes, at its discretion, the above title upon the request of individuals or institutions.

Signature of Author

To the Memory of Birhan and Kibnesh

Table of Contents

List of Tables

List of Figures

Acknowledgements

Accomplishment of a study of such scale cannot be anticipated without contribution of many individuals and institutions. It would be thus fair to mention people and institutions that have lend a hand for the successful completion of the research project.

Primarily, I am sincerely indebted to my advisor, Prof. V.N. Ma'lnev, for his insightful professional assistance and academic support all through the duration of the study.

I thankful to Addis Ababa University Office of Research and Graduate Studies who support funding for my research work. I thankful to Dr. Mulugeta Bekele who have made a serious editing and suggestion for the work. I thankful to staff members of Department of Physics of the Addis Ababa University. Special thanks goes to W/o Tsilat Adinew whose support is always sensible and generous, where I need.

I thankful to Jimma University and to staff members of Department of Physics for sponsoring my study leave.

I express my deep gratitude to my dearest wife W/o Adugnash Seyoum, for all her patience, courage and sacrifice of loneliness you put up with when I was completely occupied in this pursuit. I love you and I am honestly humbled by your never-ending support. I thankful to my children Efrata Sisay and Yonatan Sisay for your patience. Special thanks to my father Ato shewamare, and to my mother W/o Belaynesh, and to my sisters and to my brothers who were always beside me in supporting my work.

Finally, I thankful to my friends and colleagues for their comments and supports.

Sisay Shewamare
Mach, 2013

Abstract

The Thesis is devoted to the theoretical and numerical study of the enhancement of the local electric field and the induced optical bistability (IOB) in metal ellipsoidal and spherical dielectric nanoparticles covered by a metal shell with nonlinear dielectric functions. In the electrostatic approximation, specification of the IOB domain reduces to an analysis of the algebraic cubic equation for the local electric field in the particle as a function of the external electric field. The comparatively simple analysis of roots of a cubic equation, proposed in the Thesis, allowed us to find the range of the amplitudes of incident electromagnetic wave and their frequencies where the IOB exists and study its dependence on the parameters of the problem. The results of numerical computations for metal and metal covered semiconductor nanoparticles are presented graphically.

It is shown that the local field in metal spherical particles with dielectric core in an external varying electric field has two maxima at two different frequencies. The second maximum becomes more important with increment in the metal fraction. Due to the nonlinear dielectric function of the core, the composite of these inclusions may have two optically induced bistability domains at different frequencies. At rather high metal fraction, two bistability domains merge and form one entire bistability domain. The parameters of these domains are studied numerically. In the Thesis we focuses on the second bistability domain. This domain exists in a comparatively narrow frequency range and its onset fields are lower than those of the first bistability domain. The lowest bistability onset fields are obtained in the entire domain. This peculiarity of the optical induced bistability in the metal composite with small dielectric cores can be attractive for possible applications.

In the Thesis it is shown that the enhancement factor of the local electric field in metal spherical or cylindrical nanopacticles with dielectric cores imbedded in a dielectric matrix have two maxima on two resonant frequencies. The second maxima for

the inclusions with large dielectric cores covered by a thin metal shell is comparatively small. With increasing in a metal fraction in the inclusion, both enhancement factors grow. For large metal fractions, the maxima of the enhancement factors become the same order of magnitude and considerably large. At a special relation between the dielectric constants of the core and the host matrix, the two maxima merge and show further increment. The numeric calculations show that the real and imagine parts of the refractive index of the composites of metal inclusions having "small" dielectric cores have new interesting features.

The optical properties of metal/dielectric composites (metal with dielectric core and pure metal inclusions) in passive and active host matrices are studied. It is shown that the real and imaginary parts of the refractive index of the composites with metal covered inclusions have two maxima at two resonant frequencies. Both types of the composite show a strong anomalous dispersion of the real part of refractive index. The active host matrices can considerably reduce the absorption and provide the conditions for propagation of weakly damping electromagnetic waves on the resonant frequencies. The weakly spreading wave packets of light of a negative group velocity can be experimentally observed in these composites.

General Introduction

The linear and nonlinear response of the medium strongly effects on the propagation of electromagnetic wave in the optical material and can even result in the permanent modification of its physical properties. In turn, the linear and nonlinear optical features of composite materials with metal nanostructures are dominated by surface plasma oscillations. The fact that the surface plasmon (SP) strongly depends on size, shape, distribution of metal nanoparticles as well as on surrounding dielectric matrix offers an opportunity for manufacturing of new promising nonlinear materials, nanodevises and optical elements.

Composite materials, consisting of small, nonlinear metallic particles (existing in the shape of sphere or cylinder) randomly embedded in a linear dielectric host, are well known for their complex responses to incident light fields [1], [2].

Nonlinear optical effects are useful for many different applications. Some examples of areas of science and technology in which nonlinear optics discussed in nonlinear microscopy [3], ultrafast laser systems [4], wavelength conversion [5], material processing [6], the characterization of surfaces [7], optical routing and switching based on optically induced bistability both on networks [8], [9], [10] and on chips [11]. Metals have a fast and strong nonlinear response [12] and may be good candidates for nonlinear optical applications if they are combined with dielectrics [13], [14].

Combining metals and dielectrics has two main purposes. One is allowing light to enter more deeply into metals, and the other is achieving light localization which in turn leads to an enhanced nonlinear response.

An outstanding property of metal nanoparticle is the presence of extinction bands in the visible or infrared that result from the so called plasmon resonances these resonances do not exist in bulk metals, can be interpreted as a result of the confinement of free electrons in a space smaller than one wavelength of the light and controlled by changing the shape of the nanoparticle and its orientation with respect to the electric field.

Plasmon resonances in metal nanoparticles can be put to many practical uses for example they enhance the sensitivity of optical sensors [15] and show great potential to be applied in the therapy of cancer [16]. Plasmon resonances are also the reason why the nonlinear optical properties of nanoparticle systems are enhanced with respect to those of bulk metals [17].

The evaluation of the effective optical properties of composite materials were first devoted to the analysis of linear media [18] and considering the contribution of the local field of the particle extended to the study of materials with one nonlinear component [19, 20] in addition with very low concentration of the nonlinear component [19, 21], contributions being treated as purely real and as small perturbations (low field approximation) to the assumed leading linear behavior [20, 22]. Due to these limitations, in the case of relatively high concentration of the nonlinear components, the above-mentioned approximations are generally unable to predict (and control) the appearance of effects such as the optical bistability associated with the nonlinear optical response of composite materials [2, 19].

The velocity of propagation of light in a material system can be controlled and modified to a large extent, extreme values of pulse velocity slow light ($v << c$), superluminal light ($v > c$), and v negative) have been reported [23], [24]. The pioneering demonstrations of slow and fast light were all based on the exploitation of narrow spectral resonances, mainly created by electromagnetically-induced transparency [23] or coherent population oscillation [24]. Narrow spectral resonances induce an anomalous situation for the optical propagation, since any sharp spectral change in the medium transmission results in a steep linear variation of the effective refractive index along wavelength. This in turn results in a strong group velocity change at the exact center of the resonance [25]. The phenomenon of slow light has received a lot of attention since the spectacular experimental demonstration of light slow-down to 17 meters per second in an ultracold atomic gas [23].

0.1 Outline

Chapter 1 presents the back ground of the thesis starting from the electrodynamical description for the physical system and continuing to the mathematical description for the propagation of light in a composite system.

Chapter 2 describes the enhancement factor of the local field of metal nanoinclusion with a dielectric core considering a linear dielectric functions of the system. It is shown that maxima at different plasma resonant frequencies. It is very interesting to study the second maximum because it gives an opportunity to have additional optical induced bistability (OIB). In the case of large dielectric core (thin metal cover) the second maxima is not important. It is also proposed a comparatively simple analysis of roots for a cubic equation that allowed us to carry out the analytic study of the

OIB domains and may be useful while studying the processes that are described by an S-type characteristic curve of the local field in particles versus the applied field.

Chapter 3 describes the OIB domains in the plane of applied electromagnetic field-the applied radiation frequency. It is complementary to the widely used S-type characteristics. This method allows us to analyze OIB domains analytically and numerically for small metalic fraction. It is analyzed the local field enhancement inside an ellipsoidal metal particle embedded into a dielectric matrix when the incident electric field is parallel to one of the ellipsoid axes. In addition it is studied the analysis of the OIB domain for elliptical particles and the OIB of a two layer nonlinear dielectric spherical particle covered by a metal shell.

Chapter 4 describes the second OIB for large metallic fraction for both analytical and numerical results. We proposed the analytic formulas to specifying OIB domain in the plane of "frequency of the incident radiation - modulus squared of the amplitude of incident radiation". This method can be considered as a complementary plot for the method of $S-$like curves. With increment in the metal fraction, the two bistability domains merge into one with comparatively low onset fields. In Chapter five and six devoted to the real and the imaginary part of the refractive index studied in Chapter 5. Chapter 6 is devoted to the group velocity index and the group velocity of light in pure metal composite and metal/dielectric composite in active and passive host matrices.

Chapter 1

Literature Review

1.1 Description of Electrodynamical Properties of Physical Systems

1.1.1 The Maxwell Equations

Maxwell combined Coulomb's results on the forces between charged particles and Faraday's investigations on the effects of currents and magnetic fields into four partial differential equations, which reveal the electromagnetic nature of light.

Maxwell realized that the solution to the equations of electromagnetism can be expressed as a transverse electromagnetic field [26]. Maxwell's hypothesis was confirmed in 1887 by Hertz who was able to produce and to detect electromagnetic waves.

The Maxwell equations relate the space and time derivatives of the electric and magnetic fields to each other throughout the continuous medium. In this section we only present the main definitions and results which are needed for the scopes of this work . If we adopt cgs units, Maxwell equations can be expressed as follows [27]

$$\nabla \times \mathbf{E}(\mathbf{r},t) = -\frac{1}{c}\frac{\partial \mathbf{B}(\mathbf{r},t)}{\partial t}, \tag{1.1.1}$$

$$\nabla \times \mathbf{H}(\mathbf{r},t) = \frac{4\pi}{c}\mathbf{J}(\mathbf{r},t) + \frac{1}{c}\frac{\partial \mathbf{D}(\mathbf{r},t)}{\partial t}, \tag{1.1.2}$$

$$\nabla \cdot \mathbf{D}(\mathbf{r}, t) = 4\pi\rho(r, t), \tag{1.1.3}$$

$$\nabla \cdot \mathbf{B}(\mathbf{r}, t) = 0, \tag{1.1.4}$$

where $\mathbf{r}$ is the 3-dimensional coordinate vector and t indicates time. Here $\mathbf{D}(\mathbf{r}, t)$ denotes the electric displacement, $\rho(\mathbf{r}, t)$ is the charge density, $\mathbf{B}(\mathbf{r}, t)$ is the magnetic induction, $\mathbf{E}(\mathbf{r}, t)$ is the electric field, $\mathbf{H}(\mathbf{r}, t)$ is the magnetic field, and $\mathbf{J}(\mathbf{r}, t)$ is the current density. The electric displacement and the magnetic induction are connected to the electric and magnetic field, respectively, by the constitutive equations

$$\mathbf{D}(\mathbf{r}, t) = \mathbf{E}(\mathbf{r}, t) + 4\pi\mathbf{P}(\mathbf{r}, t), \tag{1.1.5}$$

$$\mathbf{B}(\mathbf{r}, t) = \mathbf{H}(\mathbf{r}, t) + 4\pi\mathbf{M}(\mathbf{r}, t), \tag{1.1.6}$$

where $\mathbf{P}(\mathbf{r}, t)$ and $\mathbf{M}(\mathbf{r}, t)$ are the polarization and magnetization of the medium, respectively, these quantities describe the electromagnetic response of the medium. The current density also given by the following equation

$$\mathbf{J} = \sigma\mathbf{E}, \tag{1.1.7}$$

where σ is the conductivity of the medium.

At optical frequencies the materials are usually non-magnetic. The magnetic permeability is unity practically and the magnetization can be omitted. Under this fairly good approximation, the optical response of a medium to an electromagnetic perturbation is completely described by the constitutive relation between the polarization and the electric field inducing it.

1.2 Linear and Nonlinear Susceptibility of Media

In this section we first introduce the linear optical response of a medium to an external electromagnetic perturbation by using very basic macroscopic electromagnetic theory. In this context we provide the definition of susceptibility and of the most relevant optical constants that can be derived from it. We also present a treatment of local field effects regarding a homogenous media. We will discuss the linear and nonlinear optical features of composite materials with metal nanostructures.

1.2.1 Local Field and Effective Medium Approximation in Linear Optics

The response of a medium to an external electric field cannot be described exactly by means of the macroscopic electric fields. The external field drives the bound charges of the medium apart and induces a collection of dipole moments [28]. In an optically dense medium, the interaction of the induced dipoles is taken into account by a local field factor, which relates the macroscopic fields to the local ones. The local field is considered by starting from the macroscopic properties of the medium. The linear polarization provides an extensive description of the light-matter interaction when low radiation intensities are considered.

1.2.2 Fundamentals of Nonlinear Optics

Nonlinear optics concerns the process that appears when a material medium is subject to a light beam sufficiently intense to modify the response of the medium to an electromagnetic field. Nonlinear optics is the study of phenomena that occur as a consequence of the modification of the optical properties of a material system by the presence of light. Typically, only laser light is sufficiently intense to modify

the optical properties of a material system. The beginning of the field of nonlinear optics is often taken to be the discovery of second-harmonic generation by Franken et al. (1961), shortly after the demonstration of the first working laser by Maiman in 1960. Nonlinear optical phenomena are "nonlinear" in the sense that they occur when the response of a material system to an applied optical field depends in a nonlinear manner on the strength of the optical field. For example, second-harmonic generation occurs as a result of the part of the atomic response that scales quadratically with the strength of the applied optical field. Consequently, the intensity of the light generated at the second-harmonic frequency tends to increase as the square of the intensity of the applied laser light.

In order to describe more precisely what we mean by an optical nonlinearity, let us consider how the dipole moment per unit volume or polarization $\mathbf{p}(t)$, of a material system depends on the strength $\mathbf{E}(t)$ of an applied optical field. In the case of conventional (i.e., linear) optics, the induced polarization depends linearly on the electric field strength in a manner that can often be described by the relationship

$$\mathbf{P}(t) = \chi^{(1)}\mathbf{E}(t), \tag{1.2.1}$$

where the constant of proportionality $\chi^{(1)}$ is known as the linear susceptibility. In nonlinear optics, the optical response can often be described by generalizing Eq.1.2.1 by expressing the polarization $\mathbf{P}(t)$ as a power series in the field strength $\mathbf{E}(t)$ as

$$P(t) = \chi^{(1)}E(t) + \chi^{(2)}E^2(t) + \chi^{(3)}E^3(t) + ... = P^{(1)}(t) + P^{(2)}(t) + P^{(3)}(t) + ... \tag{1.2.2}$$

The quantities $\chi^{(2)}$and $\chi^{(3)}$are known as the second- and third-order nonlinear optical susceptibilities and $P^{(2)}$, $P^{(3)}$ are the second and the third order polarizations respectively. The applied field $\mathbf{E}$ is of the order of the characteristic atomic electric

field strength shown [29] as $E_{at} = e/(4\pi\varepsilon_0 a_0^2)$, numerically $E_{at} = 5.14 \times 10^{11} V/m$. The second order $\chi^{(2)}$ will be of the order of $\chi^{(1)}/E_{at}$. For the condensed matter $\chi^{(1)}$ is unity, and we have expected that $\chi^{(2)}$ will be of the order of $1/E_{at}$, or that $\chi^{(2)} \approx 1.94 \times 10^{-12} m/V$. Similarly we expect $\chi^{(3)}$ to be of the order of $1/E_{at}^2$ which is $\chi^{(3)} \approx 3.76 \times 10^{-24} m^2/V^2$.

Considering the Maxwell equations given from equations 1.1.1-1.1.7 the electromagnetic wave equation can be derived as follow

$$\nabla \times \nabla \times \mathbf{E} + \frac{4\pi}{c^2}\sigma\frac{\partial \mathbf{E}}{\partial t} + \frac{1}{c^2}\frac{\partial^2 \mathbf{E}}{\partial t^2} + 4\pi\frac{\partial^2 \mathbf{P}}{\partial t^2} = 0. \tag{1.2.3}$$

The polarization $\mathbf{P}$ is stated in equation 1.2.2 therfore, equation 1.2.3 can be written as

$$\nabla \times \nabla \times \mathbf{E} + \frac{4\pi}{c^2}\sigma\frac{\partial \mathbf{E}}{\partial t} + \frac{1+\chi^{(1)}}{c^2}\frac{\partial^2 \mathbf{E}}{\partial t^2} + 4\pi\frac{\partial^2 \mathbf{P}_{NL}}{\partial t^2} = 0. \tag{1.2.4}$$

For weak incident optical field the nonlinear contribution can be neglected ($\mathbf{P}_{NL} \rightarrow 0$, and equation 1.2.4 becomes the well known ordinary wave equation:

$$\nabla \times \nabla \times \mathbf{E} + \frac{4\pi}{c^2}\sigma\frac{\partial \mathbf{E}}{\partial t} + \frac{1+\chi^{(1)}}{c^2}\frac{\partial^2 \mathbf{E}}{\partial t^2} = 0. \tag{1.2.5}$$

The nonlinear term containing $\mathbf{P}_{NL}$ in equation 1.2.4 can be recognized as a source that can emit coherent radiation at new frequency. Thus, nonlinear polarization induced in the media by propagating monochromatic electromagnetic wave is responsible for optical harmonic generation.

1.3 Lorentz Local Field

The concept of a local field was originally introduced by Lorentz [28]. The response of a medium to an external electric field cannot be described exactly by means of the

macroscopic electric fields. The external field drives the bound charges of the medium apart and induces a collection of dipole moments [30]. In an optically dense medium, the interaction of the induced dipoles is taken into account by a local field factor, which relates the macroscopic fields to the local ones. The macroscopic electric field and the effective electric field that each atom experiences should be distinguished. The effective electric field is also known as the Lorentz local field. We calculate this Lorentz local field through use of a procedure described by Lorentz in different text books (see for example [31], [32]).

It is well-known that the field driving an atomic transition in a material medium, the local field, is different in general from both the external field and the average field inside the medium. The difference from the average field does not play a significant role when one considers a low-density medium. To describe the optical properties of such a system, one can use the macroscopic (ensemble average) field. However, if the atomic density of a system exceeds $\approx 10^{15} cm^3$ [33], the influence of local-field effects becomes significant and cannot be neglected.

In order to account for local-field effects on the optical properties of a material, one needs to apply a proper model relating the local field to its macroscopic counterparts, namely the average field and polarization. The choice of the model strongly depends on the medium of interest. For example, local field in a homogeneous medium can be related to the macroscopic average field according to

$$\mathbf{E}_{Loc} = L\mathbf{E}, \tag{1.3.1}$$

where L is the local-field correction factor and E is the macroscopic average field . In order to find the local field acting on a typical dipole of the medium, one surrounds the dipole of interest with an imaginary spherical cavity of radius much larger than

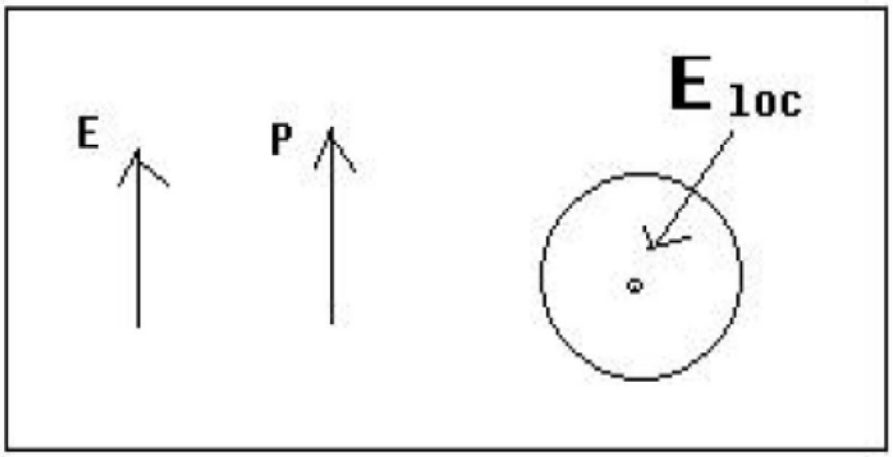

Figure 1.1: Calculation of the Lorentz local field

the distance between the dipoles, and much smaller than the optical wavelength. The contributions to the local field from the dipoles situated within the spherical cavity are accounted for exactly, while the dipoles outside the cavity are treated as uniformly distributed, characterized by some average macroscopic polarization shown in Fig.1.1. For material with linear optical response, the local field determines the microscopic polarization $p(\omega)$, expressed as the product of the local electric field times the polarizability $\alpha(\omega)$ of the single microscopic constant:

$$\mathbf{p}(\omega) = \alpha(\omega)\mathbf{E}_{loc}(\omega) \tag{1.3.2}$$

The macroscopic polarization of the medium is derived by averaging 1.3.2 over the investigated volume V, as follows [29]:

$$P(\omega) = \frac{1}{v}\int_{v} p(\omega)dv = N\alpha(\omega)E \tag{1.3.3}$$

where dv is the unit volume for integration and N is the density of microscopic

constituents. Considering for a homogeneous medium, we have the following relation

$$n_e = \frac{N}{V} \tag{1.3.4}$$

where $\frac{N}{V}$ is the number of electrons per unit volume and n_e is the number of electrons per elementary constituent of the medium. The polarization can be expressed in terms of the external electromagnetic field as follows

$$\mathbf{P}(\omega) = \chi^{(1)}_{eff}(\omega)\mathbf{E}(\omega). \tag{1.3.5}$$

Hence, in order to express the effective susceptibility in terms of the microscopic polarizability, we have to express the local electric field in terms external electric field. We have that the local electric field can be expressed as follows [31], [34], [32]

$$\mathbf{E}_{Loc} = \mathbf{E} + \frac{4\pi}{3}\mathbf{P}, \tag{1.3.6}$$

for the local field $\mathbf{E}_{Loc}$ in terms of the average macroscopic field $\mathbf{E}$ and the macroscopic polarization $\mathbf{P}$. Local field given by Eq.(1.3.6) is called Lorentz local field [29].

The concept of a local field was originally introduced by Lorentz [35] and it is further derive the Lorentz-Lorenz (or Clausius-Mossotti) relation for the dielectric permittivity ε and microscopic polarizability α. Let us assume for now that the medium is lossless and dispersionless. We represent the dipole moment induced in a typical molecule (or atom) of the medium as

$$\mathbf{P} = \alpha\mathbf{E}_{Loc}. \tag{1.3.7}$$

The macroscopic polarization of the material is given by the equation

$$\mathbf{P} = N\mathbf{p}. \tag{1.3.8}$$

where N denotes molecular (or atomic) number density. Using equations (1.3.3) through (1.3.7), we find that the polarization and macroscopic field are related by

$$\mathbf{P} = N\alpha[\mathbf{E} + \frac{4\pi}{3}\mathbf{P}]. \tag{1.3.9}$$

We assume the polarization $\mathbf{P}$ to be linear in the average field:

$$\mathbf{P} = \chi^{(1)}\mathbf{E}, \tag{1.3.10}$$

where $\chi^{(1)}$ is the linear optical susceptibility of the medium. Substituting the expression 1.3.9 into 1.3.10, solving for $\chi^{(1)}$, and eliminating the field $\tilde{E}$, we find that

$$\chi^{(1)} = \frac{N\alpha}{1 - \frac{4\pi}{3}N\alpha}. \tag{1.3.11}$$

Expressing the optical susceptibility of the medium

$$\chi^{(1)} = (\varepsilon^{(1)} - 1)/4\pi \tag{1.3.12}$$

($\varepsilon^{(1)}$ is the dielectric permittivity of the medium), we obtain the well-known Lorentz-Lorenz (or Clausius- Mossotti) relation

$$\frac{\varepsilon^{(1)} - 1}{\varepsilon^{(1)} + 2} = \frac{4\pi}{3}N\alpha. \tag{1.3.13}$$

Through rearrangements of Eq 1.3.13we can express the linear susceptibility as

$$\chi^{(1)} = \frac{\varepsilon^{(1)} + 2}{3}N\alpha. \tag{1.3.14}$$

Substituting the expression 1.3.14 in to 1.3.10 then 1.3.10 in to 1.3.8 and using the relationship 1.3.2 between the local field and dipole moment, we obtain the equation relating the local field to the average field.

$$\mathbf{E}_{Loc} = \frac{\varepsilon^{(1)} + 2}{3}\mathbf{E}. \tag{1.3.15}$$

Where

$$L = \frac{\varepsilon^{(1)} + 2}{3}, \tag{1.3.16}$$

is known in the literature as the Lorentz local-field correction factor [31], [34], [32]. The expression 1.3.15 for the local-field correction factor is valid in the case of homogeneous media, where all the particles (molecules or atoms) are of the same sort. It is also valid in materials where the emitters enter as inclusions that do not influence the correlation between the host molecules or atoms [36], [37].

1.3.1 Source of Polarizability

The polarizability [32, 38, 39] describes the distortion of the dipole field on an atomic scale induced by the interaction with the external oscillating field. Geometry suggests that the ratio between the polarization and the polarizability is simply the number of elementary components of the medium per unit volume. Effectively, this is not precisely the case, since in the definition of the averaged macroscopic quantity not only the external applied field but also the local dipole fields induced by the single elementary components of the medium yield contributions. Therefore, the electric field inducing the polarization is not the macroscopic external field of the incoming radiation.

The constitutive equation that includes the response of the material to the applied electromagnetic field is written as;

$$\mathbf{D} = \mathbf{E} + 4\pi\mathbf{P}, \tag{1.3.17}$$

where $\mathbf{D}$ is the electric displacement. The term $\mathbf{P}$ is the electrical polarization of the matter. The macroscopic polarization created by the dipoles adds to the vacuum contribution and sums up to the displacement field $\mathbf{D}$. For different frequencies,

different types of oscillators will dominate the response. The strength of this response depends also on the oscillator density and on the inertia of the excitation mechanism. For a pure dielectric response, the polarization is proportional to the electric field in a linear approximation by

$$\begin{aligned} \mathbf{P} &= \chi^{(1)}\mathbf{E}, or \\ \mathbf{D} &= \varepsilon\mathbf{E}. \end{aligned} \tag{1.3.18}$$

In general case the polarizability α is a tensor. It considerably complicates the calculation. In this work for the ellipsoidal inclusions we consider only one direction of the external field $\mathbf{E}_h$ parallel to the larger axes of the ellipsoid when the polarizability can be characterized by one parameter.

1.4 Optically Induced Bistability (OIB)

The optical properties of metal nanoparticles embedded in a dielectric medium have been a subject of immense interest in recent years because of their novel characteristics and possible device applications [40], [41],[42],[43].

The induced optical bistability (OIB) means that some nonlinear optical systems can produce two different output intensities for a given input intensity [29] or, in particular, given value of the external electric field may produce several values for the local field and polarization. Optical switching is an essential component in the all-optical network. A feasible approach to all-optical switching is based on optical bistability, an important subject in nonlinear optics [41].

Since its theoretical prediction in 1969 [44] and experimental realization in 1976 [40, 41, 42] the OIB has been intensively studied because of its potential applications for optical logic [43], optical memory element [11], and optical switching devices [45],

the phenomenon of intrinsic optical bistability in composite media has received much attention [46]. Recently it has received a new attention because of the intensive study of the properties of composite media and the nonlinear photonic crystals [47], [48], [49].

Composite materials, consisting of small, nonlinear metallic particles (existing in the shape of sphere or cylinder) randomly embedded in linear dielectric host matrix, are well known for their complex responses to incident light fields [50], [51] and shown that both interfacial property and size of metallic particles can affect the optical bistability behaviour[52].The study of optical bistability and bistable devices is a special branch of nonlinear optics. Optical bistability can be realized in many types of structures see Fig.1.2. However, in this thesis we will consider the detailed theoretical and numerical analysis of the local field enhancement and the bistability domain in small metal and metal covered semiconductor particles in the electrostatic approximation when $a \ll \lambda$ (a is a typical size of particles and λ is the wave length of the electromagnetic wave). At the same time, the particles must be large enough that the dielectric function preserve the physical meaning which can be corresponds to the nano scaled particles.

We account for a cubic nonlinearity in the polarization with respect to the local electric field. The nonlinear part of the dielectric function (DF) is important only in the electric fields that are comparable with the inner atomic fields. At present, such fields may be achieved in the laser radiation. But even the laser fields are often not enough for the experimental realization of the OIB. The important property of pure metal and metal covered dielectric nanoparticles is the considerable enhancement of the local field inside the particle if the frequency of incident electromagnetic wave

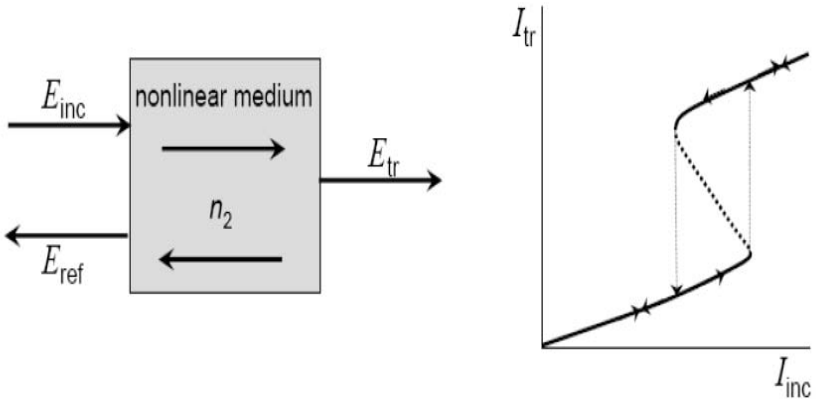

Figure 1.2: a) the nonlinear material b) The Bistability response of the nonlinear materials

approaches the surface plasmon frequency of the metal.

1.5 Refractive Index

The development of nanostructured media with electronic and optical properties vastly different from that usually found in natural material. Metamaterials exhibits abnormal dispersion characteristics at optical scales and can behave as a medium with negative [53], high [54],[55], [56], [57], [58] small [58] or unit [59], [60], [61] effective refractive index. From the practical point of view it is interesting that the optical response of such artificial media may be tuned by specific choice of constituents and their concentration or by the detailed morphology of the medium [56, 62, 63].

In the case of metal-dielectric composite media, their application can practically be limited by absorbtion of incident electromagnetic radiation due to the presence of metal components. In a number of papers [55, 56, 59, 64], it was proposed to

use active (amplifying) host matrix in order to compensate absorption at metallic inclusion.

We use a classical oscillator model for our calculation of index of refraction for both pure metal and metal with dielectric core inclusion in a host matrix. The index represented by n and given by the square root of the dielectric constant ε, which is in turn related to the atomic polarizability α using $D = \varepsilon E$ and the refractive index is given by

$$n = \sqrt{\varepsilon}. \tag{1.5.1}$$

Considering equation 1.3.12 the dielectric constant given by

$$\varepsilon = 1 + 4\pi\alpha. \tag{1.5.2}$$

1.6 Phase Velocity and Group Velocity

Let us consider the narrow wave packet centered at k_0 is given by the following equation

$$E(t) = \int_{-\infty}^{\infty} e^{-i(kx-\omega_k t)} e^{\frac{-(k-k_0)^2}{2\Delta^2}} dk. \tag{1.6.1}$$

From the dispersion relation at $k \to k_0$ expanding with Taylor series we have the following equation

$$\omega_k = \omega_{k_0} + \frac{d\omega}{dk} \mid_{k=k_0} (k - k_0) + \frac{d^2\omega}{dk^2} \mid_{k=k_0} (k - k_0)^2 + ... \tag{1.6.2}$$

The relation 1.6.2 shows that the third therm in Taylor expansion can be neglected provided that $\triangle k \ll V_g/(\frac{dV_g}{dk})$. It means that dV_g/dk should not be very large. In other words, $V_g(k)$ must be a slow function of k.

Further using equation 1.6.2 and substituting in equation 1.6.1 one can find the propagation of the light wave in the following form

$$E(t) = \int_{-\infty}^{\infty} e^{-i(k_0 x - \omega_{k_0} t)} e^{-\frac{\Delta^2}{2}(x - V_g t)^2} \int_{-\infty}^{\infty} e^{-\frac{((k-k_0) - i\Delta^2(x - V_g t))^2}{2\Delta^2}} d(k - k_0). \tag{1.6.3}$$

$$E(t) = \sqrt{2\pi} E(k_0) e^{i(k_0 x - \omega_{k_0} t)} e^{\frac{-\Delta^2 (x - V_g t)^2}{2}}. \tag{1.6.4}$$

The concept of group velocity was firstly introduce in [65]. The first recorded observation of the group velocity of a wave is presented [66]. A continuous wave light beam propagating in a medium with refractive index n has a phase velocity

$$V_p = \frac{c}{n} \tag{1.6.5}$$

where c is the speed of light in vacuum, and the refractive index is given by 1.5.1, $n = kc/\omega$ for the phase velocity. If the intensity of the signal varies in time, i.e. the spectrum of the signal has a finite width, the propagation speed of the intensity modulation is instead given by the group velocity

$$\begin{aligned} V_g &= \frac{c}{n_g}, \\ n_g &= \frac{c}{n + \omega \frac{dn}{d\omega}}. \end{aligned} \tag{1.6.6}$$

The real part of equation 1.6.4 presents the group velocity. The group velocity thus differs from the phase velocity in media and at frequencies, where the refractive index has a non-zero first-order derivative with respect to frequency. If the light intensity is modulated, e.g. sinusoidally, the group velocity thus describes the velocity with which this intensity pattern is transmitted through the device.

Chapter 2

Two Resonances in Metal/Dielectric Composites

2.1 Introduction

The enhancement of the local electric field of the incident electromagnetic radiation in the composites of metal covered nanoparticles with dielectric cores is of great importance because of different possible applications of these systems. It is known that the local field in metal inclusions can be considerably enhanced if a frequency of the incident radiation is close to the surface plasmon frequency [67]. This problem was intensively studied in connection with the optically induced bistability [68, 69]. It is generally accepted that a such enhancement can take place only on one resonant frequency depending on the dielectric constants of the system.

In this chapter, we present that the enhancement factor of the local field in the spherical and cylindrical inclusions with dielectric cores has two maxima. The second maximum in the inclusions with a large dielectric cores covered by thin metal shell (at higher frequencies) is small comparing with the first one. With increasing in the metal fraction of the inclusion, the second maximum grows and must be taken into account. This situation has not been discussed in the literature so far.

2.2 Enhancement Factor of the Local Field in Spherical and Cylindrical Nanoinclusions

Let us consider an individual metal spherical or cylindrical inclusion with a dielectric core embedded in a dielectric host matrix. In the electrostatic approximation, when a wave length of the incident electromagnetic radiation is much greater than a typical size of the inclusion, the distribution of the electric potential in the system is described by the following expressions

$$\begin{aligned} \Phi_1 &= -E_h A_d r cos\theta, r \leq r_1, \\ \Phi_2 &= -E_h (B_d r - C_d / r^{d-1}) cos\theta, r_1 \leq r \leq r_2, \\ \Phi_h &= -E_h (r - D_d / r^{d-1}) cos\theta, r \geq r_2. \end{aligned} \tag{2.2.1}$$

They are the solutions of the Laplace equations in the core and metal shell of the inclusion, and in the host matrix, respectively. Here E_h is the applied field (for the cylindrical inclusion it is perpendicular to its axis), r and θ are the coordinates of the observation point (the beginning of the coordinate in the center of the inclusion and the $z-$ axis is along $\mathbf{E}_h$), A_d, B_d, C_d, and D_d are unknown coefficients, r_1 and r_2 are the radiuses of the dielectric core and the metal shell of the inclusion, respectively. Here d is the dimension of the problem: $d = 3$ for the spherical and $d = 2$ for the cylindrical inclusion, respectively. It is necessary to note that 2.2.1 is true for infinitively long cylinder. In our case we consider $r_2/L \ll 1$ (L is a length of the cylinder) when the effect of the cylinder ends is small. We also assume that the external radius of cylindric inclusions is much smaller that their length and the wave of radiation.

From the continuity conditions of the electric potential and the displacement vector on the interface dielectric core - metal and metal - host matrix, we obtain the system of linear algebraic equations for the unknown coefficients. Further, we need

only the coefficients A_d and D_d that enter into the potential of the local field in the inclusion core and the induced dipole moment of the inclusion. They can be presented in the form

$$A_d = Q_d \frac{\varepsilon_2 \varepsilon_h}{p_d \Delta_d}, \tag{2.2.2}$$

with $Q_d = d^2/(d-1)$,

$$D_d = \{1 - \frac{d}{d-1} \frac{\varepsilon_h[(d-p_d)\varepsilon_2 + p_d\varepsilon_1]}{p_d \Delta_d}\} r_2^d, \tag{2.2.3}$$

$$\Delta_d = \varepsilon_2^2 + q_d \varepsilon_2 + \varepsilon_1 \varepsilon_h. \tag{2.2.4}$$

Here

$$q_d = (d/((d-1)p_d) - 1)\varepsilon_1 + (d/p_d - 1)\varepsilon_h, \tag{2.2.5}$$

where $p_d = 1 - (r_1/r_2)^d$ is a metal fraction in the inclusion, ε_1, ε_2, and ε_h are the dielectric functions (DF)s of the core, metal, and the host matrix, respectively. We note that the expressions 2.2.2 have been used in [52] while studying the optical induced bistability in dielectric matrix with spherical metal inclusions with small nonlinear dielectric cores. The expression 2.2.3 at $d = 3$ gives the corresponding result of [1] for the polarizability of a coated sphere.

The local field $\mathbf{E}$ in the dielectric core of the inclusion can be obtained with the help of relation

$$\mathbf{E} = A_d \mathbf{E}_h, \tag{2.2.6}$$

where A_d is given by 2.2.2. In general, it is a complex function. Further, it would be convenient to deal with the real quantity $|A_d|^2$, which we call the enhancement factor. It can be presented as follows

$$|A_d|^2 = \frac{Q_d^2}{p_d^2} \frac{\varepsilon_h^2(\varepsilon_2'^2 + \varepsilon_2''^2)}{(\varepsilon_2'^2 - \varepsilon_2''^2 + q_d\varepsilon_2' + \varepsilon_1\varepsilon_h)^2 + \varepsilon_2''^2(q_d + 2\varepsilon_2')^2}. \tag{2.2.7}$$

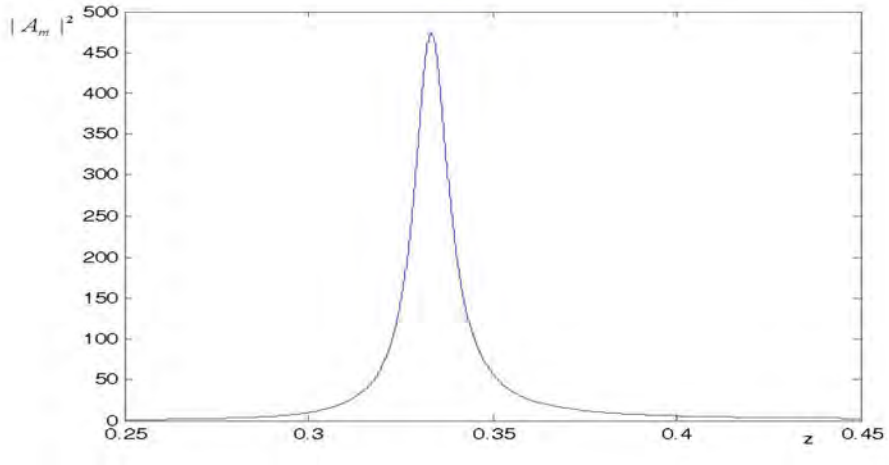

Figure 2.1: The enhancement factor $|A_m|^2$ for a pure silver spherical nanoparticle versus z. We use the following parameters of the system: $\omega_p = 1.46 \times 10^{16}$ (silver plasma frequency), $\nu = 1.68 \times 10^{14}, \gamma = 1.15 \times 10^{-2}$; $\varepsilon_\infty = 4.5, \varepsilon_h = 2.25$.

The DF of metal ε_2 is chosen in the Drude form.

$$\varepsilon_2 = \varepsilon_\infty - \frac{\omega_p^2}{\omega(\omega + i\nu)}, \tag{2.2.8}$$

where ω_p is the plasma frequency given by $\omega_p^2 = Ne^2/(\varepsilon_0 m)$, ω is the frequency of the incident wave, e is the electron, m is the mass of electron, N is the concentration of electron.

The real and imaginary part of equation 2.2.8 given by ε_2' and ε_2'' respectively as follows

$$\begin{aligned} \varepsilon_2' &= \varepsilon_\infty - \frac{1}{z^2 + \gamma^2}, \\ \varepsilon_2'' &= \frac{\gamma}{z(z^2 + \gamma^2)}. \end{aligned} \tag{2.2.9}$$

The DF of the core ε_1, in general case, includes a nonlinear part with respect to the local field. Further, for the sake of simplicity, we will ignore the imaginary parts of ε_1 and ε_h.

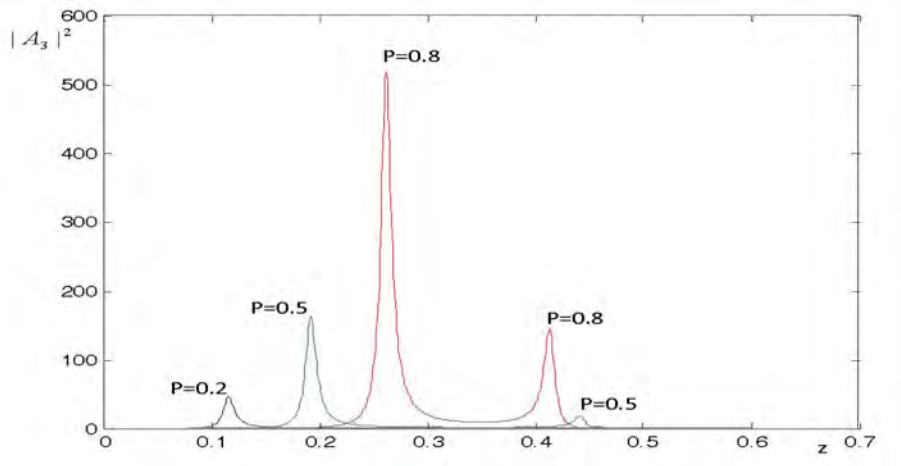

Figure 2.2: The enhancement factor $|A_3|^2$ for a silver spherical coated nanoparticle versus z at $p = 0.2, 0.5, 0.8$. Here and further we use the following parameters: $\varepsilon_\infty = 4.5, \varepsilon_{10} = 6, \varepsilon_h = 2.25$. Rest parameters are the same as in Fig.2.1

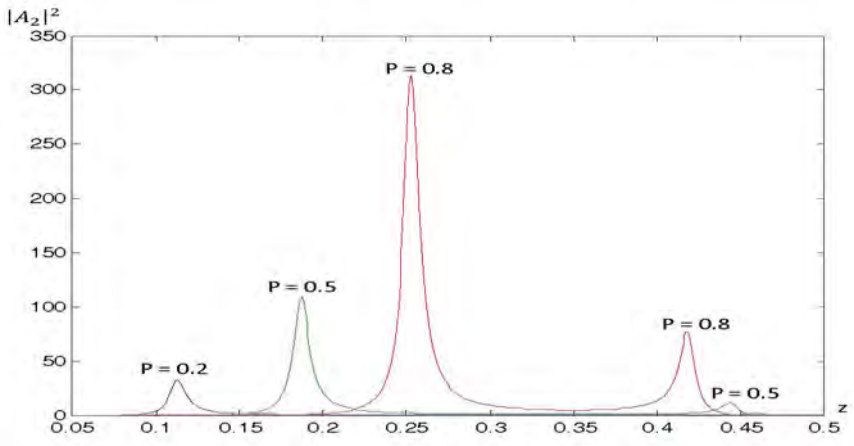

Figure 2.3: The enhancement factor $|A_2|^2$ for a silver cylindrical coated nanoparticle versus z at $p = 0.2, 0.5, 0.8$. Here and further we use the following parameters: $\varepsilon_\infty = 4.5, \varepsilon_{10} = 6, \varepsilon_h = 2.25$. Rest parameters are the same as in Fig.2.1

For the analytic analysis, we consider the practically non-decaying plasma vibrations in the metal when $\gamma << 1$. A maximum of the enhancement factor in this case is obtained setting zero the first term in the denominator 2.2.7. It gives the quadratic equation with respect to ε_2'

$$\varepsilon_2'^2 + q_d\varepsilon_2' + \varepsilon_1\varepsilon_h = 0. \tag{2.2.10}$$

Considering equation 2.2.10 we can find the analytical results of the resonant frequency in two limiting cases, the first limiting case is for thin metal cover ($p << 1$) and the second limiting case is for small dielectric core $p \approx 1$.

With account the first limiting case for thin metal of the composite for equation 2.2.5 given by

$$q_d = d[\varepsilon_1/(d-1) + \varepsilon_h]/p_d >> 1. \tag{2.2.11}$$

substituting equation2.2.11 in equation 2.2.10

$$\begin{aligned} \varepsilon_{21'}' &= -q_d, \\ \varepsilon_{22'}' &= -\varepsilon_1\varepsilon_h/q_d \end{aligned} \tag{2.2.12}$$

.

Considering in the first limiting case, using equation 2.2.12 and equation 2.2.9 we obtain the following two resonant frequencies

$$\begin{aligned} z_{1'} &= \sqrt{1/(\varepsilon_\infty + q_d)} \approx \sqrt{1/q_d}, \\ z_{2'} &= \sqrt{1/(\varepsilon_\infty + \varepsilon_1\varepsilon_h/q_d)} \approx \sqrt{1/\varepsilon_\infty}, \\ q_d &>> \varepsilon_\infty, \varepsilon_1\varepsilon_h. \end{aligned} \tag{2.2.13}$$

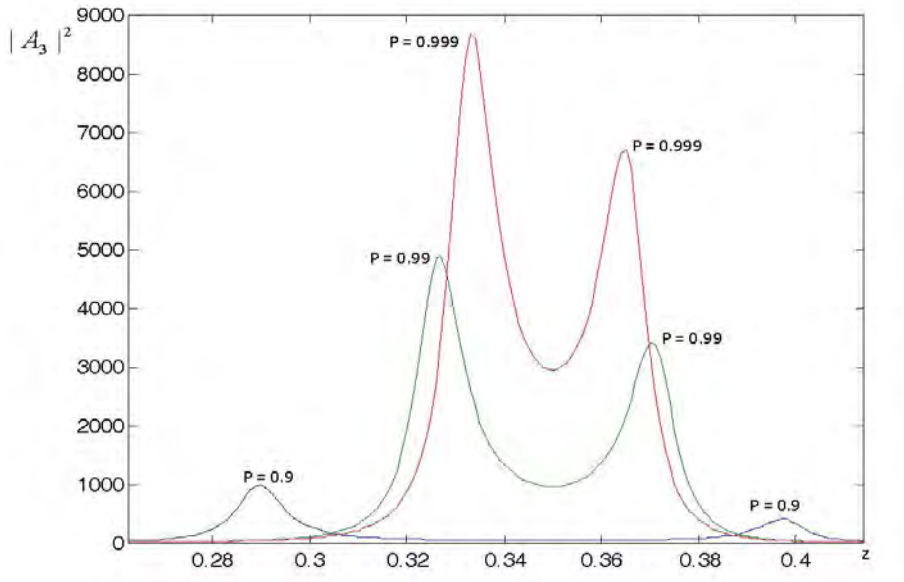

Figure 2.4: The enhancement factor $|A_3|^2$ for a silver spherical coated nanoparticle versus z at "large" p. Rest parameters are the same as in Fig.2.1

The corresponding two maxima of the enhancement factor can be calculated by substituting equation 2.2.13 in equation 2.2.7

$$\begin{aligned} |A(z_{1'})|^2 &= \frac{Q_d^2 \varepsilon_h^2}{(d[\varepsilon_1/(d-1)+\varepsilon_h])^3} \frac{p_d}{\gamma^2}, \\ |A(z_{2'})|^2 &= p_d \frac{\varepsilon_1^2 \varepsilon_h^2}{d[\varepsilon_1/(d-1)+\varepsilon_h]\varepsilon_\infty^3} |A(z_{1'})|^2, \\ \gamma &<< p_d. \end{aligned} \tag{2.2.14}$$

It is clear that the first maxima of $|A_d|^2$ is much greater than the second one for the first limiting condition $p_d << 1$.

Now we calculate the resonance frequency by considering the second limiting case for the large metal fractions (small dielectric cores). we rewrite equation 2.2.5 using $p \simeq 1$ as

$$q_d = \varepsilon_1/(d-1) + (d-1)\varepsilon_h. \tag{2.2.15}$$

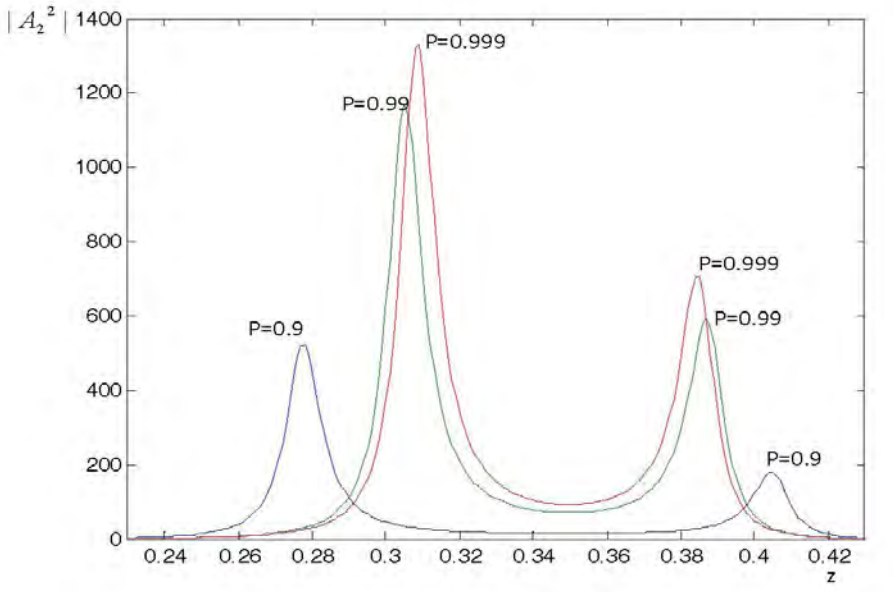

Figure 2.5: The enhancement factor $|A_2|^2$ for a silver cylindrical coated nanoparticle versus z for "large" p. Rest parameters are the same as in Fig.2.1

Substituting equation 2.2.15 in equation 2.2.10 we find the following equations

$$\begin{aligned} \varepsilon'_{21} &= -(d-1)\varepsilon_h, \\ \varepsilon'_{22} &= -\varepsilon_1/(d-1), \end{aligned} \tag{2.2.16}$$

compering equation 2.2.9 and 2.2.16 the resonance frequency can be written as

$$\begin{aligned} z_1 &= \sqrt{1/[\varepsilon_\infty + (d-1)\varepsilon_h]}, \\ z_2 &= \sqrt{1/[\varepsilon_\infty + \varepsilon_1/(d-1)]}. \end{aligned} \tag{2.2.17}$$

We find the maximum enhancement at the resonance frequency of equation 2.2.17 using equation 2.2.7

$$\begin{aligned} |A(z_1)|^2 &= \frac{Q_d^2 \varepsilon_h^4 (d-1)^4}{[\varepsilon_1 - (d-1)^2\varepsilon_h]^2(\varepsilon_\infty + (d-1)\varepsilon_h)^3} \frac{1}{\gamma^2}, \\ |A(z_2)|^2 &= \frac{\varepsilon_1^2}{\varepsilon_h^2} \frac{(\varepsilon_\infty + (d-1)\varepsilon_h)^3}{(\varepsilon_\infty + \varepsilon_1/(d-1))^3} \frac{|A(z_1)|^2}{(d-1)^4}, \\ \varepsilon_1 &\neq (d-1)^2\varepsilon_h. \end{aligned} \tag{2.2.18}$$

While obtaining 2.2.14 and 2.2.18, we used $\varepsilon_2'' = \gamma/z_r^3$ with resonant frequencies 2.2.13 and 2.2.17, respectively. Both maxima of the enhancement factor 2.2.18 of inclusions with small cores ($p \simeq 1$) are of the same order. A comparison of 2.2.18 and 2.2.14 shows that the maxima of the enhancement factor of the inclusions with small cores are much larger than those for the inclusions with large cores $p << 1$ 2.2.14.

The further increment of the enhancement factor happens to be possible by tuning the DFs of the core and host matrix. At

$$\varepsilon_1 = (d-1)^2\varepsilon_h, \tag{2.2.19}$$

the positions of the resonant frequencies coincide at,

$$z_1 = z_2 = z_r = 1/\sqrt{\varepsilon_\infty + (d-1)\varepsilon_h} \tag{2.2.20}$$

with the accuracy $\varepsilon_2'' << 1$. Two enhancement factors merge and their maximum becomes very large $\sim 1/\gamma^4$

$$|A_d(z_r)|^2 = \frac{Q_d^2 \varepsilon_h^4 (d-1)^2}{[\varepsilon_\infty + (d-1)\varepsilon_h]^6} \frac{1}{\gamma^4}. \tag{2.2.21}$$

Equation 2.2.21 shows at the condition of tunned DFs give us the highest enhancement.

2.3 Numerical Results

2.3.1 Spherical Inclusions

In the real inclusions, γ is not extremely small but finite. The behavior of $|A_d|^2$ as a function z in this case can be analyzed only numerically. The results of this study are presented below. They qualitatively confirm the above reported analytical ones.

We start our numerical calculations with the enhancement factor of a pure metal particle $|A_m|^2$. It can be obtained from 2.2.7 by setting $p = 1$ and making substitution $\varepsilon_1 \rightarrow \varepsilon_2$:

$$|A_m|^2 = \frac{9\varepsilon_h^2}{(\varepsilon_2' + 2\varepsilon_h)^2 + \varepsilon_2''^2}. \tag{2.3.1}$$

In Fig.2.1, we present 2.3.1 $|A_m|^2$ versus z and will compare it further with $|A_d|^2$ of metal covered inclusions with different dielectric cores. This quantity is calculated with the help of 2.2.7 for silver particles embedded in the host matrix with typical numerical value which present the enhancement of pure metal by considering the limiting transition parameters.

Figure 2.2 shows $|A_3|^2$ for spherical inclusions at different p. At $p = 0.2$, the second maxima which presented is practically invisible against a background of the first maxima, which can be observed nearly 9 times less than the maximum of $|A_m|^2$

as shown in Figure 2.1. The maxima of $|A_3|^2$ grow very fast with increasing p that is metallic ratio. In particular, at $p = 0.8$, the first maximum is slightly above the maximum in Fig.2.1 for pure metallic sphere. The second maximum is practically equal to the first maximum of $|A_3|^2$ at $p = 0.5$. The most interesting inclusions with $0.9 \leq p \leq 0.999$, where absolute values of both maxima considerably large. The enhancement factor of cylindrical inclusions p shows the same behavior. At small p, the second maximum is not important. At large p, it becomes comparable with the first one as it seen from Fig.2.3. The resonant frequencies are practically the same for the spherical and cylindric inclusions but the absolute values of maxima of $|A_2|^2$ which is shown in Figure 2.3 are 2-4 times less than those of $|A_3|^2$. The further increment in p practically does not change the resonant frequencies and absolute values of the maxima of enhancement factor. It is interesting to note that at the above parameters

Table 2.1: Maximum values of $|A_3|^2$ and the resonant frequency z_r for some tuned ε_1 and ε_h at $p = 0.999$.

material	ε_1	material	ε_h	z_r	$\lvert A_3\rvert^2$
GaAs	10.9	KI	2.7	0.316	6.35×10^4
Ge	15.8	AgCl	4	0.282	7.022×10^4
Si	11.7	MgO	2.95	0.309	6.66×10^4

of the composite the second (smaller) maximum is blue shifted with respect to the first one. But choosing $\varepsilon_\infty = 1$ [70] along with the same rest DFs, one can find that the second maximum becomes higher that the first one.

2.3.2 Cylindrical Inclusions

According to the above presented analytic analysis, the further increment in the enhancement factor is possible if we use the "tuned" inclusions when the condition 2.2.19 holds true. It gives $\varepsilon_1 = 4\varepsilon_h$ and $\varepsilon_1 = \varepsilon_h$ for the spherical and cylindrical inclusions, respectively. It was obtained for very small decay constant γ and p very close to unit. The numerical calculations show that at $p = 0.999$, two maxima of the enhancement factor of spherical and cylindrical inclusions merge into one peak. Its absolute value is about of one order higher than the maxima of the untuned inclusions with $p = 0.999$ (Fig.2.4, 2.5). The values of maxima of the enhancement factor of tuned spherical inclusions of different composites are presented in Table.2.1. In addition the figures presented for different metallic fraction ($p = 0.9$ and $p = 0.99$) for spherical and cylindrical inclusion shown in Fig. 2.6, 2.7.

For nanoinclusions with "small" dielectric cores one has to check is it possible to use the bulk dielectric permittivity. Our approach is applicable to the Raleigh particles. A typical wave length corresponding to the resonant frequency $0.35\omega_p$ for inclusions with $p = 0.999$ (see Fig.2.4- 2.5) is about 400nm. Taking inclusions of a radius $\sim$ 20nm and using the relation $r_1 = (1-p)^{1/d} r_2$ that connect the radiuses of core and inclusion, we get $r_1 = 2$nm and $r_1 = 0.06$nm for the spherical and cylindrical inclusion at $p = 0.999$, respectively. It means that we can use the bulk DF for $p \leq 0.999$ for the spherical inclusions shown in Fig. 2.8. For the cylindrical inclusions it is questionable. The existence of two maxima of the enhancement factor of the local field in metal inclusions with dielectric cores seems to be a result of two interfaces dielectric - metal and metal - host. In particular, for small cores, the resonant frequencies depend only on ε_∞ and ε_1 or ε_h 2.2.17. Two maxima of

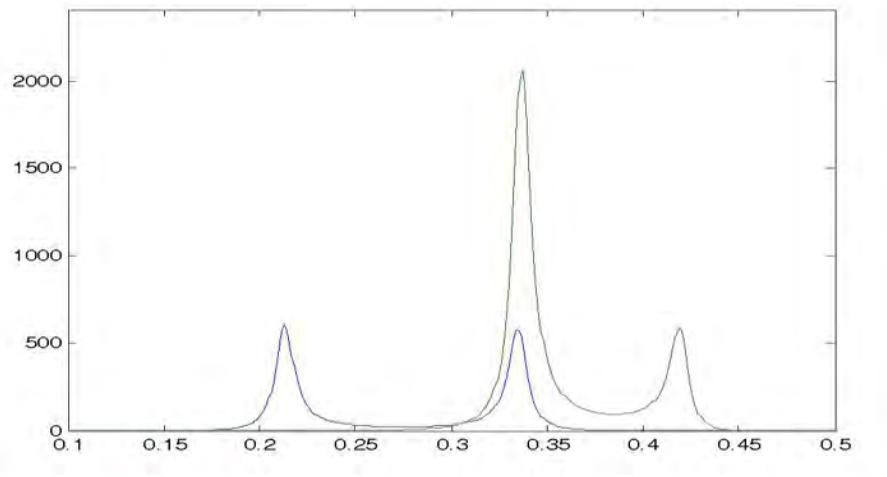

Figure 2.6: The enhancement factor $|A_2|^2$ and $|A_3|^2$ for a silver cylindrical and spherical coated nanoparticle versus z for metallic fraction of $p = 0.9$ with a parameter forcylinder $\varepsilon_h = 2.25, \varepsilon_1 = 2.25$. and for sphere $\varepsilon_h = 4.4, \varepsilon_1 = 17.6$ Rest parameters are the same as in Fig.2.1

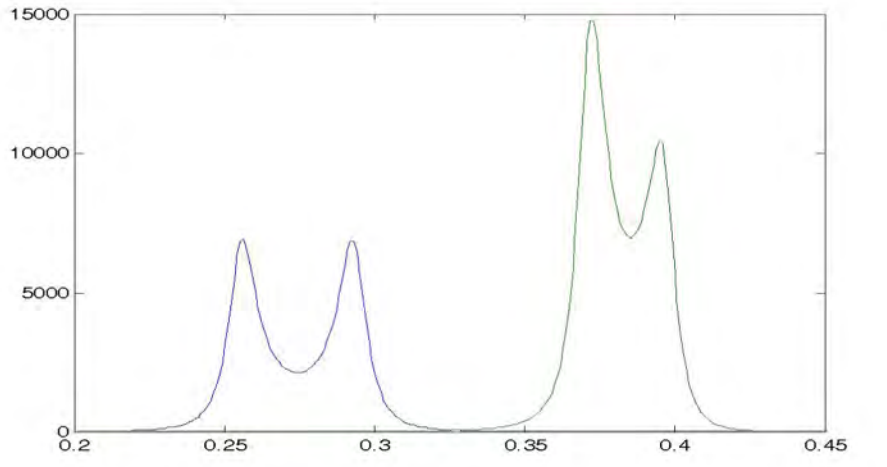

Figure 2.7: The enhancement factor $|A_2|^2$ and $|A_3|^2$ for a silver cylindrical and spherical coated nanoparticle versus z for metallic fraction $p = 0.99$ with a parameter for cylinder $\varepsilon_h = 2.25, \varepsilon_1 = 2.25$ and for sphere $\varepsilon_h = 4.4, \varepsilon_1 = 17.6$. Rest parameters are the same as in Fig.2.1

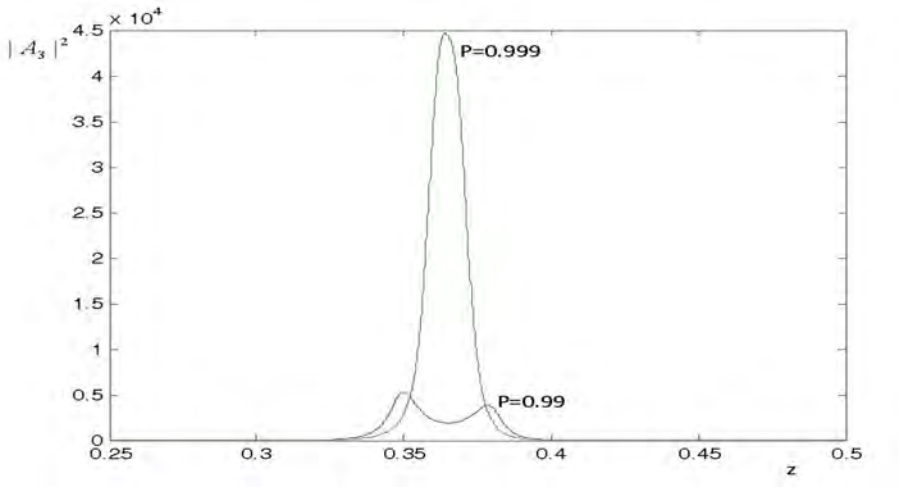

Figure 2.8: The enhancement factor $|A_3|^2$ for a silver spherical coated nanoparticle versus z for metallic fraction $p = 0.99$and $p = 0.999$ with a parameter for sphere at resonant parameter $\varepsilon_h = 4.4, \varepsilon_1 = 17.6$ Rest parameters are the same as in Fig.2.2

$|A_d|^2$ or two minima in $|\Delta|^2$, which enters in the polarazibility of inclusion 2.2.19, results in some peculiarities in the frequency dependence of the optical parameters of composites.

2.4 Conclusion

The conclusion about the existence of two maxima of the enhancement factor of the local field in metal inclusions with small dielectric cores at two different frequencies and their comparatively large amplitudes was made in [71]. It must change the linear and nonlinear properties of the composites of these inclusions. In particular, account of the second maximum of $|A_3|^2$ is considerably affects the picture of the optically induced bistability. We have seen considerably enhanced for the second maxima when metallic fraction increased. It is very interesting result we got at a tuned frequency

those two resonance merged for spherical and cylindrical inclusion.

The results of this chapter have been obtained with the help of the Drude model for the dielectric function of the electrons in the metal shell of the inclusion. We use here these simplest model. It would be interesting to note that the Drude model can be generalized with account of intra and inter band transition as well as the electron mean free path dependence on the particle size see for example (Phys Let., 446, 115 (2007), J. Phys. Chem. C, 113, 21604 (2009)). We focus on the second maxima of the enhancement factor, which is blue shifted compering to the first one. We hope that the above mentioned factors will not affect much our conclusions.

In the next Chapter we consider the nonlinear effect of induced optical bistability in the metal covered inclusions with large dielectric cores when the second maximum of the local field is not important.

Chapter 3

Induced Optical Bistability in Metal and Metal Coated Nanoparticles Composites

3.1 Introduction

The electronic properties of noble metal materials change drastically as a consequence of reducing their size and dimensionality to nanoscale proportions. The density of states and spatial length scale of the electronic motion are reduced with decreasing size, the energy eigenvalue are now determined by the system's boundaries thus surface effect become very important [72, 73].

The optical properties have attracted a large amount of work pioneered by the work of Mie [74] Gans [75]. Mie first described these phenomena theoretically by solving Maxwell's equation for the absorption and scattering of a radiation field interacting with a spherical metal particle under the appropriate boundary conditions as long as the material dielectric function is known and the size is smaller than the wavelength of light [1, 2].

A theoretical description of particle plasmons involves analyzing the interaction of

a sub-wavelength metal particle with an electromagnetic field using the electrostatic approximation. Indeed, if the particle is much smaller than the wavelength of light, the oscillating electromagnetic field is practically constant over the particle volume, so that we can calculate the spatial field distribution assuming the simplified problem of a particle in an electrostatic field [1], [32], [76].

Metallic nanoparticles have the ability to sustain coherent electron oscillations known as surface plasmon (SP) leading to electromagnetic fields confined to their surface. The formation of surface plasmon (SP) are due to the electric field of an incoming radiation that induces the formation of a dipole or a polarization of charges on the nanoparticle surface.

In this chapter, we derive the analytical expression for the enhancement factor for the elliptical small particle. And we drive the analytical and numerical results for the enhancement factor of for different depolarize factor at incident electromagnetic wave frequency approach to the surface plasmon frequency. In our approach we can find a simple relation for optical induced bistability and optical bistability domain which can help us to find a simple relation to construct optical bistability at a particular tuned incident radiation. In addition we derive the analytical and numerical results of the enhancement factor and optical bistability domain for the elliptical metals with dielectric function embedded in the dielectric host. We also discussed for optical bistability domain for spherical nanometalic particle (silver nanoparticle)

3.2 Enhancement of the Local Field in Small Metal Ellipsoidal Particles

A theoretical description of particle plasmons involves analyzing the interaction of a sub-wavelength metal particle with an electromagnetic field using the electrostatic approximation. Indeed, if the particle is much smaller than the wavelength of light, the oscillating electromagnetic field is practically constant over the particle volume, so that we can calculate the spatial field distribution assuming the simplified problem of a particle in an electrostatic field [1], [32], [76].

Following the treatment of Bohren et al [1], we derive the field distribution of an ellipsoidal particle, which is the most general smooth particle (one without edges or corners), then we extract the field for spheroidal particles which are a special class of ellipsoids.

First, we calculate effective field-dependent permittivity of the nonlinear small metal ellipsoidal particle. In this regard, we indicate that the characteristic particle size is far less than the incident wavelength, and the quasi-static approximation is valid. Moreover, we assume that the metal particle is uniaxial ellipsoids with the shape characterized by the depolarization factor L along x axis. In this notation, a sphere has $L = 1/3$, while a needlelike particle has $L \to 0$, and a plate like particle has $L \to 1$ [77]

Let the electromagnetic wave incident on a metal particle in the form of a rotational ellipsoid embedded in a dielectric host matrix. The dielectric function (DF) of the particle is assumed to depend on frequency ω and the local electric field $\vec{E}$ (inside the particle). Since the local field in nonlinear metal components cannot be solved

exactly, we shall use mean-field approximation [1] to estimate the field-dependent permittivity of metal,and may be presented in the form [78]

$$\varepsilon_2(\omega, \vec{E}) = \varepsilon_2(\omega) + \chi(\omega) \left|\vec{E}\right|^2, \tag{3.2.1}$$

where $\chi(\omega)$ is the complex Kerr coefficient, $\varepsilon_2(\omega) = \varepsilon_2'(\omega) + i\varepsilon_2''(\omega)$ is the linear part of DF (with respect to $\vec{E}$) and taken in the Drude form

$$\varepsilon_2 = \varepsilon_\infty - \frac{\omega_p^2}{\omega(\omega + i\nu^2)}, \tag{3.2.2}$$

the real and imaginary part of equation 3.2.2 is given

$$\varepsilon_2'(\omega) = \varepsilon_\infty' - \frac{\omega_p^2}{\omega^2 + \nu^2}, \quad \varepsilon_2''(\omega) = \varepsilon_\infty'' + \frac{\nu}{\omega} \cdot \frac{\omega_p^2}{\omega^2 + \nu^2}. \tag{3.2.3}$$

Here, ω_p is the plasma frequency of electrons in the metal, ν is their collision frequency and ε_∞ is a constant that may be a function of frequency and depends on the type of metal.

The potential and the electric field in side the ellipsoid, in the electrostatic approximation, is given

$$\phi = \frac{\phi_h}{1 + \frac{L(\varepsilon - \varepsilon_h)}{\varepsilon_h}} \tag{3.2.4}$$

$$\vec{E} = \frac{\varepsilon_h}{\varepsilon_h + L(\varepsilon - \varepsilon_h)} \vec{E_h}. \tag{3.2.5}$$

Consider the case when the electric vector of the incident wave $\vec{E_h}$ be parallel to the large semi-axis of the ellipsoid. It is known [79] that in the electrostatic approximation the electric field $\vec{E}$ inside the particle is uniform and parallel to $\vec{E_h}$ for an arbitrary dependence of $\varepsilon(\omega, \vec{E})$. This electric field in terms of the enhancement factor and applied field may be expressed in the form [79]

$$\vec{E} = F \cdot \vec{E}_h, \quad F = \frac{\varepsilon_h}{\varepsilon_h\,(1-L) + L\,\varepsilon_2(\omega, \vec{E})}, \tag{3.2.6}$$

where F is an enhancement factor, L is a depolarization factor along the field direction in our case coincides with the larger semi axis of the ellipsoid, ε_h is the dielectric function of the host matrix. Combining 3.2.6, and 3.2.1, we obtain the following expression for the enhancement factor

$$F = \frac{\varepsilon_h}{L} \cdot \frac{1}{\tilde{\varepsilon'} + \chi' \left|\vec{E}\right|^2 + i\left(\tilde{\varepsilon''} + \chi'' \left|\vec{E}\right|^2\right)}, \tag{3.2.7}$$

where $\tilde{\varepsilon}'$ and $\tilde{\varepsilon}''$ are real and imaginary parts of the combination of the dielectric function for the host matrix and the dielectric function for the ellipsoidal particle

$$\tilde{\varepsilon} \equiv \frac{\varepsilon_h\,(1-L) + L\,\varepsilon(\omega)}{L}, \tag{3.2.8}$$

and χ' and χ'' are real and imaginary parts of $\chi(\omega)$.

Let the electric field in the ellipsoidal particle be small enough that the nonlinear term of DF 3.2.1 may be ignored. In this case, 3.2.7 with account of definitions 3.2.3 and 3.2.8 the enhancement factor will be

$$|F_0|^2 = \left|\frac{\varepsilon_h}{L}\right|^2 \frac{1}{\left(\dfrac{1}{z_s^2} - \dfrac{1}{z^2+\gamma^2}\right)^2 + \left(\dfrac{1}{\bar{z}_s^2} + \dfrac{\gamma}{z(z^2+\gamma^2)}\right)^2}. \tag{3.2.9}$$

Here F_0 stands for the enhancement factor for ellipsoidal particle 3.2.7 when the nonlinear electric field terms in the DF are neglected due to its smallness. We have also introduced the dimensionless frequencies as one of the input parameter for our further calculation.

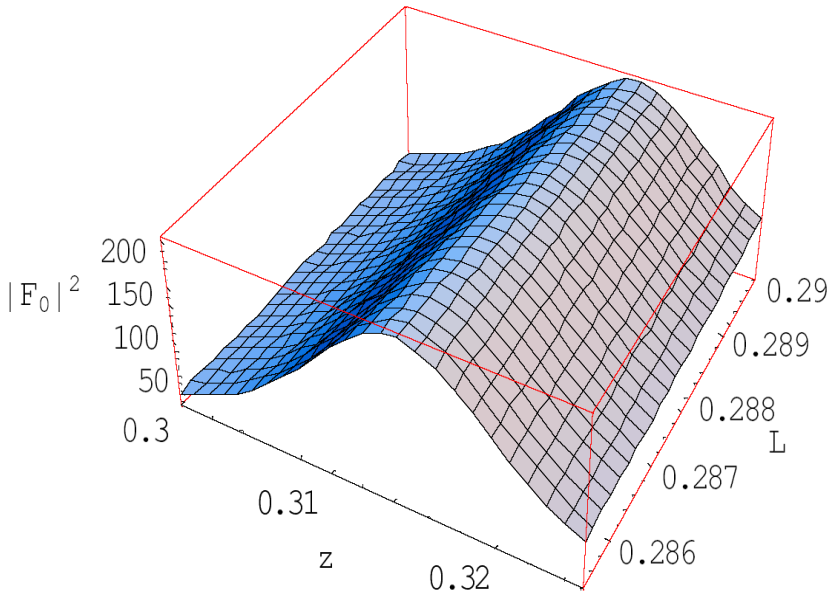

Figure 3.1: Enhancement factor $|F_0|^2$ for a silver nanoparticle versus z and L; $\varepsilon'_h = 2.25$, $\varepsilon''_h = 0$, $\varepsilon'_\infty = 4.5$, $\varepsilon''_\infty = 0.16$, $\omega_p = 1.46 \times 10^{16}$ (frequency of the silver surface plasmons), $\nu = 1.68 \times 10^{14}$, $\gamma = 1.15 \times 10^{-2}$.

$$
\begin{aligned}
&z = \frac{\omega}{\omega_p}, \quad \gamma = \frac{\nu}{\omega_p}, \quad z_s = \frac{\omega_s}{\omega_p}, \quad \bar{z}_s = \frac{\bar{\omega}_s}{\omega_p}, \\
&\omega_s = \omega_p \sqrt{\frac{L}{\varepsilon'_h(1-L) + \varepsilon'_\infty L}}, \\
&\bar{\omega}_s = \omega_p \sqrt{\frac{L}{\varepsilon''_h(1-L) + \varepsilon''_\infty L}}.
\end{aligned}
\tag{3.2.10}
$$

It is important to obtain the largest possible values of $|F_0|^2$ in relation to the local and applied field 3.2.9. It is clear that it can happen if the first term in the denominator 3.2.9 is close to zero which means that the applied electromagnetic wave frequency approach to the surface plasma frequency. We have decided to plot $|F_0|^2$ because of the multi parametrical dependence of $|F_0|^2$ and we use its 3D representation

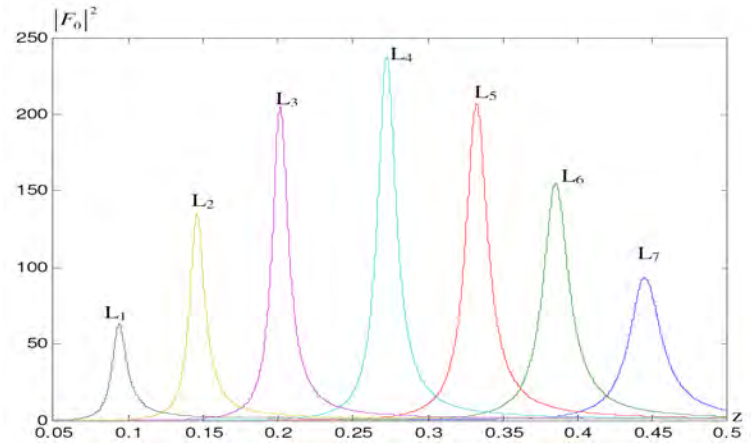

Figure 3.2: The enhancement factor $|F_0|^2$ 3.2.9 as a function of the dimensionless frequency z at different L ($L_1 = 0.02, L_2 = 0.05, L_3 = 0.1, L_4 = 0.2, L_5 = 0.33, L_6 = 0.5, L_7 = 0.8$) with the same parameters of the particle and ε_h as in Fig.3.1

versus z and L. Figure 3.1 presents such a graph in the range of parameters where $|F_0|^2$ is the largest.

One can see that the enhancement factor has a rather sharp maximum when the frequency ω approaches the frequency of the surface plasmon ω_s 3.2.9 if $\gamma \ll z$. To clarify the dependence on L, we present $|F_0|^2$ as a function of z at different constant L (Fig. 3.2). Inspecting graphs on Fig.3.1 and Fig.3.2 one can see that the enhancement factor $|F_0|^2$ in the physically interesting range parameters sharply depends on the frequency of incident electromagnetic wave ω and comparatively weakly depends on the depolarization factor decreasing with L. It can be seen from 3.2.9 that $|F_0|^2 = 1$ at $L \to 0$.

The maximum value of $|F_0|^2$ at the accepted parameters of the particle and the host matrix is around 200. By changing ε_h and L one can obtain even larger $|F_0|^2$. Here we can plot the enhancement factor will be maximum at the depolarization factor

at $L/3$ and given as in Fig.3.1 where the shape of the particle is spheroid. It means that at comparatively large applied fields E_h in the vicinity of the corresponding plasma resonance it is necessary to account the nonlinear terms in the dielectric function 3.2.1. This will be done in the next section.

3.3 Bistability in Ellipsoidal Metal Particles with Nonlinear Dielectric Functions

In this section, we consider the local field in metal ellipsoidal [44] particles which account for the nonlinear part of $\varepsilon(\omega, \vec{E})$ in 3.2.1. We have calculated optical induced bistability in ellipsoidal metal particles with nonlinear dielectric function with the help of equation 3.2.6. But direct usage of this equation is inconvenient since it contains complex coefficients. And to avoid this complex coefficient we have taken the square modulus of 3.2.6with respect to $\left|\vec{E}\right|^2$ and $\left|\vec{E}_h\right|^2$. Let us introduce with the following denotations for $X = |\chi| \left|\vec{E}\right|^2$ and for $Y = (\frac{\varepsilon_h}{L})^2 |\chi| \left|\vec{E}_h\right|^2$, using some rearranging the equation we obtain the cubic equation for Y in terms of X

$$X^3 + aX^2 + bX = Y, \tag{3.3.1}$$

where we use for the variable in the 3.3.1 as follows

$$a = 2\left(\frac{\tilde{\varepsilon}'\chi' + \tilde{\varepsilon}''\chi''}{|\chi|}\right), \quad b = |\tilde{\varepsilon}|^2 .$$

Equation 3.3.1 determines a dependence of the "local field" X on the "applied field" Y, dimensionless frequency z, depolarization factor L and other parameters of the system. The enhancement factor with account of the above specified quantities

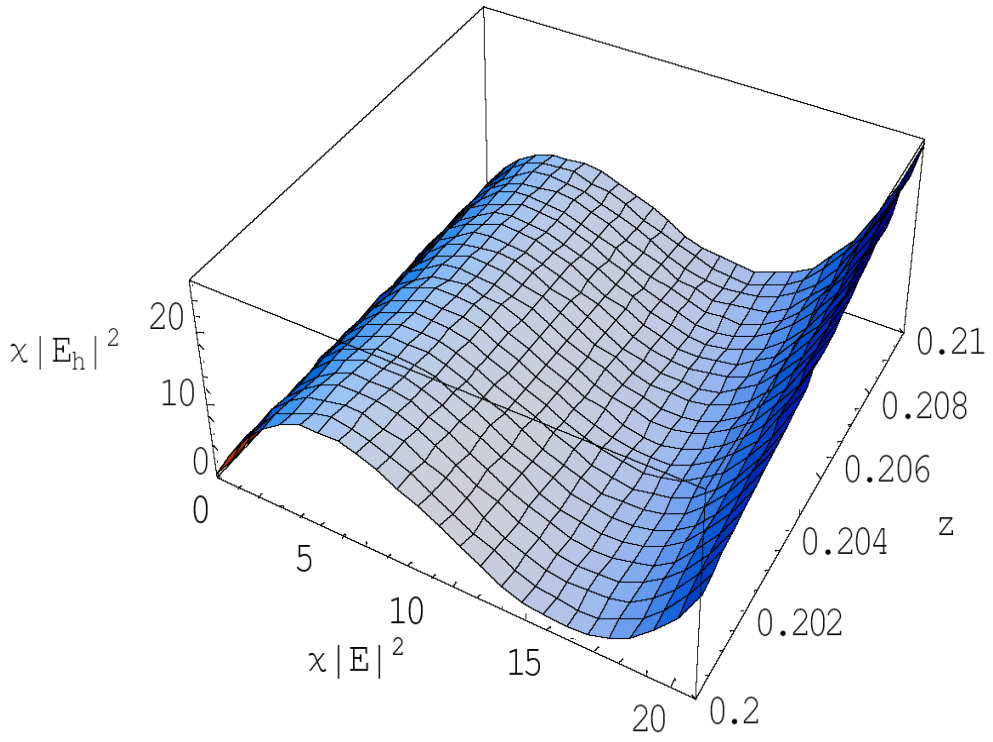

Figure 3.3: The applied field $\chi|E_h|^2$ versus local field $\chi|E|^2$ and frequency z at $L = 0.33$ with the rest parameters as in Fig.3.1.

is given by a simple relation

$$|F|^2 = \frac{X}{Y}. \tag{3.3.2}$$

Further, we are interested only in real and positive roots of cubic equation 3.3.1. If this equation has one real positive root then the local field in the inclusion is a single-valued function of the applied field. If equation 3.3.1 has three positive roots then the local field is not a single valued function of the applied field and the system becomes unstable. This situation is called induced optical bistability (IOB)as it was mentioned above.

To obtain the general picture of the connection between the applied field, local

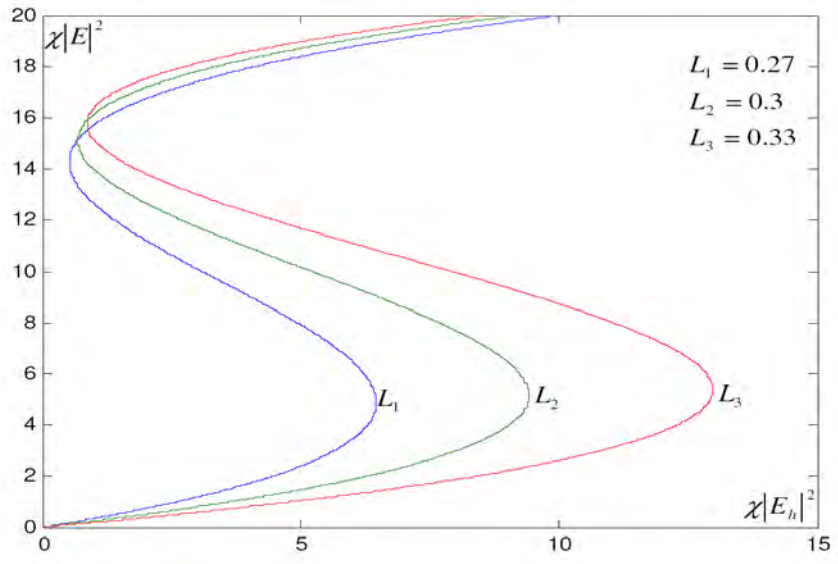

Figure 3.4: Local field $\chi|E|^2$ versus applied field $\chi|E_h|^2$ at frequency $z = 0.2$ for different L; the rest parameters as in Fig.3.1.

field, and the frequency we decided to present 3D graph involving these quantities. The $3D$ graph depicted in Fig.3.3 is obtained with the help of 3.3.1 and shows such a graph in the most interesting range of these parameters when three different values of the local field correspond to one value of the applied field.

While analyzing the bistability phenomena in the system, it is more convenient to consider a dependence of the local field on the applied field. Figure 3.3 shows such dependencies obtained with the help of 3.3.1 at $z = 0.2$ for different depolarization factors. One can see that the bistability region (three different values of $\chi\,|E|^2$ for one value of $\chi\,|E_h|^2$) broads with increase with the depolarization factor L. Unfortunately Fig.3.3 is obtained for a fixed frequency of the incident electromagnetic wave. The bistability domain in the plane $\left(z, \chi\left|\vec{E}_h\right|^2\right)$ can be specified from an analysis of roots

of the cubic equation 3.3.1.

There are two ways of finding the root location of a cubic equation, which are described in Appendices A and B. From the analysis the roots of 3.3.1 one can find the IOB domain in the plane of $\left(z, \chi \left|\vec{E}_h\right|^2\right)$.

The equation 3.3.1 has three real positive roots provided the conditions (.0.7) of Appendix A are satisfied. In the case under consideration, these conditions may be written in the form

$$\begin{aligned} &a \leq -\sqrt{3b}, a < 0, \\ &-\frac{2}{9}\left[DX_2 + \frac{ab}{2}\right] < Y < -\frac{2}{9}\left[DX_1 + \frac{ab}{2}\right], \end{aligned} \tag{3.3.3}$$

where

$$X_{1,2} = \frac{-a \mp \sqrt{D}}{3}, \quad D = a^2 - 3b, \tag{3.3.4}$$

where $X_{1,2}$ are the position of extremum points of the function presented by the left hand side of 3.3.4. They are determined from the equation $3X^2 + 2aX + b = 0$. It is easy to show that

$$D = \frac{[(\tilde{\varepsilon}'\chi' + \tilde{\varepsilon}''\chi'')^2 - 3(\tilde{\varepsilon}''\chi' + \tilde{\varepsilon}'\chi'')^2]}{|\chi|^2}. \tag{3.3.5}$$

It follows from 3.3.3 and 3.3.4 that IOB emerges if $\tilde{\varepsilon}'' > 0$, $\chi'' > 0$, and quantities χ' and $\tilde{\varepsilon}'$ have different signs. Below, we carry out a detailed analysis of the case $\tilde{\varepsilon}' < 0,\ \chi' > 0$.

In the case $x_1 = x_2$ it is possible to find the IOB frequency domain analytically. The general case requires numerical calculations [80].

Let us consider the non-absorbing host medium ($\varepsilon_h'' = 0$) containing the metal inclusion with the non-absorbing nonlinear part of the dielectric function ($\chi'' = 0$,

and $\chi' > 0$). In this case, equation 3.3.1 takes the form

$$X^3 + 2\tilde{\varepsilon}' X^2 + |\tilde{\varepsilon}|^2 X = Y, \tag{3.3.6}$$

where

$$\tilde{\varepsilon}'(z) = \frac{1}{z_s^2} - \frac{1}{z^2+\gamma^2}, \tag{3.3.7}$$

$$\tilde{\varepsilon}''(z) = \varepsilon''_\infty(z) + \frac{\gamma}{z(z^2+\gamma^2)}. \tag{3.3.8}$$

The dimensionless frequencies z, z_s, γ were specified in 3.3.7. From the first inequality 3.3.3 follows that IOB exists at frequencies z that satisfy the inequality

$$z^3\beta - z(z_s^2 - \gamma^2\beta) + \sqrt{3}z_s^2\gamma \leqslant 0, \tag{3.3.9}$$

where $\beta = (1+\sqrt{3}z_s^2\varepsilon''_\infty) > 0$. To solve inequality 3.3.9 we consider the cubic equation

$$z^3\beta - z(z_s^2 - \gamma^2\beta) + \sqrt{3}z_s^2\gamma = 0. \tag{3.3.10}$$

This equation at $z_s^2 - \gamma^2\beta > 0$, has two positive roots (z_2, z_3) and one negative root, provided that its discriminant Q is negative and the coefficients of this equation are positive and close to the surface plasmon frequency $z^2 \lesssim z_s^2 - \gamma^2$ (see Appendix B). The boundary frequencies of the IOB domain may be found from the cubic equation 3.3.10. Differentiating the function, which is the left hand side of 3.3.10 with respect to z, we find the extremum points $\pm\sqrt{(z_s^2 - \gamma^2\beta)/(3\beta)}$. Substituting them into 3.3.10, we obtain the following inequality

$$-(z_s^2 - \gamma^2\beta)^3 + \frac{81}{4}z_s^4\gamma^2 \leqslant 0. \tag{3.3.11}$$

According to Appendix A, at points z_2 and z_3, $a^2 - 3b = 0$ $a = 2\tilde{\varepsilon}'$, $b = |\tilde{\varepsilon}|^2$). The critical magnitudes of the electric fields at these points are (.0.9)of Appendix A

$$\begin{aligned} (x_c)_{2,3} &= -\frac{2}{3}\left(\frac{1}{z_s^2} - \frac{1}{z_{2,3}^2+\gamma^2}\right), \\ (y_c)_{2,3} &= (x_c)_{2,3}^3. \end{aligned} \tag{3.3.12}$$

At $Q = 0$, $z_1 = z_2 = z_c$, the critical magnitude of the field y_c, according to 3.3.12, coincides with a minimum value of the external electric field when bistability emerges in the system. Therefore, in the case under consideration, the IOB in the system emerges in the frequency band

$$z_2 \leqslant z \leqslant z_3. \tag{3.3.13}$$

The range of the applied fields is again specified by the second inequality 3.3.3. Roots $z_2 > 0$, $z_3 > 0$ may be found from 3.3.11, which has three real roots. Inequality 3.3.11 at fixed β and z_s, and at $\dfrac{\gamma^2\beta}{z_s^2} \ll 1$ allows one to obtain the critical γ_c

$$\gamma_c = \frac{2}{9} z_s \left(1 - \frac{4}{81}\beta\right)^{3/2}. \tag{3.3.14}$$

If the collision frequency $\gamma > \gamma_c$, then the IOB disappears. We may suggest that any increase in the damping existing in the inclusion makes the conditions of the IOB emergence more restrictive. A minimum critical value of the external electric field for the IOB onset may be found from 3.3.12. It is given by the relation

$$|\chi| \cdot \left|\vec{E}_h\right|_c^2 = \left(\frac{L}{\varepsilon_h}\right)^2 \cdot \left(\frac{1}{z_3^2 + \gamma^2} - \frac{1}{z_s^2}\right)^3 \tag{3.3.15}$$

where z_3 is the larger of roots z_2 and z_3 of equation 3.3.10. If ε''_∞ and γ tend to zero, the critical electric field tends to zero as well.

The curves $f_{1,2}$ restricting the IOB domain in the plane $\left(z, \chi\left|\vec{E}_h\right|^2\right)$ can be obtained from the equations

$$f_i = -(2/9)[Dx_i + ab/2](L/\varepsilon_h)^2, \quad i = 1, 2. \tag{3.3.16}$$

Figure 3.5 depicts the IOB domain (shaded area) in the plane $\left(z, \chi\left|\vec{E}_h\right|^2\right)$ for the ellipsoidal silver particle. The boarders of the IOB domain (curves f_1 and f_2) have been calculated with the help of formula 3.3.16.

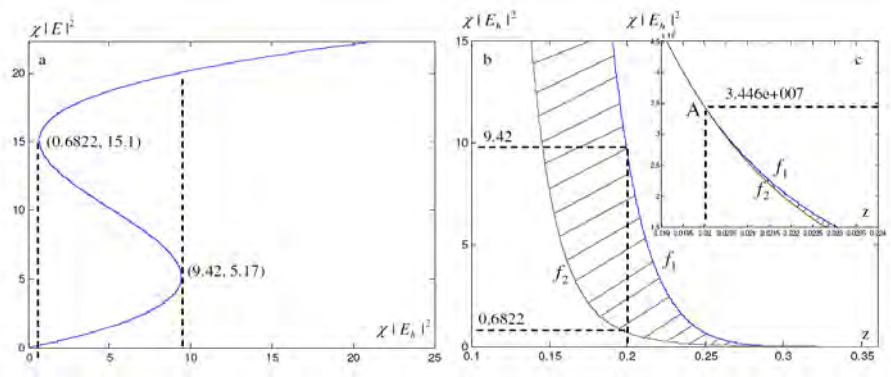

Figure 3.5: The ellipsoidal silver particle with the parameters $L = 0.3$, $\varepsilon'_h = 2.25$, $\varepsilon''_h = 0$, $\varepsilon'_\infty = 4.5$, $\varepsilon''_\infty = 0.16$, $\gamma = 1.15 \times 10^{-2}$ (a) The IOB for local field $\chi\,|E|^2$ versus applied field $\chi\,|E_h|^2$ at frequency $z = 0.2$. The IOB domain in the plane $(z,\ \chi|E_h|^2)$ (shaded area). (b)High frequency limit part of the IOB domain. (c) Low frequency limit part of the IOB domain

.

Below we present the IOB domain for the curve $L_2 = 0.3$. It corresponds to the lowest applied and local fields comparing to the bistability domains for the curves $L_1 = 0.27$ and $L_3 = 0.33$. The bistability domains for the polarization factors corresponding to L_1 and L_3 have the same style as depicted in Fig.3.5. But the bistability domain for L_1 is narrower and for L_3 is wider than for L_2 in accordance with the range of the applied fields.

The limiting values of the amplitudes of incident electric field are shown in Figure 3.5 by a dashed line at $\omega = 0.2\omega_p$. Fig.3.5b shows the bistability domain near a point z_2 (the smaller root of equation 3.3.10). The entire bistability domain looks like an area enclosed by a hysteresis-type curve. Its upper gets narrowing with increasing in the external field.

We would like to note the upper end of the bistability domain in Fig.3.5(c) point

A corresponds to $z = 0.02$, $\gamma = 0.0115$, and considerably high applied fields. We also have calculated $\chi|E|^2$ versus $\chi|E_h|^2$ for different γ with the same rest parameters as in Fig.3.3 The results show that the IOB practically disappears at $\gamma > 3 \times 0.0115$.

3.4 Bistability in Coated Spherical Particles with Large Dielectric Core

We now consider a spherical dielectric particle (the core) of a radius r_1 covered by a metal shell of radius r_2. Let the core be a nonlinear dielectric of the Kerr type with nonlinear DF

$$\varepsilon_1 = \varepsilon_{10} + \chi \left|\vec{E}\right|^2, \tag{3.4.1}$$

where ε_{10} is the linear part of DF, χ is the nonlinear Kerr coefficient that in a general case depends on the frequency of the electromagnetic field and $\vec{E}$ is the amplitude of the local field in the core. The dielectric function of the metal shell is of the Drude type[79]

$$\varepsilon_2 = \varepsilon_\infty - \frac{1}{z(z + i\gamma)}, \tag{3.4.2}$$

where z and γ are given by 3.2.10. In the long wavelength limit (the electrostatic approximation), the electric field within the inclusion or the local field may be found from the relation 3.4.1 with the enhancement factor F given by the following expression

$$\begin{aligned} F &= \frac{3}{2p} \cdot \frac{\varepsilon_2 \varepsilon_h}{\Delta}, \\ \Delta &= \varepsilon_2^2 + [(3/2p - 1)\varepsilon_1 + (3/p - 1)\varepsilon_h]\varepsilon_2 + \varepsilon_1 \varepsilon_h. \end{aligned} \tag{3.4.3}$$

Here, $p = 1 - r_1^3/r_2^3$ is the metal fraction in the inclusion particle. One can easily see that 3.4.3 for a completely metallic particle ($p = 1$) gives the same enhancement

factor as 3.2.6 for a spherical metallic particle ($L = 1/3$).

A considerable increase in the local electric field can be obtained if the denominator of 3.4.3 tends to a minimum. This condition can be realized by tuning the parameters that comprise Δ.

In the limit $\gamma \ll 1$ (the collision frequency of electrons is small compared to the plasma frequency)the imaginary part of 3.4.2 can be neglected and the "resonance" condition ($\Delta = 0$) reduces to a quadratic equation in ε_2 with the following roots

$$\begin{aligned} &\varepsilon_{2\pm} = (-s \pm \sqrt{s^2 - 4\varepsilon_1\varepsilon_h})/2, \\ &s = (3/2p - 1)\varepsilon_1 + (3/p - 1)\varepsilon_h. \end{aligned} \tag{3.4.4}$$

In the case under consideration $s < 0$ and $\varepsilon_{2\pm} < 0$. Moreover, $\varepsilon_{2-} < \varepsilon_{2+}$. In the limiting case of a small metal fraction, $p \ll 1$, expressions 3.4.4 may be simplified

$$\begin{aligned} &\varepsilon_{2-} = -\frac{3(\varepsilon_1 + 2\varepsilon_h)}{2p}, \quad \varepsilon_{2+} = -\frac{2\varepsilon_1\varepsilon_h}{3(\varepsilon_1 + 2\varepsilon_h)}p, \\ &p \ll 1. \end{aligned} \tag{3.4.5}$$

Since $\varepsilon_{2\pm} < 0$, realization of the local field enhancement requires $Re\varepsilon_2(\omega) < 0$ as well. One can see from 3.4.2 that it takes place at frequencies $\omega < \omega_0 = \omega_p/\sqrt{\varepsilon_\infty}$ (we assumed that $\omega_0 \gg \nu$). The frequency ω_0 corresponds to the bulk plasmon frequency. It also follows from 3.4.1, 3.4.3, and 3.4.4 that maximum enhancement of the local field occurs when the frequency of electromagnetic wave approaches

$$\omega_{s\pm} = \frac{\omega_p}{\sqrt{\varepsilon_\infty - \varepsilon_{2\pm}}}. \tag{3.4.6}$$

For example, at $p \ll 1$, when the metal fraction of inclusion is comparatively small, $\omega_{s-} \to 0$, $\omega_{s+} \to \omega_0$. We would like to note that the polarizability of a two-layer spherical inclusion may be presented in the following form [81]

$$\alpha = 4\pi r_2^3 \frac{\bar{\varepsilon} - \varepsilon_h}{\bar{\varepsilon} + 2\varepsilon_h}, \tag{3.4.7}$$

where $\bar{\varepsilon}$ is the effective dielectric function of the individual two-layer inclusion in the dipole approximation given by the relation

$$\bar{\varepsilon} = \varepsilon_2 \frac{\varepsilon_1(3/p-2)+2\varepsilon_2}{\varepsilon_1+\varepsilon_2(3/p-1)}. \tag{3.4.8}$$

Combining 3.4.7 and 3.4.8 one can easily show that the enhancement factor 3.4.3 and the polarizability coefficient 3.4.7 have the same denominator Δ 3.4.3. This means that α considerably increases when the frequency ω approaches one of the frequencies 3.4.6. At the same time, the absorption of radiation by the particle increases due to an increase in the polarization.

The considerable local field enhancement within the coated spherical particle requires that the nonlinear term in 3.4.1 must be taken into account. The enhancement factor F 3.4.3 depends on the local field $\vec{E}$. Acting in the same manner as in section 3 while obtaining 3.3.10, we obtain the cubic equation for computation of the "local field" $|\chi||\vec{E}|^2$ in the particle

$$\begin{aligned}
&X^3 + a_1 X^2 + b_1 X = \eta Y, \\
&a_1 = 2Re\left(\frac{\Delta_0}{\delta}\right), b_1 = \left|\frac{\Delta_0}{\delta}\right|^2, \\
&\Delta_0 = (\varepsilon_2)^2 + \varepsilon_2\left[\varepsilon_{10}\left(\frac{3}{2p}-1\right)+\left(\frac{3}{p}-1\right)\varepsilon_h\right] + \varepsilon_{10}\varepsilon_h, \\
&\eta = \frac{9}{p^2}\left|\frac{\varepsilon_2\varepsilon_h}{\delta}\right|^2, \delta = \varepsilon_h + \frac{\varepsilon_2}{2p}(3-2p).
\end{aligned} \tag{3.4.9}$$

Here Δ_0 is obtained from 3.4.3 by substitution $\varepsilon_1 \to \varepsilon_{10}$.

We consider the range of parameters where this cubic equation has real coefficients and has three real positive (Appendixes A and B) . The domain of IOB can be specified in the same manner as it was done in the previous section.

Here we briefly discuss the results obtained. The IOB in the coated spherical particle emerges at the following conditions (in notations 3.4.9):

$$\begin{aligned} &a_1 \le -\sqrt{3b_1}, \quad a_1 < 0 \\ &-\frac{2}{9}\left[D_1 X_2 + \frac{a_1 b_1}{2}\right] < Y < -\frac{2}{9}\left[D_1 X_1 + \frac{a_1 b_1}{2}\right]. \end{aligned} \tag{3.4.10}$$

The boarders of the IOB domain are specified by the curves

$$\begin{aligned} &f(X_i) = -\frac{2}{9\eta}\left[D_1 X_i + \frac{a_1 b_1}{2}\right], i = 1, 2, \\ &X_{1,2} \text{ are the extremum points of ,} \\ &f(X) = X^3 + a_1 X^2 + b_1 X, \\ &D_1 = a_1^2 - 3b_1. \end{aligned} \tag{3.4.11}$$

Since in our case $\varepsilon_{10} > 0$ and $\varepsilon_h > 0$, there is no IOB in the frequency range where $Re\varepsilon_2(\omega) > 0$. The second inequality of 3.4.10 determines the range of the applied field where the IOB can appear.

Now we return to the simplified version of our theory when the imaginary parts of ε_1 and ε_2 can be ignored. In this case, the first condition of the IOB emergence reduces to

$$\Delta_0 \delta < 0. \tag{3.4.12}$$

This inequality may be presented in the following form

$$(\omega - \omega_{S-}^{(0)})(\omega - \omega_{S+}^{(0)})(\omega - \omega_{S1}) < 0, \tag{3.4.13}$$

where the frequencies $\omega_S^{(0)}$ are given by 3.4.6 with ε_1 substituted by ε_{10}

$$\omega_{S1} = \frac{\omega_p}{\sqrt{\varepsilon_\infty - \varepsilon_0}}, \quad \varepsilon_0 = \frac{2p}{3 - 2p}. \tag{3.4.14}$$

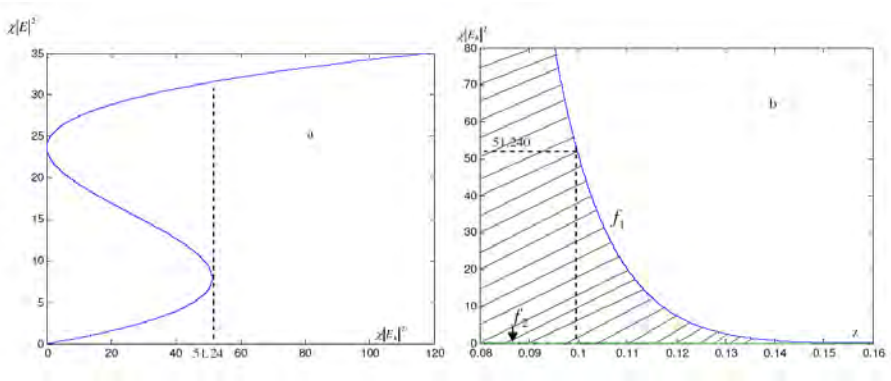

Figure 3.6: IOB in the coated spherical particle: $\varepsilon_{10} = 6.00$,$\varepsilon_\infty = 4.5$, $\varepsilon_h = 2.25$,$p = 0.4$,$\gamma = 0$; a) The local field $\chi |E|^2$ versus the applied field $\chi |E_h|^2$ at $z = 0.1$ b) IOB domain (shaded area) in the plane $(z,\ \chi |E_h|^2)$. The curves f_1 and $f_2 = 0$ are calculated with the help of 3.4.10.

It is clear that $\omega_{S-}^{(0)} < \omega_{S+}^{(0)} < \omega_{S1}^{(0)}$. In addition, in this case

$$\begin{aligned} x_1 &= -\frac{\Delta_0}{\delta}, \qquad & x_2 &= -\frac{3\Delta_0}{\delta}, \\ f(x_1) &= -\frac{4}{27}\left(\frac{\Delta_0}{\delta}\right)^3, \quad & f(x_2) &= 0. \end{aligned} \tag{3.4.15}$$

Summing up these results, we can claim that the IOB emerges in the two-layer spherical particle with a Kerr type nonlinear dielectric core 3.4.1 covered with a metal shell with no decay (the Drude type dielectric function 3.4.2 with zero imaginary part) in the following two frequency bands:

$$0 < \omega < \omega_{S-}^{(0)} \quad \text{and} \quad \omega_{S+}^{(0)} < \omega < \omega_{S1}^{(0)} \tag{3.4.16}$$

IOB does not exist if the external field exceeds the critical value

$$E_c = \frac{4p\varepsilon_h}{27\,|\varepsilon_2|}\sqrt{\frac{|\Delta_0|^3}{3\,\chi\,\delta.}} \tag{3.4.17}$$

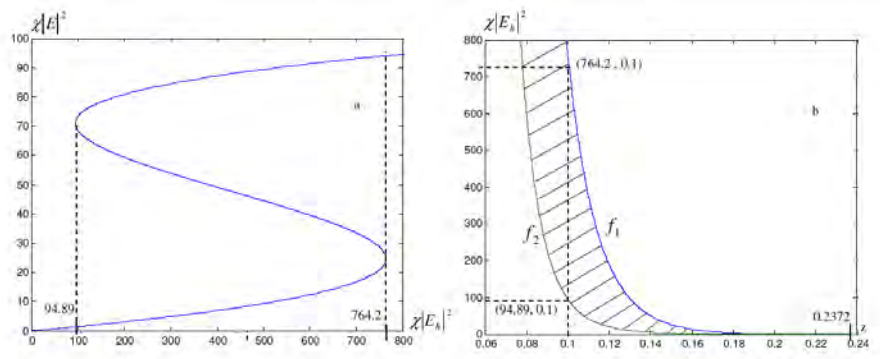

Figure 3.7: IOB in a spherical particle with a silver cover: $\varepsilon_{10} = 6.00$,$\varepsilon_\infty = 4.5$, $\varepsilon_h = 2.25$,$p = 0.7$,$\gamma = 0.0115$; a) The local field $\chi\,|E|^2$ versus the applied field $\chi\,|E_h|^2$ at $z = 0.1$ b) the IOB domain (shaded area) in the plane (z, $\chi\,|E_h|^2$).

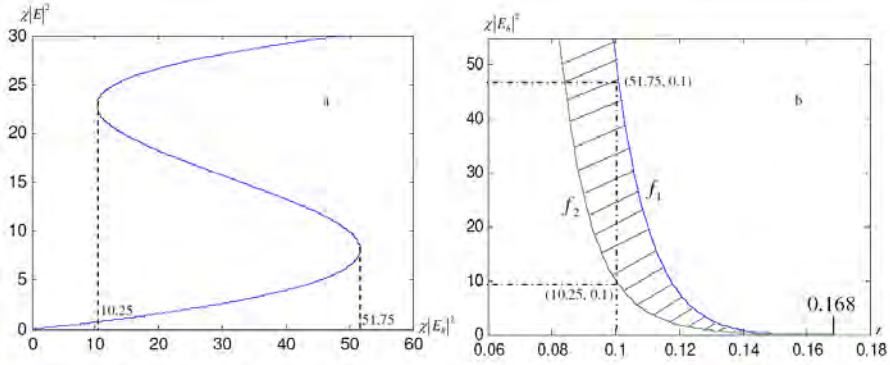

Figure 3.8: IOB in a spherical particle with a silver cover: $\varepsilon_{10} = 6.00$,$\varepsilon_\infty = 4.5$, $\varepsilon_h = 2.25$,$p = 0.4$,$\gamma = 0.0115$ a) The local field $\chi\,|E|^2$ versus the applied field $\chi\,|E_h|^2$ at $z = 0.1$ b) the IOB domain (shaded area) in the plane (z, $\chi\,|E_h|^2$) .

We illustrate typical dependencies of the local field on the applied field (Fig.3.7a and Fig. 3.8a) that are obtained from the solution of the cubic equation 3.4.9 and the IOB domains (Fig.3.7b and Fig. 3.8b) from the bistability conditions (relation 3.4.10). We have calculated the IOB domains for different p in the range $1 - 0.25$ at $\gamma = 0.0115$. The results show that the IOB domain decreases with decreasing the metallic fraction.

3.5 Conclusion

This Chapter presents the theoretical and numerical study of the optically induced bistability (IOB) in metal and metal covered nanoparticles in the electrostatic approximation. We focus on the possible analytic treatment based on the analysis of the roots of a cubic equation of the local field in the nanoparticles that considerably reduce the numerical calculations. The calculations have been carried out in the dimensionless frequencies normalized by the the plasma frequency ω_p of the metal (silver) cover. The the local field inside the particles E as a function of the applied field E_h, frequency and other parameters was calculated by introducing $\chi^{(3)}|E|^2$ and $\chi^{(3)}|E_h|^2$ including the third order nonlinear optical susceptibility $\chi^{(3)}$. It allows one to use the graphs presented in the paper for evaluation the parameters of the IOB domain for the particular systems with the help of the corresponding ω_p, $\chi^{(3)}$, and the dielectric permittivity of the host matrix ε_h.

The entire domain of the IOB has not been studied in the literature according to our best knowledge. The paper presents a such study for ellipsoidal metal particles. In the intensity-frequency plane of the incident electromagnetic wave this domain is the area restricted by a hysteresis-like curve. The upper part of the domain area

becomes narrower with an increase the amplitude of the electromagnetic wave and corresponds rather high fields.

The study of the electrodynamic properties of small spherical particles with a nonlinear dielectric and covered by the metal shell shows that the IOB in this type of inclusion may emerge in two-frequency bands. The metal covering of the nonlinear dielectric makes it easier for an enhancement of the local field to the required level for the IOB emergence. The IOB is very critical to all decaying mechanisms. In particular, if γ increases three times the IOB completely disappears in the elliptical metal particles.

Finally, one more interesting fact is worth noting. We considered the local fields by solving the corresponding equations for systems different from those onces considered in this paper. In particular, a two-layer plane structure of metal and nonlinear dielectric, a sphere with nonlinear dielectric in a metal host matrix, and a two-layer ellipsoid with a nonlinear dielectric and a metal covering if the external electric field is parallel to one of its axes. In the case of two-layer ellipsoid at arbitrary orientation of the external electric field, the order of this equation becomes higher. Change in the order of equations may produces more complex pictures of the IOB in these systems.

In the next Chapter, we present the two optical bistability domain in metal/ dielectric composite in large metal fraction.

Chapter 4

Two Optical Bistability Domains in Metal/ Dielectric Composites

4.1 Introduction

Optical induced bistability (OIB) is still of great interest since its theoretical discovery and experimental realization [29, 44, 80], because of its numerous possible applications. The most attractive systems for a study of the OIB are composites consisting of metal covered dielectric particles with nonlinear dielectric functions embedded in a linear host matrix [67, 68]. The point is that OIB is based on the nonlinear properties of the dielectric function of inclusions. The amplitude of the electric field of the incident intensive radiation is enhanced in the inclusion (local field) on the frequency close to the surface plasmon frequency of the metal. This enhancement makes the nonlinear part of the dielectric function (DF) of the core significant.

Usually, OIB is demonstrated with the help of $S-$like curves in the plane "applied field - local field (in an inclusion)" [19], [67], [68]. They show that three values of the local field correspond to one value of the applied field which implies the system to be unstable. These curves allow one to specify the onset and offset values of the applied

fields of OIB at a particular frequency of the incident radiation.

In this thesis, we show that the enhancement factor of the local field of metal nanoinclusion with a dielectric core has two maxima at different frequencies. The second maximum is important at comparatively high metal fractions. The composite with these inclusions has two bistability domains in different frequency range. In our previous paper [82], we proposed the analytic formulas specifying OIB domain in the plane of "frequency of the incident radiation - modulus squared of the amplitude of incident radiation". This method can be considered as a complementary to the above mentioned method of $S-$like curves. With the help of this method, we study domains of bistability in the composite of spherical metal inclusions with "small" nonlinear dielectric core. The plasma resonant frequency for the optical induced bistability (OIB) occur with the same values of the plasma resonance frequency for the formation of the enhancement of the local field. We are interested to focus on the second bistability domain. With increment in the metal fraction, the two bistability domains merge into one with comparatively resulting low onset fields.

4.2 Resonant Frequencies and Enhancement Factor of Local Field in Metal Covered Spherical Inclusion

We present the calculation for the enhancement factor for the local field and the polarizebility of the spherical particle with the help of the distribution of the potential. The potential distribution in a spherical metal nanoparticle with a dielectric core embedded in a dielectric matrix in an external constant electric field can be obtained

from 2.2.1 setting $d = 3$

$$\begin{aligned} \Phi_1 &= -E_h A r cos\theta, r \leq r_1, \\ \Phi_2 &= -E_h (Br - C/r^2) cos\theta, r_1 \leq r \leq r_2, \\ \Phi_h &= -E_h (r - D/r^2) cos\theta, r \geq r_2. \end{aligned} \tag{4.2.1}$$

Here Φ_1, Φ_2, and Φ_h are potentials in the dielectric core, metal, and the host matrix, respectively, E_h is the applied field, r and θ are the spherical coordinates of the observation point (the $z-$ axis is chosen along the vector $\mathbf{E}_h$), r_1, r_2 are radiuses of the dielectric core and the metal shell, respectively.

From the continuity conditions of the potential and the displacement vector at the boundaries dielectric core-metal and metal-host matrix, we obtain a system of linear algebraic equations for A, B, C, D 2.2.1. The solution of this system can be presented as

$$A = \frac{9\varepsilon_2 \varepsilon_h}{2p\Delta}, \tag{4.2.2}$$

$$B = \frac{3\varepsilon_h(\varepsilon_1 + 2\varepsilon_2)}{2p\Delta}, \tag{4.2.3}$$

$$C = \frac{3\varepsilon_h(\varepsilon_1 - \varepsilon_2)}{2p\Delta} r_1^3, \tag{4.2.4}$$

$$D = \{1 - \frac{3\varepsilon_h[(3-p)\varepsilon_2 + p\varepsilon_1]}{2p\Delta}\} r_2^3 \tag{4.2.5}$$

where

$$\Delta = \varepsilon_2^2 + q\varepsilon_2 + \varepsilon_1 \varepsilon_h. \tag{4.2.6}$$

Here $q = (3/2p - 1)\varepsilon_1 + (3/p - 1)\varepsilon_h$, $p = 1 - (r_1/r_2)^3$ is a metal fraction in the inclusion, $\varepsilon_1, \varepsilon_2$, and ε_h are the dielectric functions (DFs) of the core, metal shell, and the host matrix, respectively. We note that equation 4.2.1 describe the electric field of the electromagnetic wave in the electrostatic approximation when the wave length of the incident radiation is much larger than a typical size of the inclusion [69].

In particular,equation4.2.2 for the enhancement of the local field and equation 4.2.5 coincides with the polarizability of a coated sphere, which follows from the general expression of a coated ellipsoid [69].

The dielectric function for a metal in the inclusion is given to be in the Drude form 2.2.9. The dielectric function in the core of the metal and the dielectric function for the host taken to be linear for the sake of simplicity.

$$\varepsilon_1 = \varepsilon_{10} + \chi|\mathbf{E}|^2, \tag{4.2.7}$$

where ε_{10} is the linear part of DF, χ is the nonlinear Kerr coefficient, and $\mathbf{E}$ is the local field in the core.

The enhancement factor of the local field in the inclusion for the weak incident fields $\chi|\mathbf{E}|^2 << \varepsilon_{10}$, the local field is presented as in the form of equation 3.2.6 $\mathbf{E} = A\mathbf{E}_h$. In this relation A is given by 4.2.2 which is a complex quantity. Further, it would be convenient to consider with $|A|^2$, which represent a real quantity. We call $|A|^2$ the enhancement factor and express it as

$$|A|^2 = \frac{81\varepsilon_h^2}{4p^2} \frac{\varepsilon_2'^2 + \varepsilon_2''^2}{[\varepsilon_2'^2 - \varepsilon_2''^2 + q\varepsilon_2' + \varepsilon_1\varepsilon_h]^2 + \varepsilon_2''^2(q + 2\varepsilon_2')^2}. \tag{4.2.8}$$

Here ε_2' and ε_2'' are the real and imaginary part of ε_2 2.2.9, respectively. For the sake of simplicity, we ignore the imaginary parts of ε_1 and ε_h.

We considering the ideal case when the decay of plasma vibration is extremely small ($\gamma <<< 1$). In this case, the second term in the denominator of 4.2.8 proportional to $\varepsilon_2''^2 \sim \gamma^2$ is negligible. The maximum of $|A|^2$ is reached when the first term in the denominator of 4.2.8 is zero. This condition gives a quadratic equation with respect to ε_2', which has two roots with two different resonant frequencies. For not very small γ and arbitrary p, the situation can be traced only numerically.

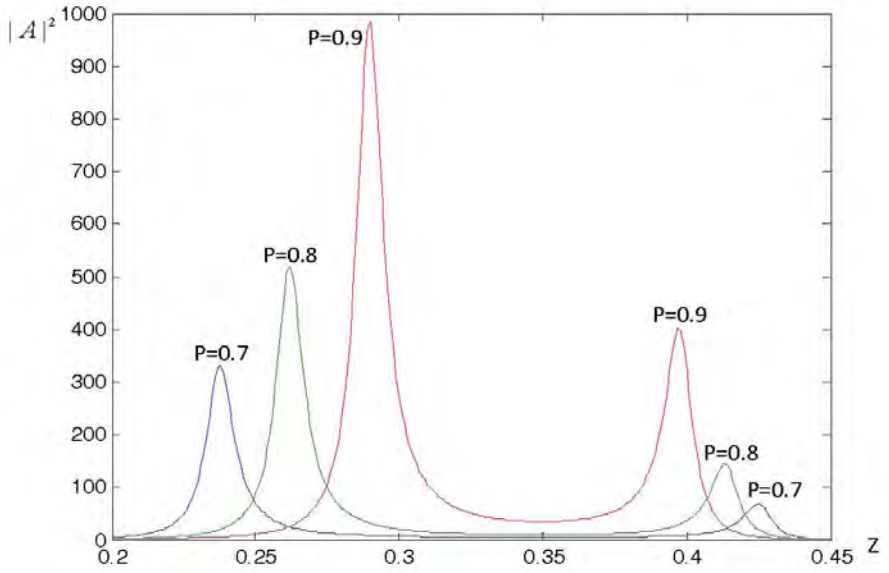

Figure 4.1: Enhancement factor $|A|^2$ versus z of metal inclusion with dielectric core at different p; $\varepsilon_\infty = 4.5$, $\varepsilon_1 = 6$, $\varepsilon_h = 2.25$; $\omega_p = 1.46 \times 10^{16}$ (frequency of the silver surface plasmons), $\nu = 1.68 \times 10^{14}, \gamma = 1.15 \times 10^{-2}$.

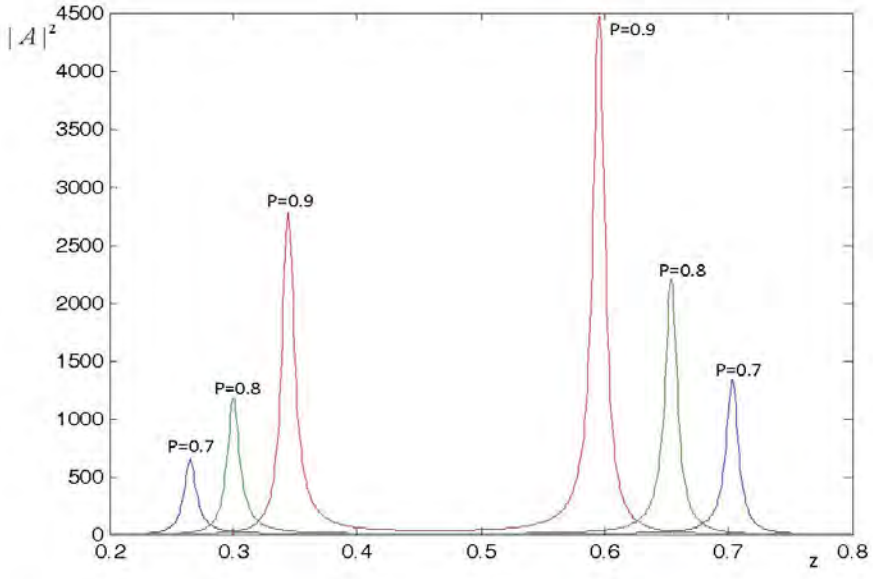

Figure 4.2: Enhancement factor $|A|^2$ versus z of metal inclusion with dielectric core at different p with $\varepsilon_\infty = 1$. Rest of the parameters are the same as in Fig. 4.1.

Figure 4.1 shows $|A|^2$ versus z for different p. These curves are obtained with the help of 4.2.8 neglecting the nonlinear term in ε_1 given by 4.2.7. The numerical values of the DFs of the composite are taken from [82].

The most interesting feature of these graphs is the appearance of two peaks of the enhancement factor at two different frequencies. The positions and values of these maxima strongly depend on p (for fixed other parameters). For example, for $p < 0.4$, the second maximum is lower then the first one and very small. May be because of this the second maximum of $|A|^2$ was not specified earlier chapter devoted to the study of OIB in coated particles [68, 67, 82]. For $p > 0.4$, it becomes more important and with further increase in p, both maxima become higher and move closer to each other.

It is necessary to note that p should not be very close to unity, so that ε_1 should be physical meaningful. However, "closeness" of p to unity does not mean that the radius of dielectric core r_1 is close to 0. The point is that r_1 is related to a radius of the inclusion r_2 as

$$r_1/r_2 = (1-p)^{1/3}. \tag{4.2.9}$$

For example, for inclusions with $p = 0.9$ it gives $r_1 = 0.46r_2$ and even for $p = 0.999$, we get $r_1 = 0.1r_2$.

One more parameter that strongly affects the enhancement factor is ε_∞. For example, using $\varepsilon_\infty = 1$ [70] with identical other dielectric constants, we obtain the second maximum of $|A|^2$ to be larger than the first one. At the same time, the width of the maxima get narrower and the corresponding resonant frequencies show the blue shift. It is illustrated in Fig.4.2.

We emphasize that the second maximum in $|A|^2$ becomes important in inclusions

with "large" fraction of metal that exceeds the fraction of the dielectric. In this chapter, we are exploring the OIB in composites of metal inclusions with small dielectric cores which has not been done before. It is worth noting that appearance of two maxima in the enhancement factor of covered inclusions requires special conditions. It can be shown with the help of 4.2.8 that the metal inclusions covered by the dielectric, used in [52], have only one resonant frequency and one maximum of the enhancement factor.

4.3 Two Bistability Domains in Composite with Metal Inclusions with Nonlinear Dielectric Core

Considering the contribution of the nonlinear part ε_1 and the polarization inclusions in the Clausius-Mossotti approximation, we obtain the equation specifying the local field. Following [1], the average Lorentz local field in the dielectric core of the inclusion $\mathbf{E}_L$ is given by

$$\mathbf{E}_L = \mathbf{E}_h + \frac{4\pi}{3}\mathbf{P}, \tag{4.3.1}$$

where the polarization of the system is $\mathbf{P} = nD_d\mathbf{E}_L$ (n being a density number of the inclusions). As it was mentioned above, the polarizability of the inclusion is given by 4.2.5. Introducing the volume fraction of inclusions in the composite $f = \frac{4\pi}{3}nr_2^3$, using equations 4.2.2, 4.3.1, and for the local field $\mathbf{E} = A_d\mathbf{E}_L$we get

$$\mathbf{E} = \frac{9\varepsilon_2\varepsilon_h}{2p\Delta(1 - fD/r_2^3)}\mathbf{E}_h. \tag{4.3.2}$$

From 4.3.2, we obtain the cubic equation for the square modulus of the local field $X = \chi|\mathbf{E}|^2$ in the form

$$X^3 + a_1X^2 + b_1X = \eta Y, \tag{4.3.3}$$

where

$$\begin{aligned} a_1 &= 2Re\frac{\Delta_0+\alpha\beta}{\delta+\alpha}, \\ b_1 &= |\frac{\Delta_0+\alpha}{\delta+\alpha}|^2, \\ Y &= \chi|\mathbf{E}_h|^2, \\ \eta &= \frac{81\varepsilon_h^2|\varepsilon_2|^2}{4p^2|\delta+\alpha|^2(1-f)^2}, \end{aligned} \tag{4.3.4}$$

with $\Delta_0 = \varepsilon_2^2 + q\varepsilon_2 + \varepsilon_{10}\varepsilon_h$, $\alpha = 3f\epsilon_h/[2(1-f)]$, $\beta = (3/p-1)\varepsilon_2 + \epsilon_{10}$, and $\delta = \varepsilon_2(3/2p-1)+\varepsilon_h$. The quantity X depends on the applied field $\mathbf{E}_h$ and the parameters of the composite. Equations 4.3.3 differ from 3.3.1 by their coefficient.

If the cubic equation 4.3.3 has one real positive root, the local field in the nanoparticle is a single-valued function of the applied field. If it has three real positive roots, the local field is not a single-valued function of the applied field and the system becomes unstable. This is what we called optical induced bistability (OIB)[29]. OIB is usually illustrated in the $Y-X$ plane and connected with S-like curves showing that three different values of the local field correspond to one value of the applied field [68, 1]. Below, we use the method developed in [82], which allows one to study the shape and the parameters of the bistability domain in the $z-Y$ plane. This domain is restricted by the curves

$$f_i(z) = -\frac{2}{9\eta}\left[DX_i + \frac{a_1 b_1}{2}\right], i = 1, 2, \tag{4.3.5}$$

where $X_{1,2} = (-a \mp \sqrt{D})/3$ are the extremum points of the function ηY, $D = a_1^2 - 3b_1$ with a_1, b_1, and η given by 4.3.4. The curve $f_2(z)$ presents a set of maxima of ηY and the curve $f_1(z)$ presents a set minima of ηY in the $z-Y$ plane. We note that the curves $\eta Y(X)$ are the $N-$type unlike the $S-$type curves $X(Y)$. If positions of maxima and minima coincide, the curves $f_{1,2}$ merge and there is no bistability at all.

The curves enveloping the bistability domain allow one to obtain the same information as that from $S-$ type curves, particularly, the onset and offset bistability

fields at a particular frequency. This method can be considered as complementary to the $S-$curves method.

We have shown that the local field in the metal inclusions with the "small" nonlinear dielectric core has two maxima. This allows one to hope that the composites consisting such inclusions have two OIB domains in the frequency ranges, where the local field has maxima. Below, we show that there are two domains of OIB in the composites consisting of inclusions with small nonlinear dielectric cores. We call them the first and second optical induced bistability, OIB1 and OIB2 respectively. In the next subsection we consider the main features of OIB1.

4.3.1 First Domain of OIB

The OIB1 in metal covered inclusions have been studied in many papers [68]-[1], [83], [20]. Here, we consider the OIB1 domain in the $z - Y$ plane. Figure 4.3 shows this domain for the composite $p = 0.9, f = 0.03$ and other parameters taken the same as before. It can be seen that the domain of this bistability ends at $z \simeq 0.27$. With decrease in frequency, the OIB1 requires higher and higher applied fields. It is understandable because the inequality $z << \gamma$ gets weaker and eventually violates. This domains stronger driving applied fields for plasma vibrations. The shape of the OIB1 domain at low frequencies is shown in the inset of Fig.4.3.

To obtain the onset and offset applied fields of OIB at a particular frequency z, one has to draw a vertical line from the point z parallel to the $Y = \chi|\mathbf{E}_h|^2$ axis. The crossing points with lines f_2 (the left curve) and f_1 (the right curve) give the onset and offset bistability fields, respectively. In Fig.4.3, this procedure is illustrated for the OIB1 at $z = 0.2$. Considering the corresponding crossing points (0.2, 0.2306)

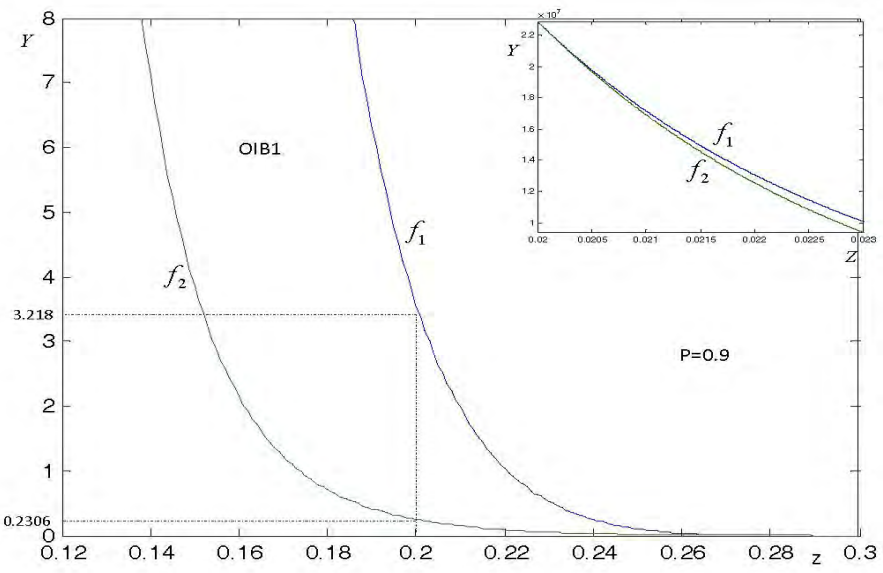

Figure 4.3: OIB1 domain. Curves f_2 and f_1 for composite of silver inclusions with nonlinear dielectric core in the plane $z - Y$; $p = 0.9$ and the volume fraction of inclusions $f = 0.03$. Rest of the parameters are the same as in Fig. 4.1.

and (0.2, 3.2180), one can get the onset and offset fields from the relations $Y_{off} = \chi|E_h|^2 = 0.2306$ and $Y_{on} = \chi|E_h|^2 = 3.2180$. We used this method for an analyzing the OIB domain in a single silver coated inclusion with $p = 0.4$ in a linear host matrix $\varepsilon_h = 2.25$ [82]. It is clear now, that in these conditions there is no second bistability domain. In the next subsection, we discuss the main features of the OIB2.

4.3.2 Second Domain of OIB

The OIB2 domain emerges at higher frequencies than the IOB1. Our numerical calculations allow us to find OIB2 domain in the frequency range $0.368 < z < 0.378$ for the composite with $p = 0.9, f = 0.03$. This bistability domain is rather narrow.

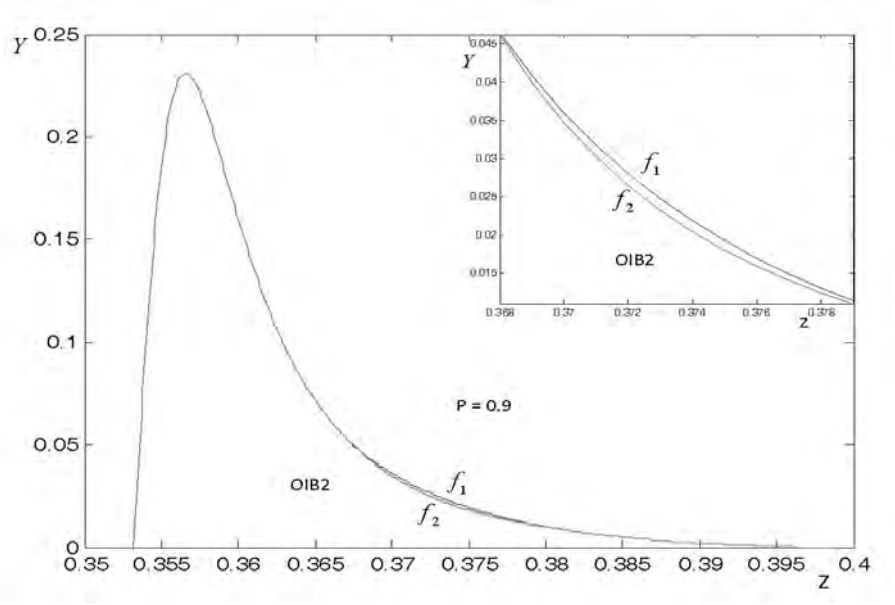

Figure 4.4: OIB2 domain. Curves f_2 and f_1 for composite of silver inclusions with nonlinear dielectric core in the plane $z - Y$; $p = 0.9$ and $f = 0.03$. Rest of the parameters are the same as in Fig. 4.1.

For $p \leq 0.85$ it is practically invisible. Increasing p OIB2 domain becomes more pronounced. Figure 4.4 shows the OIB2 domain in the $z - Y$ plane. The domain exists in a comparatively narrow frequency range $0.368 < z < 0.378$ (inside curves f_2 and f_1). Out of this frequency range the curves f_1 and f_2 coincide and there is no bistability. The enlarged OIB2 domain is shown in the inset of Fig.4.4. The onset and offset fields in this case are very close. For example, at the frequency $z = 0.374$, we obtain Y_{off} to be 0.021 and Y_{on} to be 0.023, which allow us to calculate the values of the onset and offset fields. Comparing these above values with the same values of OIB1 shows that the latter are approximately one order smaller.

Figure 4.5 shows the typical $S-$like bistability curves in the $Y - X$ plane for the same composite parameters. We present this figure to show that our approach

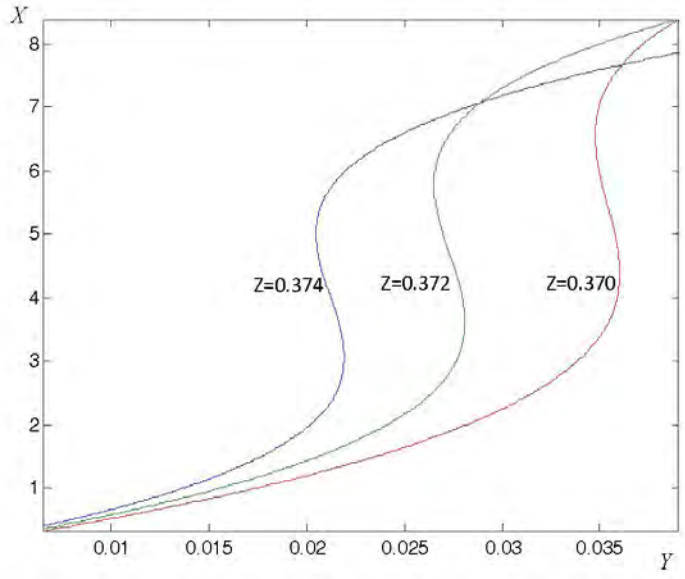

Figure 4.5: OIB2 domain. X versus Y for composite of silver inclusions with nonlinear dielectric core; $p = 0.9$ and $f = 0.03$. Rest of the parameters are the same as in Fig. 4.1.

which is different from the traditional one equivalently gives the same information regarding OIB. The frequency of OIB2 domain according to Fig.4.4 equals $\Delta z_2 = 0.01$. Comparison it with the frequency range of OIB1 domain $\Delta z_1 = 0.24$ shows that the frequency range of OIB2 domain is approximately one order smaller.

Table 4.1 shows the onset and offset values of Y of OIB1 and OIB2 for different frequencies within the relevant ranges. It can be seen that those values related to OIB2 are approximately one order smaller than those related to OIB1.

Table 4.1: Onset and offset values of Y of IOB1,2 for different z at $p = 0.9$ and $f = 0.03$. Rest of the parameters of the composite specified in Fig.4.1

IOB 1			IOB 2		
z	offset Y	onset Y	z	offset Y	onset Y
0.14	6.64	92.92	0.368	0.04620	0.04655
0.16	2.00	30.47	0.370	0.03476	0.03602
0.18	0.66	10.10	0.372	0.02650	0.02809
0.20	0.23	3.22	0.374	0.02047	0.02192

Table 4.2: Onset and offset values of $Y \times 10^{-3}$of OIB1,2 for different z at $p = 0.99$ and $f = 0.03$. Rest of the parameters are specified in Fig.4.1

IOB 1			IOB 2		
z	offset Y	onset Y	z	offset Y	onset Y
0.311	0.5527	0.9986	0.344	0.6945	0.8351
0.312	0.5081	0.8138	0.348	0.5106	0.6666
0.313	0.4659	0.6595	0.352	0.3993	0.4988
0.314	0.4256	0.5328	0.356	0.3133	0.3427

The p specifying the metal fraction in the inclusion considerably affects the enhancement factor of the local field. It is understandable that it must strongly affect

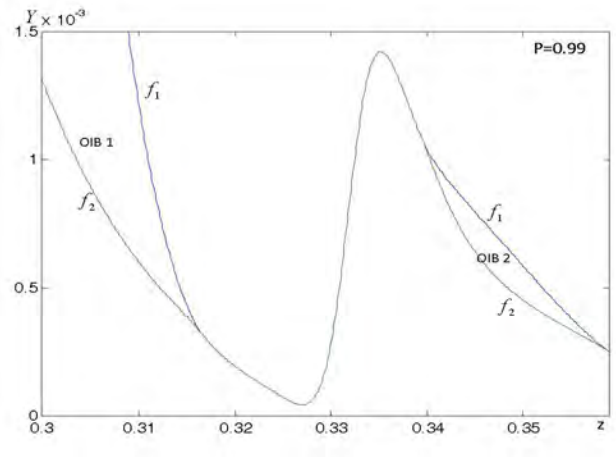

Figure 4.6: OIB1 and OIB2 domains. Y versus z for composite of silver inclusions with nonlinear dielectric core; $p = 0.99$ and $f = 0.03$. Rest of the parameters are the same as in Fig. 4.1.

both types of the bistability. To illustrate the role of p, we consider the bistabilty domains in the composite with inclusions having metal fraction $p = 0.99$ and $p = 0.999$. The results are presented in Fig.4.6 and 4.7.

Figure 4.6 shows the end of the OIB1 and the entire OIB2 domains. The first one ends at $z = 0.316$. The second domain exists in frequency range $0.339 \leq z \leq 0.358$. In agreement with Section 4.2, these domains get closer compared with the case $p = 0.9$ since the corresponding resonant frequencies get closer each other. Increase in the metal fraction of inclusions results in widening the frequency ranges of both bistability domains and decrease in the onset fields of OIB2. Comparison Fig.4.4 and Fig.4.6 one clearly sees a considerable widening the range of the onset and offset fields of the OIB2 domain. Fig.4.6 shows that OIB1 and OIB2 can exist at the same onset fields but at different frequencies. In particular, in the same range of onset fields $3.9 \times 10^{-4} < Y < 10^{-3}$, the OIB1 and OIB2 exist in the frequency ranges of $0.30 < z < 0.32$ and $0.34 < z < 0.35$. The onset fields for this composite can be

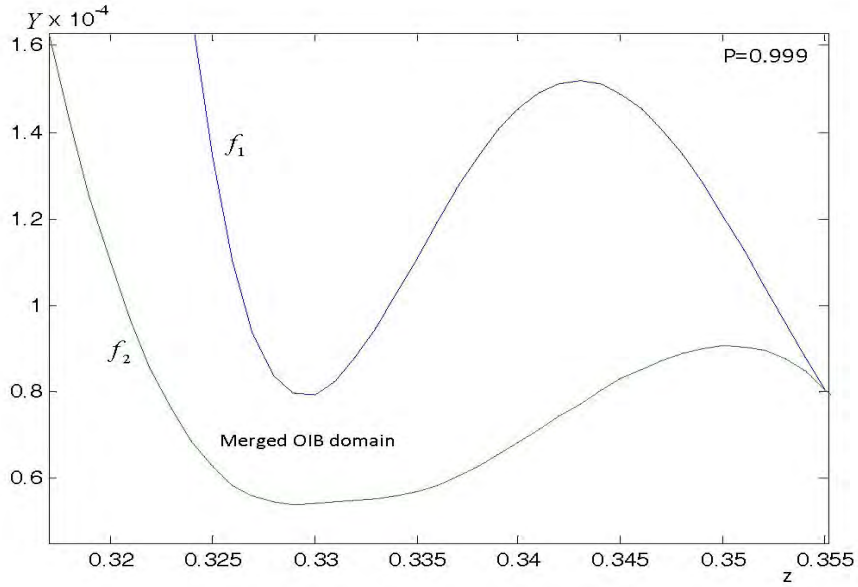

Figure 4.7: Entire OIB domain (merging OIB1 and OIB2). Y versus z for composite of silver inclusions with nonlinear dielectric core; $p = 0.999$ and $f = 0.03$. Rest of the parameters are the same as in Fig. 4.1.

calculated from the relation $Y \sim 10^{-4}$. They are considerably smaller than for the composite with $p = 0.9$. The end of OIB1 domain shows a blue shift. The onset and offset fields for both types of bistability in this case are given in Table 4.2.

A further increase in the metallic fraction p in the composite makes the frequency gap between the domains of OIB1 and OIB2 narrower. For example, in the composite $p = 0.999$ the frequency gap disappears. In Fig.4.7, we show the bistability domain enveloped by curves f_1 and f_2. In this case, there is only one bistability domain in the frequency range $0.02 < z < 0.35$. We may note that the phenomena described above for two separate bistability domainstake place in one merged domain. The lowest onset field corresponding to the frequency $z = 0.329$ can be found from the relation $Y = 5.3 \times 10^{-5}$. This onset field is lower than the onset fields for the

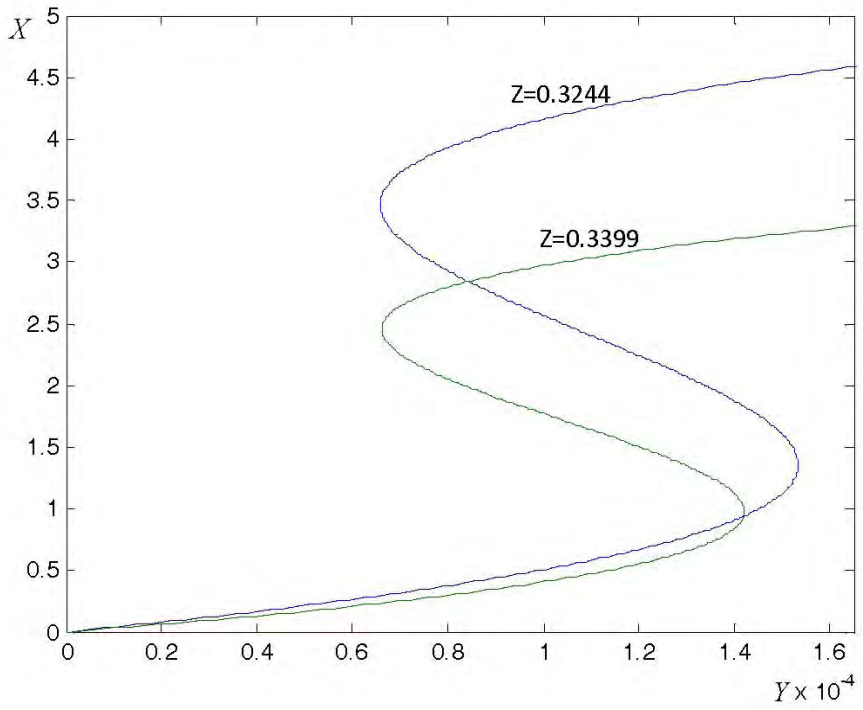

Figure 4.8: Entire OIB domain. X versus Y for composite of silver inclusions with nonlinear dielectric core with the same onset fields; $p = 0.999$ and $f = 0.03$. Rest of the parameters are the same as in Fig. 4.1.

$p = 0.99$ composite. In Fig.4.8, we present two curves X versus Y for the composite $p = 0.999, f = 0.03$ at two different frequencies $z_1 = 0.324$ and $z_2 = 0.340$. They correspond to the same onset fields $Y = 6.6 \times 10^{-5}$ but different offset fields $Y(z_1) = 1.6 \times 10^{-4}$ and $Y(z_2) = 1.4 \times 10^{-4}$. The same values of these parameters of the entire OIB domain can be obtained from Fig.4.7.

In this chapter, we specify the typical size of inclusions a when the long wave approximation is valid $a << \lambda$. The highest frequency associated with end of the OIB2 domain approximately equals to $0.4\omega_p$ that gives $\lambda \simeq 300nm$. It means that

the composites with inclusions of a typical size $20-30nm$ can be described within the frames of the long wave approximation and may have two domains of OIB. However, we have to discuss one more question. Our numerical calculations for composites $p > 0.999$ show that the shape of the entire OIB domain practically does not change. We remind that the metal fraction $p = 0.999$ means that a radius of the dielectric core r_1 equals to 0.1 of a radius of the inclusion r_2. For inclusions with $r_2 = 30$nm, we obtain that the radius of dielectric core is $r_1 = 3$nm. In other words, the core can be treated as a quantum dot. It is known [84] that the quantum dots can be satisfactory described by the macroscopic dielectric permittivity. For example, the macroscopic dielectric permittivity is used for the 2.8nm quantum dot [85]. We assume the macroscopic Kerr constant can be used for our nonlinear cores. The composite of 30nm inclusions with $p = 0.99$ is the most appropriate for realization of two OIB domains.

4.4 Conclusion

In this Chapter, we present the enhancement factor of the local field in a metal spherical inclusion with dielectric core in a linear host matrix has two maxima at two different frequencies. The second maximum corresponding to the higher resonant frequency can be specified and becomes important in inclusions with a large metal fraction $p > 0.85$. The composite of such inclusions have two domains of the optical induced bistability (OIB) in the field of intensive electromagnetic radiation.

The domain with lower frequencies is called OIB1 and have been studied in many papers. The second domain (OIB2) relates to the higher frequencies and exists in a comparatively narrow frequency range. It exists only in the composites with small dielectric cores. This type of bistability, to our best knowledge, have not been discussed

so far.

The narrowness of the frequency range of OIB2 is the main difficulty of its specification. In this work, we study the "frequency of incident radiation - squared modulus of the amplitude of the electric field of the incident radiation" plane, which is more convenient than the traditional " squared modulus of the electric field of the incident wave - squared modulus of the local field" plane.

The parameter that strongly affects the relative frequency location of both types of bistability is a metal fraction of the inclusion p, provided that rest of the parameters of the composite are the same. We consider OIB in composites with $p = 0.9 - 0.999$. There are two bistability domains in the composites $p = 0.9 - 0.99$. The frequency gap between them getting narrower with increment in p. The composite with $p = 0.999$ has only one OIB domain. The composites with higher p have lower onset fields. In particular, the composite with $p = 0.999$ (the radius of core 10 times smaller that the radius of inclusion) has the lowest onset fields. This composite have a peculiar property - the same onset fields correspond to different frequencies. These peculiarities make the composites of metal inclusions with small nonlinear dielectric cores attractive for different applications.

In the next Chapter, we consider the linear optical properties of composites with account of the second resonant frequency.

Chapter 5

Refractive Index of Composites with Metal and Metal Covered Inclusions

5.1 Introduction

It is shown the presence of two enhancement for metal core composite and one enhancement for pure composite systems in [71] and we calculate the refractive index for both real and imaginary part for passive and active media. Here we found two region of anomalous dispersion for metal core composite and one anomalous dispersion region for pure metal composite. We have done also for different f (percentage of particles in the host matrix) which is not affecting the structure and the value of real part of the refractive index. What we have seen is the effect on the absorption which is the imaginary part of the refractive index linearly depend on f for pure metal composite and for metal with dielectric core composites.

5.2 Polarizability of Spherical Nanoinclusions

The polarization of an individual metal covered spherical nanoinclusion with a dielectric core embedded in a dielectric host matrix [1], [71] can be presented in the form of 4.2.5

$$\begin{aligned} D &= \alpha r_2^3, \\ \alpha &= 1 - \frac{3\varepsilon_h[(3/p-1)\varepsilon_2 + \varepsilon_1]}{2\Delta}, \\ \Delta &= \varepsilon_2^2 + q\varepsilon_2 + \varepsilon_1\varepsilon_h, \\ q &= [\frac{3}{2p} - 1]\varepsilon_1 + [\frac{3}{p} - 1]\varepsilon_h. \end{aligned} \tag{5.2.1}$$

Here D is the effective polarizability of the inclusion, $p = 1 - (r_1/r_2)^3$ is a metal fraction in the inclusion (r_1 and r_2 are radiuses of the dialectic core and the metal cover). The dielectric functions (DFs) of the core, metal cover, and host matrix are denoted as ε_1, ε_2, and ε_h, respectively. Relation 5.2.1 holds true for the Raman particles when the radius of inclusion r_2 is much less than the wave length of incident radiation λ. Further, we use a real DF of the core 4.2.7. It is known that the frequency dependence of metals over the optical frequency range is described by the Drude model [86], [87] ε_2 is given in equation 2.2.9. Here we consider the case when the DF of the host matrix in real and imaginary form

$$\varepsilon_h = \varepsilon_h' + i\varepsilon_h'' \tag{5.2.2}$$

The negative imaginary part that decreases decay of the electromagnetic waves in the composite. In this model ε_h'' does not depend on the frequency and its value will be discussed below.

Now obtain expressions of the real α' and imaginary α'' parts of 5.2.1 and presenting them in the form

$$\alpha' = 1 - \frac{3\varepsilon_h}{2}\frac{[(3/p-1)\varepsilon_2' + \varepsilon_1]\Delta' + (3/p-1)\varepsilon_2''\Delta''}{\Delta'^2 + \Delta''^2}, \tag{5.2.3}$$

$$\alpha'' = \frac{3\varepsilon_h}{2}\frac{[(3/p-1)\varepsilon_2' + \varepsilon_1]\Delta'' - (3/p-1)\varepsilon_2''\Delta'}{\Delta'^2 + \Delta''^2}, \tag{5.2.4}$$

where the real and the imaginary part of Δ given in the following expressions

$$\begin{aligned} \Delta' &= \varepsilon_2'^2 + q\varepsilon_2' + \varepsilon_1\varepsilon_h - \varepsilon_2''^2, \\ \Delta'' &= \varepsilon_2''(q + 2\varepsilon_2'). \end{aligned} \tag{5.2.5}$$

An analytic analysis of the obtained expressions can be done in the model of a very weak damping of plasma vibrations in the metal part of the inclusion when we consider $\gamma << 1$ which is negligible. In this case from the imaginary part of equation 2.2.9 can be consider $\varepsilon_2'' \sim \gamma << 1$. The minimum of the denominators in 5.2.3 and 5.2.4 gives the maximum value of polarization at the condition of

$$\varepsilon_2'^2 + q\varepsilon_2' + \varepsilon_1\varepsilon_h = 0. \tag{5.2.6}$$

This equation 5.2.6 has two roots that in turn gives two resonant frequencies. The conclusion about existence of two plasma resonant frequencies in the metal covered inclusions with dielectric core have been done in [71]. Below, we analyze the behavior of the imaginary part of the polarizability α'', 5.2.4 which is responsible for the absorption of electromagnetic waves in the composites. The resonant frequencies given by equation 2.2.20 z_r, substituting in equation 5.2.4 we found the absorbtion at the resonant frequency as follows

$$\alpha''(z_r) = \frac{3\varepsilon_h}{2}\frac{[(3/p-1)\varepsilon_2' + \varepsilon_1](q + 2\varepsilon_2') + (3/p-1)\varepsilon_2''^2}{\varepsilon_2''[\varepsilon_2''^2 + (q + 2\varepsilon_2')^2]}. \tag{5.2.7}$$

Let us find the analytical results of the resonant frequency that maximize the polarizability 5.2.7 of the composite. Here we are considering the following two limiting cases, the first limiting case is for thin metal cover ($p << 1$) and the second limiting case is for small dielectric core $p \approx 1$.

In the first limiting case, applying in the denominator of equation 5.2.7 in equation 5.2.6 $q = 3[\varepsilon_1/2 + \varepsilon_h]/p$ which is results $>> 1$ with account of the leading terms, the solutions of 5.2.6 will be

$$\varepsilon'_{21'} = -q, \tag{5.2.8}$$

for the second term we found the result from equation 5.2.6

$$\varepsilon'_{22'} = -\varepsilon_1\varepsilon_h/q. \tag{5.2.9}$$

The resonant frequency can be calculated compering 3.2.3 with 5.2.8 and 5.2.9 which is given the result of two resonant frequencies 2.2.13

$$\begin{aligned} &z_{r1'} \approx \sqrt{1/q}, z_{r2'} \approx \sqrt{1/\varepsilon_\infty}, \\ &q >> \varepsilon_\infty, \varepsilon_1\varepsilon_h. \end{aligned} \tag{5.2.10}$$

Usage of the above relations give the following two maxima of the imaginary part of the polarizebility α''

$$\begin{aligned} \alpha''(z_{1'}) &\approx \frac{\varepsilon_h\sqrt{6}}{(\varepsilon_1 + 2\varepsilon_h)^{3/2}}\frac{\sqrt{p}}{\gamma}, \\ \alpha''(z_{2'}) &\approx \frac{\varepsilon_1\varepsilon_h(\varepsilon_1 + \varepsilon_h)}{(\varepsilon_1 + 2\varepsilon_h)\varepsilon_\infty^{3/2}}\frac{p}{\gamma}, \gamma << p. \end{aligned} \tag{5.2.11}$$

It is seen that for small p, the first maximum is larger than the second one.

The case of large metal fractions $p \simeq 1$ (small dielectric cores)is more interesting. With $q = \varepsilon_1/2 + 2\varepsilon_h$, the roots of 5.2.6

$$\begin{aligned} \varepsilon'_{21} &= -2\varepsilon_h \\ \varepsilon'_{22} &= -\varepsilon_1/2 \end{aligned} \tag{5.2.12}$$

give the following resonant frequencies

$$\begin{aligned} z_1 &= 1/\sqrt{\varepsilon_\infty + 2\varepsilon_h} \\ z_2 &= 1/\sqrt{\varepsilon_\infty + \varepsilon_1/2}. \end{aligned} \tag{5.2.13}$$

The maxima of α'' given by

$$\begin{aligned} \alpha''(z_{r1}) &\approx \frac{3\varepsilon_h}{(\varepsilon_\infty + 2\varepsilon_h)^{3/2}} \frac{1}{\gamma}, \\ \alpha''(z_{r2}) &\approx \frac{9\varepsilon_1\varepsilon_h(1-p)}{2(\varepsilon_1 - 4\varepsilon_h)(\varepsilon_\infty + \varepsilon_1/2)^{3/2}} \frac{1}{\gamma}, \end{aligned} \tag{5.2.14}$$

provided that from equation 5.2.14 $\varepsilon_1 \neq 4\varepsilon_h$. If equation 5.2.14 shows the following condition

$$\varepsilon_1 = 4\varepsilon_h. \tag{5.2.15}$$

The resonant frequencies z_{r1} and z_{r2} become very close and we get

$$\alpha''(z_{r1} = z_{r1}) \approx \frac{3\varepsilon_h}{(\varepsilon_\infty + 2\varepsilon_h)^{3/2}} \frac{1}{\gamma}. \tag{5.2.16}$$

The polarizability of pure metal which has both real and imaginary parts represented with equation as follows [38]

$$\alpha_m = \frac{\varepsilon_2 - \varepsilon_h}{\varepsilon_h + 2\varepsilon_h}. \tag{5.2.17}$$

It can be obtain from the second formula 4.2.5 setting $p = 1$ and making the substitution $\varepsilon_1 \to \varepsilon_2$.

Separating in 5.2.17 real and imaginary parts, we get

$$\begin{aligned} \alpha'_m &= \frac{(\varepsilon'_2 - \varepsilon'_h)\Delta'_m + (\varepsilon''_2 - \varepsilon''_h)\Delta''_m}{\Delta'^2_m + \Delta''^2_m}, \\ \alpha''_m &= \frac{3(\varepsilon''_2\varepsilon'_h - \varepsilon'_2\varepsilon''_h)}{\Delta'^2_m + \Delta''^2_m}, \\ \Delta'_m &= \varepsilon'_2 + 2\varepsilon'_h, \Delta''_m = \varepsilon''_2 + 2\varepsilon''_h. \end{aligned} \tag{5.2.18}$$

Here we take into account the imaginary part of the host matrix ε_h''. Assuming that the imaginary parts ε_2'' and ε_h'' are very small, we find that the maximum of α_m'' 5.2.18 obtained from the condition $\Delta_m' = 0$ has only one resonant frequency

$$z_r = 1/\sqrt{\varepsilon_\infty + 2\varepsilon_h}. \tag{5.2.19}$$

To be consistent with the results for the metal inclusions with the dielectric core, we set $\varepsilon_h'' = 0$. With the help of 5.2.19 we obtain the maximum of α_m''

$$\alpha_m''(z_r) = \frac{3\varepsilon_h}{(\varepsilon_\infty + 2\varepsilon_h)^{3/2}} \frac{1}{\gamma}. \tag{5.2.20}$$

Comparing 5.2.14 and 5.2.20, we see that the maxima of the imaginary parts of polarizability of the inclusion with dielectric core are of the same order as the one of the pure metal inclusion.

While obtaining 5.2.11, 5.2.14, and 5.2.16 we used relation $\varepsilon_2'' = \gamma/z_r^3$ with resonant frequencies 5.2.10 and 5.2.13. The maxima of the enhancement factor of the inclusions with small dielectric cores ($p \simeq 1$) 5.2.18 and 5.2.20 are of the same order.

5.3 Refractive Index of Composites of Metal Inclusions with Small Dielectric Cores

We express the refractive index as

$$n = \sqrt{\varepsilon} = \sqrt{1 + 4\pi\chi} \tag{5.3.1}$$

and obtain the general expression for the real and imaginary part of the refractive index for the pure metal composite and metal with dielectric core composite. To illustrate this, we calculated the real n' and imaginary part n'' of the refractive index. Consider the refractive index of the composites with real inclusions, when γ is not

extremely small but a finite being of the order of 10^{-2}. The optical properties of these systems can be analyzed only numerically. The results of this study are presented below. According to the Clausius-Mossoti formula the effective DF ε of the composite can be written as

$$\frac{\varepsilon - \varepsilon_h}{\varepsilon + 2\varepsilon_h} = \frac{4\pi}{3} DN, \tag{5.3.2}$$

where D given by 4.2.5, and N is a density number of the inclusions. With the help of the volume fraction of spherical inclusions $f = (4\pi/3)r_2^3 N$, the refractive index of the composite n is given by the equation

$$n^2 = \varepsilon = \varepsilon_h\{1 + 3f\frac{\alpha}{1 - f\alpha}\}, \tag{5.3.3}$$

where the polarization α for metal with dielectric core composite is given by

$$\alpha = 1 - \frac{d}{d-1}\frac{\varepsilon_h((d/p - 1)\varepsilon_2 + \varepsilon_1)}{\Delta_d}. \tag{5.3.4}$$

Equating the real and imaginary parts of 5.3.3, we obtain a system of coupled equations for the real n' and imaginary n'' parts of the composite refractive index

$$\begin{aligned} n'^2 - n''^2 &= b_1, \\ 2n'n'' &= b_2, \end{aligned} \tag{5.3.5}$$

with

$$\begin{aligned} b_1 &= \varepsilon'_h + 3f\frac{(\alpha' - f|\alpha|^2)\varepsilon'_h - \alpha''\varepsilon''_h}{(1 - f\alpha')^2 + (f\alpha'')^2}, \\ b_2 &= \varepsilon''_h + 3f\frac{(\alpha' - f|\alpha|^2)\varepsilon''_h + \alpha''\varepsilon'_h}{(1 - f\alpha')^2 + (f\alpha'')^2}. \end{aligned} \tag{5.3.6}$$

Relation 5.3.6 holds true for the Raman particles when the radius of inclusion r_2 is much less than the wave length of incident radiation λ. Further, we use a real DF of the core. The DF of metal ε_2 is chosen in the Drude form given in equation

3.2.3. Here we consider the case when the DF of the host matrix $\varepsilon_h = \varepsilon'_h + i\varepsilon''_h$ has a negative imaginary part that decreases decay of the electromagnetic waves in the composite. In this model we consider ε''_h does not depend on the frequency which is linear (constant) and its value will be discussed below.

The expressions of the real α' and imaginary α'' parts for α metal with dielectric core composite and present them in the form

$$\begin{aligned}\alpha' = 1 - \frac{d}{d-1}[&\frac{(\varepsilon'_h((d/p-1)\varepsilon'_2+\varepsilon_1) - \varepsilon''_h(d/p-1)\varepsilon''_2)\Delta'_d}{\Delta'^2+\Delta''^2} \\ &+ \frac{(\varepsilon''_h((d/p-1)\varepsilon'_2+\varepsilon_1) + \varepsilon'_h(d/p-1)\varepsilon''_2)\Delta''_d}{\Delta'^2_d+\Delta''^2_d}],\end{aligned} \tag{5.3.7}$$

$$\begin{aligned}\alpha'' = \frac{d}{d-1}[&\frac{(\varepsilon'_h((d/p-1)\varepsilon'_2+\varepsilon_1) - \varepsilon''_h(d/p-1)\varepsilon''_2)\Delta''_d}{\Delta'^2+\Delta''^2} \\ &- \frac{(\varepsilon''_h((d/p-1)\varepsilon'_2+\varepsilon_1) + \varepsilon'_h(d/p-1)\varepsilon''_2)\Delta'_d}{\Delta'^2_d+\Delta''^2_d}],\end{aligned} \tag{5.3.8}$$

where

$$\begin{aligned}\Delta' &= \varepsilon'^2_2 + q'\varepsilon'_2 - q''\varepsilon''_2 - \varepsilon''^2_2 + \varepsilon_1\varepsilon'_h, \\ \Delta'' &= 2\varepsilon''_2\varepsilon'_2) + q'\varepsilon''_2 + q''\varepsilon'_2 + \varepsilon_1\varepsilon''_h,\end{aligned} \tag{5.3.9}$$

and

$$\begin{aligned}q' &= (d/(d-1)p-1)\varepsilon_1 + (d/p-1)\varepsilon'_h, \\ q'' &= (d/p-1)\varepsilon''_h.\end{aligned} \tag{5.3.10}$$

The expression of the real and imaginary part of the refractive index using equation 5.3.5 can be written as

$$\begin{aligned}n' &= \sqrt{\frac{1}{2}(\sqrt{b_1^2+b_2^2}+b_1^2)} \\ n'' &= \sqrt{\frac{1}{2}(\sqrt{b_1^2+b_2^2}-b_1^2)}.\end{aligned} \tag{5.3.11}$$

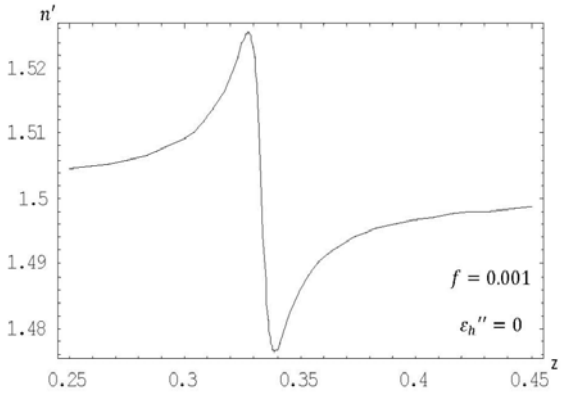

Figure 5.1: Real part of refractive index n' of composite with pure silver spherical inclusions versus z. Numerical values of the composite parameters: $\varepsilon'_h = 2.25, \varepsilon''_h = 0, f = 0.001, \varepsilon_\infty = 4.5, \omega_p = 1.6 \times 10^{16}, \gamma = 1.15 \times 10^{-2}$

.

5.4 Refractive Index Composites with Passive and Active Host Matrix

Below, we present the real and imaginary part of the refractive index in figures 5.1, 5.2, 5.3, 5.4 considering the case of the passive host matrices $\varepsilon''_h = 0$. We set the volume fraction $f = 0.001$. The numerical calculation of maxima of $f\alpha'_m$ and $f\alpha''_m$ as well as $f\alpha'$ and $f\alpha''$ shows that they are of the order of 10^{-2}. It allows us to neglect the dipole-dipole interaction between the inclusions.

The active host matrix with $\varepsilon''_h < 0$ for the composites of pure metal and metal covered inclusions with the dielectric core and we set the the volume fraction $f = 0.001$, for metal/ dielectric composite the host matrix $\varepsilon''_h = -0.13866$ and $\varepsilon''_h = -0.20722$ for the second and the first maxima respectively, for pure metal composite the host matrix is $\varepsilon''_h = -0.1159113$. We can see the numerical results $f\alpha'_m$ and $f\alpha''_m$

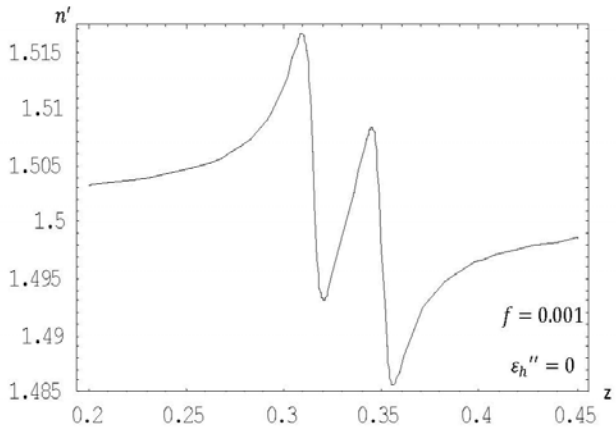

Figure 5.2: Real part of refractive index of composite with metal covered inclusions with dielectric core with metal fraction $p = 0.99$versus z. Rest of the parameters of the composite are the same as in Fig.5.1.

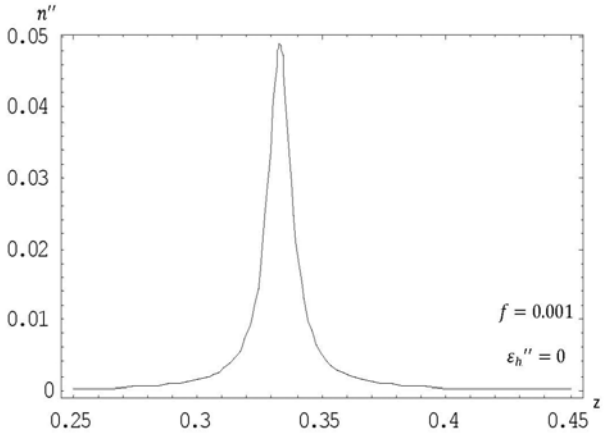

Figure 5.3: Imagine part of refractive index n'' of composite with pure silver spherical inclusions versus z. Numerical values of the composite parameters are the same as in Fig.5.1.

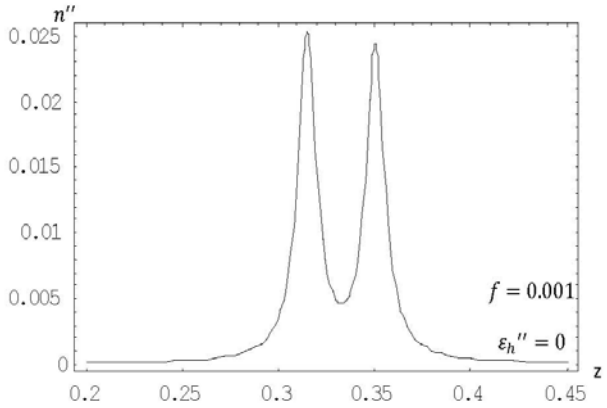

Figure 5.4: The imaginary part of the refractive index n'' versus z in the composite with passive host matrix $\varepsilon_h'' = 0$. The rest parameters of the composite are the same as in Fig.5.1.

as well as $f\alpha'$ and $f\alpha''$ give for these quantities values of the order of 10^{-2}. The same results we obtain with the help of analytical formulas 5.2.18, 5.3.7 and 5.3.8. It allows us to neglect the dipole-dipole interaction between the inclusions.

We have seen the graphical representation of the decreasing the absorbtion of the incident radiation due to the active host matrices for pure metal and metal with dielectric core shown in the figure 5.5, 5.6, 5.7.

Figure 5.5 shows the imaginary part of the refractive index versus the applied radiation frequency at given active host matrix $\varepsilon_h = -0.1159113$. In this case $n^{''} \sim 10^{-7}$.

Figure 5.6 illustrate the active host matrix at $\varepsilon_h = -0.13866$ that corresponds to the left side of the resonance frequency near to $z \sim 0.32$ and the absorption $n^{''} \sim 10^{-7}$. Figure 5.7 illustrate the active host matrix at $\varepsilon_h = -0.20722$ that corresponds to the right hand side of the resonance frequency near to $z \sim 0.35$ and the absorption

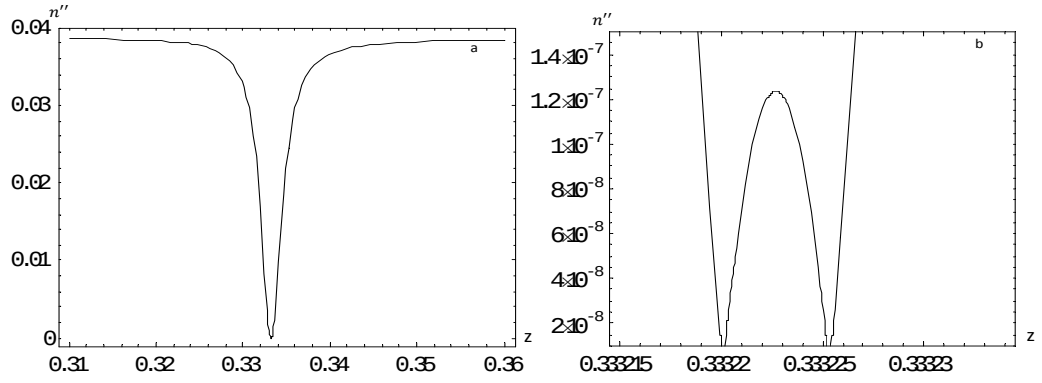

Figure 5.5: a) The Imaginary part n'' versus z for pure metal with gain matrix $\varepsilon_h'' = -0.1159113$, b) the enlarged tip of a). The rest parameters of the composite are the same as in Fig.5.1.

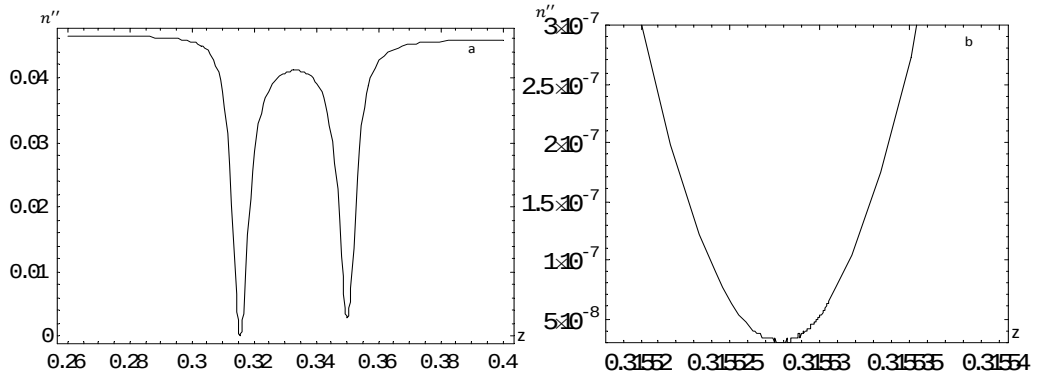

Figure 5.6: a)The Imaginary part n'' versus z in the composite with gain matrix $\varepsilon_h'' = -0.13866$, b) the enlarged left side of a). The rest parameters of the composite are the same as in Fig.5.1.

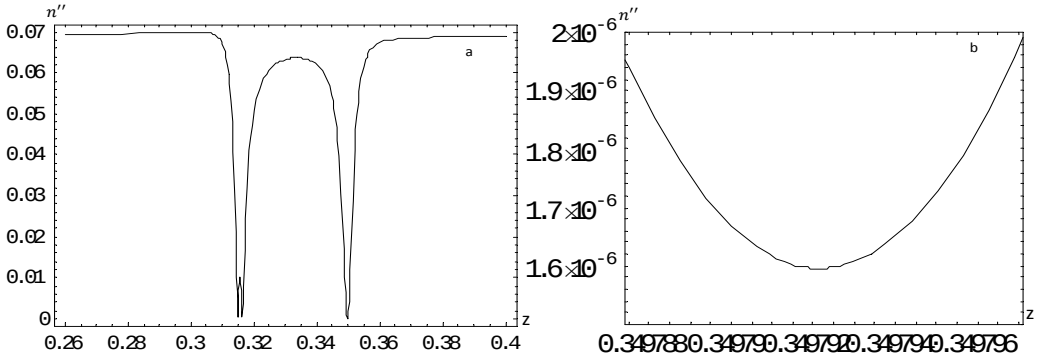

Figure 5.7: a) The Imaginary part n'' versus z in the composite with gain matrix $\varepsilon_h'' = -0.20722$, b) the enlarged right side of a). The rest parameters of the composite are the same as in Fig.5.1.

$n^{''} \sim 10^{-8}$

A typical length at which the intensity of radiation decreases by $e-$ times can be evaluated with the help of the relation [29]

$$l \approx c/2n''z_r\omega_p. \tag{5.4.1}$$

For passive matrix the negative refractive index for pure metal is $n'' = 0.05$, $z_r = 0.33$, and $\omega_p = 10^{16}$. Equation 5.4.1 gives the following $l \approx 10^3 nm$. It is of the order of the wave length $400nm$ corresponding to this frequency ω_p. The reason of this is that $n'' \sim 1$ and high ω_p in metals. This evaluation is true for the both types of composites. Therefore, the thin films of the composites practically completely absorb the radiation on the resonant frequencies and one cannot speak about propagating waves on these frequencies. To obtain propagating waves it is necessary to considerably decrease n'' [88]. It can be done by introducing the active elements in the host matrix and we shown these results by considering equation 5.4.1 and our numerical results described in the figure 5.5, 5.6, 5.7 in the order of $l \sim 10^2 cm$.

5.5 Conclusion

We have calculated the real and imaginary parts of the refractive index of the composites of spherical metal inclusions with small dielectric cores and for a pure metal embedded in equilibrium host matrix and active host matrix.

The real part of the refractive index of pure metal shows an anomalous dispersion and absorption occurs at the resonant frequency. There is a strong anomalous dispersion and absorption on these frequencies for the case of metal with dielectric core.

Considering a small negative imaginary part of the dielectric host matrix it is possible to organize conditions for propagating weakly damping light backward waves with the group velocity less than speed of light.

Figures 5.1 and 5.3 show the frequency dependence of the real and imaginary parts of the refractive index of the composite with pure metal inclusions. It has one resonant frequency.

Figures 5.2and 5.4 show the same quantities for the composites with metal covered inclusions for non-tuned and tuned DF of ε_1 and ε_h at $p = 0.99$, respectively. The second maximum of n'' becomes comparable with the first one in the tuned composite that corresponds to $\varepsilon_1 = 4\varepsilon_h = 9$.

Figures 5.5, 5.6, and 5.7 show the imaginary part of the refractive index for pure metal and metal with dielectric cores for active matrices. Tunning the negative imaginary part of host matrix it is possible to considerably decrease n''.

In the next Chapter, we present the group velocity index and the group velocity in consideration of pure metal and metal/dielectric composite.

Chapter 6

Slow and Fast Light Wave in Metal/Dielectric Composites

6.1 Introduction

The systems with anomalous dispersion show peculiar optical properties at resonant frequencies. They allow the propagation of the superluminal light pulses (with group velocity exceeding the speed of light in vacuum) and the light pulses with negative group velocity (see review [89] and references ibid). The speed of the superluminal light pulse in the gaseous gain assisted atomic caesium medium have been measured in the result of [90]. The very slow light pulses have been observed in an ultra cold sodium vapor [23].

In the previous chapter, we have shown metal/dielectric composites on the resonant frequencies close the plasma frequency of the metal cover demonstrate strong anomalous dispersion even at comparatively small volume fractions of inclusions. Obviously that they have to posses the above mentioned peculiar optical properties. A level of losses in the composites can be considerably decreased by introducing the gaining elements into the host matrix of composites or use alternative layers of composite and gaining media [91], [92]. Formally, the effect of active elements in composites

can be described by introducing a negative part in the dielectric function of the host matrix [88].

The pioneering demonstrations of slow and fast light were all based on the exploitation of narrow spectral resonances, mainly created by electromagnetically-induced transparency [23] or coherent population oscillation [24]. In this chapter we present that the composites of spherical inclusions with dielectric cores embedded in a passive host matrix strongly absorb the light on two resonant frequencies unlike the composites of pure metal inclusions having only one resonant frequency. A relatively small negative imaginary part in the dielectric function of the host matrix considerably decreases (by many orders) the imaginary part of the composite refractive index and a level of losses. It provides the propagation of weakly damping narrow pulses of slow and fast light.

In our study we consider the equilibrium (passive) host matrix when $\varepsilon_h'' = 0$ for the composites of pure metal and metal covered inclusions with the dielectric core. For equilibrium (passive) host matrix consideration the numerical values shown for α_m', α_m'' and α', α'' in the figures 5.1, 5.2, 5.3, and 5.4. We set the the volume fraction $f = 0.001$. Equation 5.3.4 help us to obtain the analytical results with neglecting the dipole-dipole interaction between the inclusions. The real and imagine parts of the refractive index are presented in Fig.5.1-5.4 for passive and Fig.5.5-5.7 for active matrices.

It is seen that values of n' are practically the same for both composites with $\varepsilon_h'' = 0$. At the same time, the maxima of n'' of the metal covered tuned inclusions are approximately two times smaller than the same quantity of the composite with pure metal inclusions with $\varepsilon_h'' = 0$.

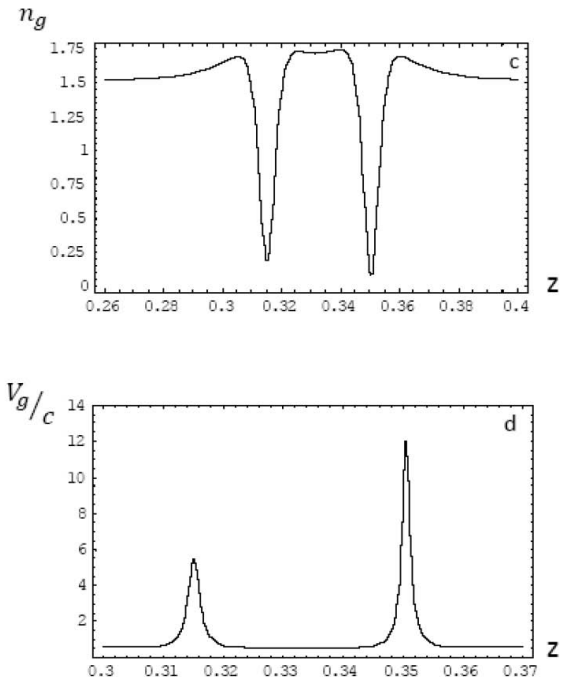

Figure 6.1: Passive composite with tuned inclusions ($\varepsilon_h'' = 0$). c)group velocity index n_g versus z; d) normalized group velocity V_g/c versus z. Numerical values of composite parameters: $\varepsilon_1 = 9, \varepsilon_h' = 2.25, p = 0.99$, $\varepsilon_\infty = 4.5$, $\omega_p = 1.6 \times 10^{16}$ (silver), $\gamma = 1.15 \times 10^{-2}$, $f = 0.001$.

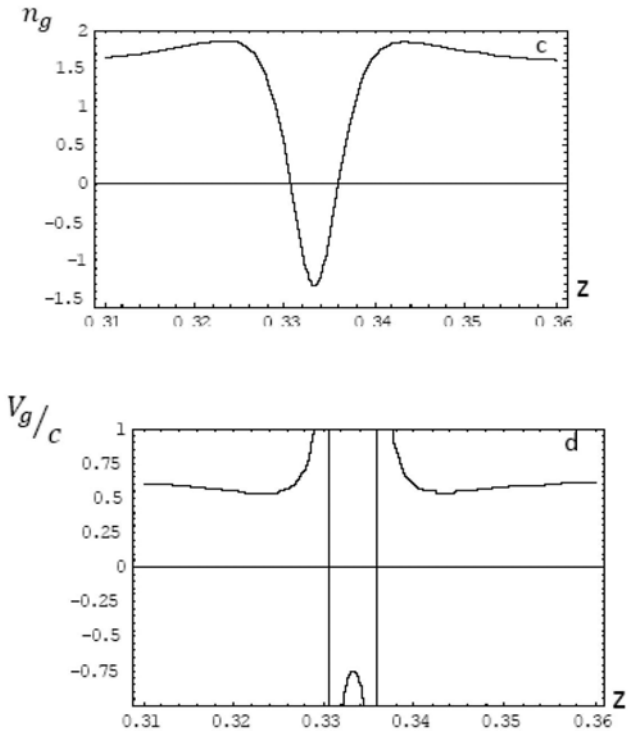

Figure 6.2: Passive composite with pure metal inclusions ($\varepsilon_h'' = 0$). c)group velocity index n_g versus z; d) normalized group velocity V_g/c versus z. The numerical values of composite parameters: $\varepsilon_h' = 2.25, \varepsilon_\infty = 4.5$, $\omega_p = 1.6 \times 10^{16}$ (silver), $\gamma = 1.15 \times 10^{-2}$, $f = 0.001$.

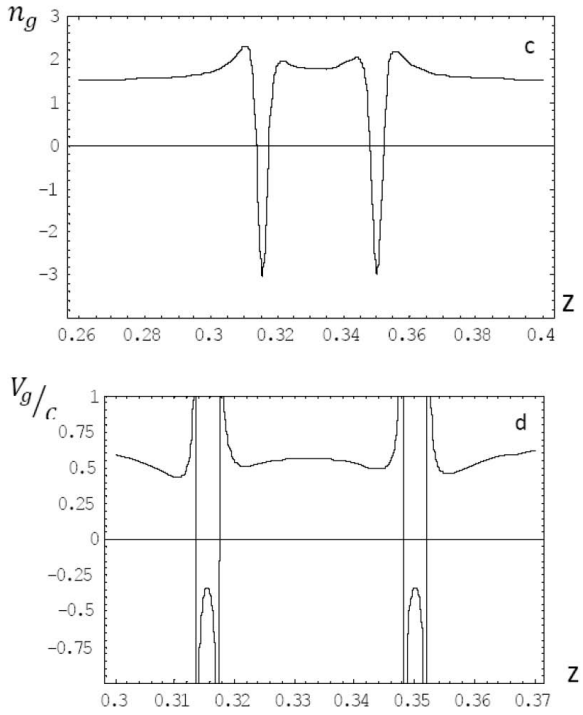

Figure 6.3: Active composite with tuned inclusions $\varepsilon_h'' = -0.13866$. c)group velocity index n_g versus z; d)normalized group velocity V_g/c versus z. The numerical values of composite parameters are the same as in Fig.6.1.

In this study we also considering the active host matrix to increase the propagation width of the incident radiation in the medium. This propagation is exists in our work and shown the decreasing absorption for pure metal composite described in figure 5.5 and for metal with dielectric core composite described in figures 5.6, 5.7

The main characteristic of the composites under consideration is a strong absorption of EMWS at resonant frequencies. In fact, a typical length on which the intensity of the decreases by $e = 2.713$ times can be evaluated with the help of [29] as given in equation 5.4.1.

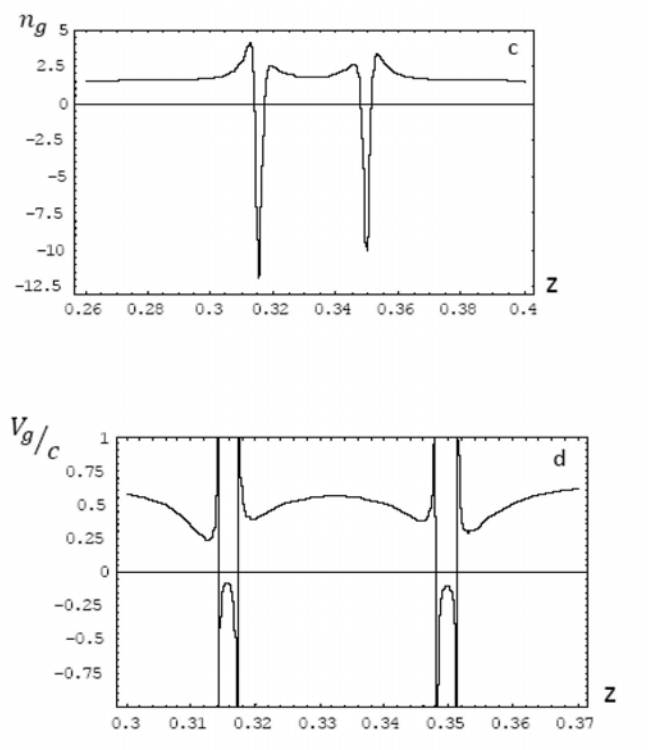

Figure 6.4: Active composite with tuned inclusions $\varepsilon_h'' = -0.20722$. c)group velocity index n_g versus z; d) normalized group velocity V_g/c versus z. The numerical values of composite parameters are the same as in Fig.6.1.

For the composite with tuned inclusions has $n'' = 0.025$ at the resonant frequency $z_r = 0.33$. Taking $\omega_p = 10^{16}$, we get $l \approx 2000nm$. For the composite with pure metal inclusions l is two times less. It is comparable with the wave length $400nm$ corresponding to the resonant plasma frequency $0.33 \times \omega_p$. Therefore, the EMWs of the resonant frequencies are strongly absorbed by the relatively thin layers of the composites.

6.2 Negative Group Velocity in Composites with Active Host Matrix

The optical pulses propagating through highly dispersive media [93], [94] show a negative value of the group velocity. In such a situation, It predicts that the peak of the transmitted pulse will exit the material before the peak of the incident pulse enters the material, and furthermore that the pulse will appear to propagate in the backward direction within the medium [95, 96, 97].

We consider the waves in the composite with the active host matrix within the frame of the simple model with a constant negative imaginary part of the DF of the host matrix $\varepsilon_h'' < 0$. It does not depend on the frequency and as we show below compensates the losses of the EMWs on the resonant frequencies. We calculate the quantity V_g with the help of the known formula [32]

$$V_g(z) = \frac{c}{n_g(z)}, n_g(z) = n'(z) + z\frac{dn'(z)}{dz}, \tag{6.2.1}$$

which is called the group velocity of a wave packet. Here c is the speed of light in vacuum and n_g is the group velocity index [89]. This relation is obtained from $V_g = d\omega/dk$ (ω is the frequency and k is the wave vector) with usage of the definition of the real part of the refractive index $n' = kc/\omega(k)$, the group velocity V_g appears in

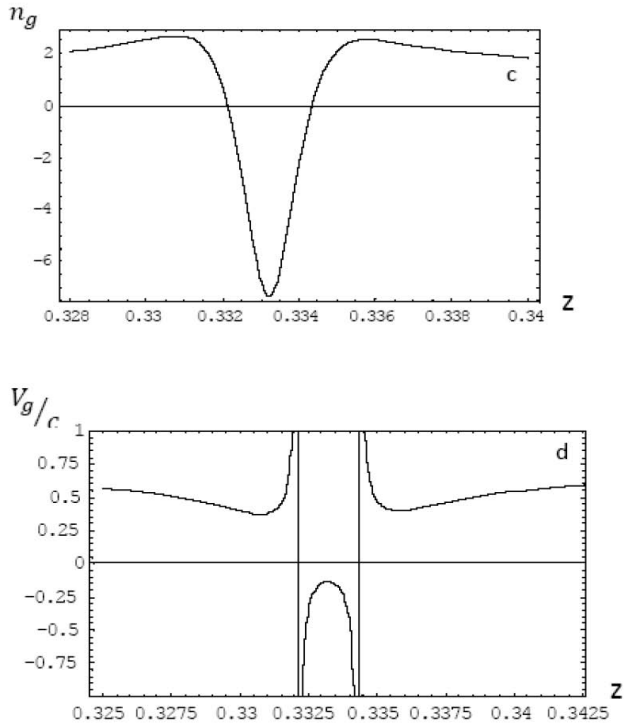

Figure 6.5: Active composite with pure metal inclusions $\varepsilon_h'' = -0.1159113$.c)group velocity index n_g versus z; d)normalized group velocity V_g/c versus z. The numerical values of composite parameters are the same as in Fig.6.2 with $f = 0.0002$.

the second term of the Taylor expansion as shown in equation 1.6.2

$$\omega_k = \omega_{k_0} + V_g(k_0)(k - k_0) + \frac{1}{2}\frac{dV_g}{dk}|_{k=k_0}(k - k_0)^2 + ... \tag{6.2.2}$$

around the center of the wave packet k_0. Therefore, 6.2.1 has a meaning of the group velocity in the case of a week dispersion of $\omega(k)$. For a strong dispersion, the higher terms in 6.2.2 must be taken into account and in this case V_g losses its physical meaning [29].

Figures 6.1c,6.1d - 6.5c,6.5d present n_g and V_g/c versus z for the passive and active composites of metal covered and pure metal inclusions. In Fig.6.1d and 6.2d

can be seen the superluminal light $V_g(z)/c > 1$ and backward light $V_g(z) < 0$, at the resonant frequencies. In the passive composites, the light is absorbed in thin layers $\sim 10^3 nm$. The graphs of $n_g(z)$ help to understand which light is typical for a particular composite [29]. In Fig.6.1c the curve $n_g(z)$ does not cross the $z-$ axis. Its minima show the maxima of $V_g(z)/c$. From Fig. 6.1d one can see that the maxima of V_g/c in the passive composite $p = 0.99, f = 0.001$ at resonant frequencies are larger than unit and close to 6 and 12. Decreasing f from this value, one we can obtain two maxima of $V_g < c$ at the same resonant frequencies. The situation becomes more interesting with increasing in f. If $n_g(z)$ touches the z axis at some points z_1 and z_2(from the positive side), there are three branches of positive $V_g(z)$ approaching two vertical lines (asymptotes) passing and tending to $+\infty$. With further increase in f, the curve $n_g(z)$ crosses $z-$ axis four times. We have two close (paired) asymptotes passing through the crossing points. In the frequency ranges between asymptotes the waves with negative V_g appear. In this case there are five frequency ranges in the composite with tuned inclusions: three positive branches of $V_g(z) \to +\infty$ if the frequency approach the paired asymptotes from outside and two negative branches $V_g(z) \to -\infty$ if the frequency approaches the paired asymptotes from inside. The narrower distance between asymptotes the "deeper" the maxima of negative $V_g(z)$.

We illustrate this for both types of active composites. Our calculations show that increase in f and in $|\varepsilon_h''|$ basically gives the same effect. In Fig.6.3d and 6.4d one can see $V_g(z)/c$ for the composite $f = 0.001$ with tuned metal covered inclusions $\varepsilon_h'' = -0.13866$ and $\varepsilon_h'' = -0.20722$. It is important that the maxima of $V_g/c = -0.3$ of the left (Fig.6.3d) and $V_g/c = -0.2$ of the right (Fig.6.4d) wings of n'' correspond to $\sim 10^{-7}$ and $\sim 10^{-6}$, respectively. It gives the typical length of propagation $l \sim (10^2 -$

10)cm, respectively. It is important that at the maxima of $V_g < 0$, the derivatives $dV_g/dz = 0$ and $dV_g/dk = 0$. Therefore, the third term in 6.2.2 disappears. In this frequency range, the negative group velocity has the physical meaning and the narrow Gaussian pulses of the slow backward waves are weakly spreading and weakly decaying. The corresponding typical frequencies of these waves are of the order of $(3-4) \times 10^{15}$ and lays in the ultra violet part of the spectrum.

Now we consider the fast positive and negative superluminal light. In the first case $|dV_g/dz|$ is very large (see Fig.6.3d and 6.4d). Moreover, the n'' is a fast function of z and it is not small. Therefore, the corresponding wave packets be strongly absorbed and their group velocity 6.2.1 have no physical meaning. The character of their propagation requires a numerical analysis. In the second case of the superluminal backward waves $|V_g| > c$, the frequency range between the two neighbor asymptotes gets narrower. A negative maximum of the group velocity getting deeper. But it is difficult to obtain small n'' for these waves for reasonable ε_h'' and f. Therefore, only very narrow wave packets of the fast negative light can be characterized by the group velocity. But there is no guarantee that are weakly decaying. This results are in agreement with [98], where it was firstly shown that the superluminal and backward waves can be characterized by the group velocity. Consider the frequencies close to the singularity of 6.2.1 or $n_g = (0)$, where $V_g(z) \to \pm\infty$. There is a strong frequency dispersion of $V_g(z)$ and it cannot be treated as the group velocity. But one can understand it with the help of the following simple example. Let us consider the condition $n_g = 0$ as a differential equation. Its solution is $n'(\omega) = n_0\omega_0/\omega$, where $\omega = z\omega_p$ and n_0 is a refraction index at ω_0. A profile of the narrow wave packet with the central frequency ω_0 propagating in the media with this refractive index can be

obtained from the integral given equations 1.6.1-1.6.4.

Therefore, at the singularity point of 6.2.1, where $n'(\omega) \sim 1/\omega$, the narrow wave packet propagate as a monochromatic wave with the exponentially decaying amplitude. The group velocity coincides with the phase velocity $V_g = V_{ph} \approx c/\sqrt{\varepsilon'_h}$.

All the above reported concerning the waves in the passive and active composites with tuned inclusions relate to the composites with pure metal inclusions that have one resonant frequency. In Fig.6.2d, one can see the branches $V_g(z)/c$ of the fast and negative light in the passive composite with $f = 0.0002$ which is show in figure 5.5. From figure 6.5d it is seen that the negative light with the group velocity $V_g = -0.12c$ can propagate in the active dielectric/pure metal composite with $\varepsilon''_h = -0.1159113$. It is necessary to note that the parameter of absorbtion n'' of EMWs is very sensitive to a value of ε''_h and practically linearly depends on small f. Due to this an experimental checking of the our theory is more reliable on the passive composites with pure metal inclusions in spite of the large absorption of EMWs. For example, the interference of two light beams with the same resonant frequency when one beam passes through a thin slab of the composite and another one propagates in empty space must show a difference between their velocities.

6.3 Conclusion

There are weakly damping narrow packets of these waves in the active composites of due to considerable decreasing in the imaginary part of the refractive index. It can be done by a fine tuning of the gain level of the composite (negative part $\varepsilon_h < 0$.)

There are slow and fast light propagating in the passive and active composites with pure metal inclusions in the vicinity of resonant frequencies. The passive composites

of pure metal inclusions can be more favorable for initial experimental studying of the dispersion properties of the slow backward waves because of the simplicity of manufacturing of these systems.

Bibliography

[1] C.F. Bohren and D.R. Huffman. *Absorption and Scattering of Light by Small Particles*. Wiley, New York, 1983.

[2] U. Kreibig and M. Vollmer. *Optical properties of metal clusters*. Springer, Berlin, 1995.

[3] B. R. Masters. *Handbook of Biomedical Nonlinear Optical Microscopy*. Oxford University Press.

[4] C. Rulliere. *Femtosecond Laser Pulses: Principles and Experiments*. Springer, 2nd edition, 2004.

[5] G. G. Gurzadyan V. G. Dmitriev and D. N. Nikogosyan. *Handbook of Nonlinear Optical Crystals*. Springer Series in Optical Sciences, Springer, 3rd rev. edition, 1999.

[6] R. W. Boyd and S. J. Bentley. Recent progress in quantum and nonlinear optical lithography. *Journal of Modern Optics*, 53:713–718, 2006.

[7] Q. Zheng G. S. He, L.-S. Tan and P. N. Prasad. Multiphoton absorbing materials: Molecular designs, characterizations, and applications. *Chemical Review*, 108:1245–1330, 2008.

[8] J. E. Midwinter. *Photonics in Switching. Quantum Electronics Principles and Applications*. Academic Press, 1993.

[9] G. P. Agrawal. *Applications of Nonlinear Fiber Optics. Optics and Photonics Series*. Academic Press, 2001.

[10] G.P.Agrawal. *Lightwave technology components and devices*. Jhon Wiley and Sons, New Jersey, 2004.

[11] H. Nihei and A. Okamoto. Photonic crystal systems for high-speed optical memory device on an atomic scale. *Proc. SPIE*, 4416:470–473, 2001.

[12] S. Kaneko K. Uchida S. Omi H. Tanji T. Tokizaki, A. Nakamura and Y. Asaharaaj. Subpicosecond time response of third-order optical nonlinearity of small copper particles in glass. *Applied Physcs Letters*, 65:941–943, 1994.

[13] V. M. Shalaev. *Nonlinear Optics of Random Media*. Springer-Verlag, 2000.

[14] Y.-K. Yoon R. S. Bennink and R. W. Boyd. Accessing the optical nonlinearity of metals with metal-dielectric photonic bandgap structures. *Optics Letters*, 24:1416–1418, 1999.

[15] M. D.Musick A.Lyon and M. J. Natan. Colloidal au-enhanced surface plasmon resonance immunosensing. *Analytical Chemistry*, 70:5177–5183, 1998.

[16] D. J. Graves J. Park T. Hyslop F. Tam N. Halas S. Surrey P. Fortina, L. J. Kricka and S. A. Waldman. Applications of nanoparticles to diagnostics and therapeutics in colorectal cancer. *Trends in Biotechnology*, 25:145–152, 2007.

[17] P. Roussignol D. Ricard and C. Flytzanis. Surface-mediated enhancement of optical phase conjugation in metal colloids.

[18] V. M. Shalaev. Electromagnetic properties of small-particle composites. *Phys. Reports*, 61:272, 1996.

[19] K.M. Leung. Optical bistability in the scattering and absorption of light from nonlinear microparticles. *Phys. Rev. A*, 33:2461, 1986.

[20] D. Stroud D.J.Bergman, Ohad Levy. Theory of optical bistability in weakly nonlinear composite medium. 49:129–134, 1994.

[21] K. M. Leung L. M. Floan T. SCALESE S. Arnold, T. R. Keeffe and A. Pluchino. Optical bistability of an aqueous aerosol particle detected through light scattering: theory and experiment. *Appl. Optics*, 29:3473, 1990.

[22] R. Nathanshon Levy and D. J. Bergman. Electrical resonance and optical bistability in periodic composite materials. *J. Appl. Phys*, 77:4263–4273, 1995.

[23] Z. Dutton L. V. Hau, S. E. Harris and C. H. Behroozi. Light speed reduction to 17 metres per second in an ultracold atomic gas. *Nature*, 397:594–598, 1999.

[24] N. N. Lepeshkin M. S. Bigelow and R. W. Boyd. Superluminal and slow light propagation in a roomtemperature solid. *Science*, 301:200–202, 2003.

[25] R. W. Boyd and D. J. Gauthie. Slow" and "fast" light. *In Progress in Optics*, 43:497–530, 2002.

[26] B. Bleaney B.I. Bleaney. *Electricity and magnetism*. Oxford University, London, 3rd ed. edition, 1976.

[27] M. Born and E.Wolf. *Principles of Optics*. Cambridge University Press, Cambrige, 7th ed. edition, 1999.

[28] B. A. van Tiggelen B. N. A. Lagendijk and P. de Vries. Microscopic approach to the lorentz cavity in dielectrics. *Phys. Rev. Lett.*, 79:657–660, 1997.

[29] R. W. Boyd. *Nonlinear Optics*. Academic Press, 1992.

[30] R. L. Sutherland. *Handbook of Nonlinear Optics*. Marcel Dekker, New York, 1996.

[31] H. A. Lorentz. *Theory of electrons,*. Teubner, Leipzing, 2rd ed. edition, 1916.

[32] J. D. Jackson. *Classical Electrodynamics*. Wiley, New York, 3rd ed. edition, 1998.

[33] J. Cooper J. Guo and A. Gallagher. Selective refraction from a dense atomic vapour. *Phys. Rev. A*, 53:1130–1138, 1996.

[34] J.van Kranendonk and J.E. Sipe. Foundations of the macroscopic electromagnetic theory of dielectric media. *Elsevier, Amsterdam*, 1977.

[35] J.E. Sipe J. J. Maki, M. S. Malcuit and R. W. Boyed. Linear and nonlinear optical measurements of the lorentz local field. *Phys. Rev. Lett.*, 68:972, 1991.

[36] P. de Vries and A. Lagendijk. Resonant scattering and spontaneous emission in dielectrics microscopic derivation of local-field effects. *Phys. Rev. Lett.*, 81:1381–1384, 1998.

[37] M. F. Reid C.K. Duan and Z. Wang. Local field effects on the radiative lifetime of emitters in surrounding media: Virtual- or real-cavity model. *Phys. Lett. A*, 343:474–480, 2005.

[38] E. M. Lifshitz L. D. Landau and L. P. Pitaevskii. *Electrodynamics of Continuous Media*. Pergamon Oxford, 2nd ed. edition, 1984.

[39] J. E. Sipe J. J. Maki, M. S. Malcuit and R. W. Boyd. Linear and nonlinear optical measurements of the lorentz local field. *Phys. Rev. Lett.*, 67:972–975, 1991.

[40] Zhenya Li Lei Gao, Liping GU. Optical bistability in nonlinear composite media. *Phys. stat. sol. (b)*, 218:591, 2000.

[41] H. M. Gibbs. *Optical Bistability: Controlling Light with Light, Quantum electronics-principles and applications*. Academic Press, 1985.

[42] W. Bogaerts D. Van Thourhout G. Morthier G. Priem, P. Dumon and R. Baets. Optical bistability and pulsating behaviour in silicon-on-insulator ring resonator structures. *Opt. Express*, 13:9623–9628, 2005.

[43] D. J. Hagan G. Assanto, Z. Wang and E. W. Vanstryland. All-optical modulation via nonlinear cascading in type ii second-harmonic generation. *Appl. Phys. Lett.*, 67:2120–2122, 1995.

[44] J.Goldhar A. Szöke, V.Daneu and N.A. Kurnit. Bistable optical element and its application. *Appl. Phys. Lett.*, 15:376, 1969.

[45] J. I. Dijkhuis A. V. Akimov V. G. Golubev D. A. Kurdyukov A. B. Pevtsov D. A. Mazurenko, R. Kerst and A. V. Sel'kin. Ultrafast optical switching in three-dimensional photonic crystals. *Phys. Rev. Lett.*, 91:213903, 2003.

[46] Zhenya Li Lei Gao, Liping GU. Optical bistability and tristability in metal/dielectric composite media of nanospherical. *Phys.Rev. E*, 68:06660, 2003.

[47] H. L. Tam K. W. Cheah F. Y. Wang, G. X. Li and S. N. Zhu. Optical bistability and multistability in onedimensional periodic metal-dielectric photonic crystal. *Appl. Phys. Lett.*, 92:211109, 2008.

[48] S. H. Fan M. F. Yanik and M. Soljacic. Uhigh-contrast all-optical bistable switching in photonic crystal microcavities. *Appl. Phys. Lett.*, 83:2739–2741, 2003.

[49] M. Soljaci M. F. Yanik, S. H. Fan and J. D. Joannopoulos. All-optical transistor action with bistable switching in a photonic crystal cross-waveguide geometry. *Opt. Lett.*, 28:2506–2508, 2003.

[50] T.Yanagawa K.Kurokawa Y.Hosoya, T.Suga. Linear and nonlinear optical properties of sol-gel-derived au nanometer-particle doped alumina. *J.Appl. Phys. Lett.*, 81:1475, 1997.

[51] J. Solis C.N. Afonso D.H. Osborne R.F. Hanglud Jr. A.K.Petford-Long. R.Serna, J.M. Ballesteros. Laser-induced modification of the nonlinear optical response of laser deposited cu:al_2o_3. *ThinSolid Films*, 318:96, 1998.

[52] Z.Y.Li T.Pan, J.P.Huang. Optical bistability in metal/dielectric composite with interfacial layer. *Physica B*, 301:190, 2001.

[53] et.al Hsiao-Kuan Yuan. A negative permeability material at red light. *Opt. Express*, 15:1076–1083, 2007.

[54] I.E. Protsenko A.N. Oraevskii. High refractive index and other optical properties of hetrogeneous media. *JETP Lett.*, 72:445, 2000.

[55] I.E. Protsenko A.N. Oraevskii. Optical properties of hetrogeneous media. *Quantum Electron.*, 31:252, 2001.

[56] I.E. Protsenko O.A. Zaimidoroga, V.N. Samoilov. The problem of realization of a high refractive index and the optical. properties of heterogeneous media. *Phys. Elem. Part. At. Nucl.*, 33:101, 2002.

[57] S. Fan J.T. Shen, P.B. Catrysse. Mechanism for designing metallic metamaterials with a high index of refraction. *Phys. Rev. Lett.*, 94:197401, 2005.

[58] L. Wang E.D. Jones S.Y. Lin, V.M. Hietala. A high dispersive photonic band gap prism. *Phys. Rev. Lett.*, 21:1771, 1996.

[59] S.V. Sukhov S. G. Moiseev, E.A. Pashinina. On problem of transparency of metal-dielectric composite media with dissipative and amplifying component. *Quantum Electronics*, 37:446–452, 2007.

[60] S.V. Sukhov. Nanocomposite material with the unit refractive index. *Quantum Electron.*, 35:741–744, 2005.

[61] L.A. Blanco A.G. Borisov S.V. Shabanov F.J. Garcia de Abajo, G. Gomez-Santos. Tunneling mechanism of light transmission trough metallic fillms. *Phys. Rev. Lett.*, 95:067403, 2005.

[62] V.N. Samoilov I.E. Protsenko, O.A. Zaimidoroga. Hetrogeneous medium as a filter of electromagnetic radiation. *J. Opt. A: Pure Appl. Opt.*, 9:363–368, 2007.

[63] S.G. Moiseev. Metal-dielectric composite as a. weakly reflecting coating in the optical range. *Nonlinear World*.

[64] S.V.Suhov S.G. Moiseev, E.A. Pashinina. Thin-film polarizer made of heterogeneous medium with uniformly oriented silver nanoparticles. *Quantum Electron.*

[65] W. R. Hamilton. Research respecting vibration, connected with the theory of light. *Proc. Roy. Irish Acad.*, 1:341, 1832.

[66] J. S. Russell. Report on waves. this report features the first, recorded pbservations of solitary waves (p.321) and of group velocity (p. 369). *Brit. Assoc. Reports)*, 1:311–390, 1844.

[67] A.E. Neeves and M.H. Birnboim. Composite structures for the enhancement of nonlinear-optical susceptibility. *J.Opt.Soc.Am.B*, 6:787, 1989.

[68] R. Inguva-M.H. Birnboim N. Kalyaniwalla, J.W. Haus. Intrinsic optical bistability for coated spheroidal particles. *Phys. Rev. A*, 42:5613, 1990.

[69] Tomoshiro Inoue-Masatoshi Nakagaki Hiroki Koizimu Kenso Yamaguchi Cai Lai Masaru Kamano Masarobu Haraguchi, Toshishiro Okamoto and Masamitsu Fujii. Linear and nonlinear optical phenomena of metallic nanoparticles. *IEEE Journal of selected topics in quantum electronics*, 14:1540, 2008.

[70] S. Banerjee K. Chattejee and D. Chaktovorthy. Plasmon resonance shift in oxid-coated silver nanoparticles. *Phys.Rev.B,*, 66:085421–1 – 085421–7, 2002.

[71] V.N.Mal'nev Sisay Shewamare. Two optical bistability domains in composites of metal nanoparticles with nonlinear dielectric core. *Physca B*, 407:4837–4842, 2012.

[72] G. Schmid. *Clusters and Colloids, From Theory to Application.* VCH Weinheim, 1998.

[73] S. Link and M. A. El-Sayed. Spectral properties and relaxation dynamics of surface plasmon electronic oscillations in gold and silver nanodots and nanorods. *J. Phys. Chem. B*, 103:8410–8426, 1999.

[74] G. Mie. Contribution to the optics of turbid media, especially colloidal metal suspensions. *Ann. Phys.*, 25:377–445, 1908.

[75] R. Gans. Form of ultramicroscopic perticles of silver. *Ann. Phys.*, 47:270–284, 1915.

[76] Stefan Alexander Maier. Plasmonics: Fundamentals and applications. *Springer, Berlin*, 2007.

[77] L. H. Shi and L. Gao. Subwavelength imaging from a multilayered structure containing interleaved nonspherical metadielectric composites. *Phys. Rev. B*, 77:195121, 2008.

[78] G. S. Agarwal and S. Dutta Gupta. T-matrix approach to the nonlinear susceptibilities of heterogeneous media. *Phys. Rev. A*, 38:5687, 1988.

[79] R. Inguva J.W.Haus, N. Kalyaniwalla and C.M. Bowden. Nonlinear-opticalproperties of conductive spheroidal particle composites. *J. Opt. Soc. Am.B*, 6:797–807, 1989.

[80] S. L. McCall H.M. Gibbs and T. N. C. Venkatesan. Differential gain and bistability using a sodium filled febry-perot interferometer. *Phys.Rev.Lett.*, 36:1135–1138, 1976.

[81] O.Levy and D.J.Bergman. Intrinsic optical bistability and resonances in nonlinear composites. *Physica A*, 207:157–162, 1994.

[82] V.N. Mal'nev Sisay Shewamare O.A. Buryi, L.G.Grechko. Induced optical bistability in small metal and metal coated particles with nonlinear dielectric function. *Ukr.J.Phys.*, 56:311, 2011.

[83] Selvakumar V.Nair Lavanya M. Ramaniah and Kailash C. Rustagi. Linear and nonlinear optical response of spherical anisotropic semiconductor microcrystallites. *Physical Review B*, 40:12423, 1989.

[84] J.H. Davies. *The Physics of Low-Dimensional Semiconductors*. Cambridge University Press, 1998.

[85] S.D. Smith A. Miller, D.A.B. Miller. Dynamic nonlinear optical processes in semiconductors. *Adv. Phys*, 30:697–800, 1981.

[86] S. Dods Zhang R. and P. Catrysse. Fdtd approach for optical metallic material. *Laser Focus World*.

[87] R. J. Bell R. W. Alexander Jr. L. L. Long Ordal, M. A. and M. R. Querry. properties of the metals al, co, au, fe, pb, ni, pd, pt, ag, ti, and w in the infrared and far infrared. *Appl. Optics*.

[88] A. A. Pnkhov A. A. Lisyansky A. P. Vingoradov A. V. Dorofeenko, A. A. Zyablovsky. Light propagation in composite materials with gain layers. *Phys. Ujp*.

[89] R.W. Boyd. Slow and fast light: fundamentals and application. *J. Mod. Opt.*, 56:1908–1915, 2009.

[90] A.Kuzmich L.J. Wang and A. Dogarlu. Gain-assisted superluminal light propagation. *Nature*, 406:277–279, 2000.

[91] G. Tartakovskii A.K. Sarychev. Magnetic plasmonic materials in actively pumped host medium amd plasmonic nanolaser. *Phys.Rev.B*, 75:085436, 2007.

[92] J.B. Pendry S.A. Ramakrishna. Removal of absorption and increase in resolution in near-field lens via optical gain. *Phys.Rev.B*, 67:201101(R), 2003.

[93] Brillouin. *Wave Propagation and Group Velocity.* Academic Press, New York, 1960.

[94] M. M. Kash et al. Ultraslow group velocity and enhanced nonlinear optical effect in a coherently driven hot atomic gas. *Phys. Rev. Lett.*, 82:5229–5232, 1999.

[95] Raymond Y.Chiao. Superluminal (but causal) propagation of wave packets in transparent media with inverted atomic populations. *Phys. Rev. A*, 48:R34, 1999.

[96] S. A. Glasgow M. Ware. The role of group velocity in tracking field energy in linear dieelectrics. *J. Peatross, Opt. Express*, 9:506=518, 2001.

[97] S. A. Glasgow M. Ware. Energy transport in linear dielectric. *J. Mod. Opt.*, 9:519, 2001.

[98] C.G.B. Garrett and D.E. McCumber. Propagation of gaussian light pulse through anomalus dispersion medium. *Phys.Rev.A*, 1:305, 1970.

[99] M. A. Palenberg and B. U. Felderhof. Optical absorption spectra of nanocrystal gold molecules. *Phys. Rev. B*, 55:10326, 1997.

Appendix A

Here we consider the location and motion of the roots to the cubic equation

$$x^3 + ax^2 + bx + c = 0 \tag{.0.1}$$

in the complex plane $x = x' + ix''$ depending on variations of the parameter$c$. In equation (.0.1), the parameters a, b, and c are real. In our case, $b \geqslant 0$, $c = -y(y > 0)$ and a may be both positive and negative. In this paper, we are concerned with the conditions imposed on the coefficients a, b and y when this equation has three (or one) real positive roots. It is known that an answer to this question is given by the Routh-Hurwitz theorem [99]. The location of the roots of (.0.1) that depend on its coefficients which follows from the Routh-Hurwitz theorem is given in the table of Appendix B. In particular, (.0.1) has three real positive roots provided that

$$D \leqslant 0, \quad b > 0, \quad y > 0, \quad ab + y > 0, \tag{.0.2}$$

where D is a discriminate of equation (.0.1)

$$D = \left(\frac{H}{3}\right)^3 + \left(\frac{q}{2}\right)^2, \; H = \frac{a^3}{3} + b, \; q = 2\left(\frac{a}{3}\right)^3 - \frac{ab}{3} - y. \tag{.0.3}$$

One can see that these conditions are rather complex for an analysis. Here we use simpler way [68]. From the graphical analysis of equation (.0.1) one may see that it has three (or one) real roots if extremum points (if they exist) of the function

$$y = x^3 + ax^2 + bx, \tag{.0.4}$$

are positive

$$x_1 > 0, \qquad x_2 > 0, \tag{.0.5}$$

and any positive y_0 lies in an interval

$$y(x_2) \leqslant y_0 \leqslant y(x_1), \tag{.0.6}$$

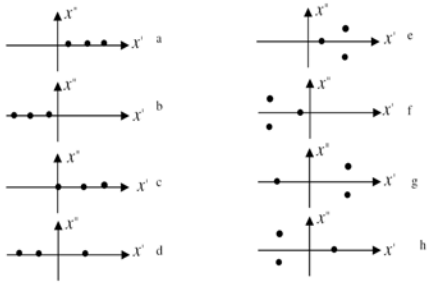

Figure 6: Location of roots on the complex plane

where $x_1 \leqslant x_2$. For (.0.1) these conditions may be written in the form

$$\begin{cases} a < -\sqrt{3b} \\ -\frac{2}{9}\left[(a^2-3b)x_2 + \frac{ab}{2}\right] < y_0 < -\frac{2}{9}\left[(a^2-3b)x_1 + \frac{ab}{2}\right] \end{cases} \tag{.0.7}$$

Therefore, the intervals where cubic equation (.0.1) has three real positive roots are given by the following expressions

$$\begin{aligned} \Delta(x) &= x_2 - x_1 = \frac{2}{3}(a^2-3b)^{1/2}, \\ \Delta(y) &= y(x_1) - y(x_2) = \frac{4}{27}(a^2-3b)^{3/2}. \end{aligned} \tag{.0.8}$$

We note that at $a^2 - 3b = 0$, $x_2 = x_1 = x_c$ and
$y_2 = y_1 = y_c$ then at the same time

$$x_c = -\frac{a}{3}, y_c = -\frac{a^3}{27}. \tag{.0.9}$$

The magnitudes x_c, y_c specify the critical values of x and y when three real positive roots appear in equation (.0.1).

Appendix B

Range of parameters	Location of roots on the complex plan
$x^3 + ax^2 + bx + c = 0$, $Q = (\frac{H}{3})^3 + (\frac{G}{2})^2 < 0$	$H = -\frac{a^3}{2} + b$, $G = 2(\frac{a}{3})^3 - \frac{ab}{3} + c$
in this case all roots are real.	
$ab - c < 0$, $c < 0$, $b > 0$, (1)	see Fig.6.a
$ab - c > 0$, $c > 0$, $b > 0$, (2)	see Fig.6.b
$ab - c < 0$, $c > 0$, $b > 0$ or $c > 0$, $b \leq 0$,(3)	see Fig.6.c
$ab - c > 0$, $c < 0$, $b > 0$,or $c < 0$, $b \leq 0$, (4)	see Fig.6.d

$x^3 + ax^2 + bx + c = 0$, $Q = (\frac{H}{3})^3 + (\frac{G}{2})^2 < 0$	$H = -\frac{a^3}{2} + b$, $G = 2(\frac{a}{3})^3 - \frac{ab}{3} + c$
in this case one root is real and two roots are complex conjugates	
$ab - c < 0$, $c < 0$, $b > 0$, (5)	see Fig.6.e
$ab - c > 0$, $c > 0$, $b > 0$, (6)	see Fig.6.f
$ab - c < 0$, $c > 0$, $b > 0$ or $c > 0$, $b \leq 0$,(7)	see Fig.6.g
$ab - c > 0$, $c < 0$, $b > 0$,or $c < 0$, $b \leq 0$, (8)	see Fig.6.h

List of Publications

1. O.A. Buryi,L.G.Grechko,V.N. Mal'nev,Sisay Shewamare, Induced Optical Bistability in Small Metal and Metal Coated Particles with Nonlinear Dielectric Function,*Ukr.J.Phys., Vol 56, Year 2011, page 311*

2. Sisay Shewamare,V.N.Mal'nev, Two Optical Bistability Domains in Composites of Metal Nanoparticles with Nonlinear Dielectric Core, "*Physica B, Vol 407,year 2012, pages 4837-4842*

3. Sisay Shewamare,V.N.Mal'nev, Slow and Fast Light in Metal/Dielectric Composites with Passive and Active Host Matrices, *to be published at the Journal of Physica B,*

List of Presentation in national and international conference

1. 7th National Ethiopian Physical Society Conference Mekele University, From February 2-3, *Optical Bistability Domains in Composites of Metal Nanoparticles with Nonlinear Dielectric core*

DECLARATION

I hereby declare that this Thesis is my original work and has not been presented for a degree in any other University. All sources of material used for the Thesis have been duly acknowledged.

Sisay Shewamare _____

email: sisayshewa20@yahoo.com

This Thesis has been submitted for examination with my approval as University advisor.

Prof. V. N. Mal'nev _____

email: vadimmalnev@yahoo.com